THE DEVELOPMENT OF A STOCHASTIC MODEL OF THE ATMOSPHERE BETWEEN 30 AND 90 KM TO BE USED IN DETERMINING THE EFFECT OF ATMOSPHERIC VARIABILITY ON SPACE SHUTTLE ENTRY PARAMETERS

by

Janet W. Campbell

Thesis submitted to the Graduate Faculty of the

Virginia Polytechnic Institute and State University

in partial fulfillment of the requirements for the degree of

DOCTOR OF PHILOSOPHY

in

Statistics

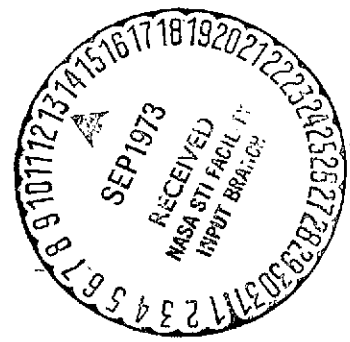

APPROVED:

R. G. Krutchkoff, Chairman

A. D. Sullivan

B. Harshbarger

R. H. Myers

B. Reed

W. B. Olstad, NASA

March 1973

Blacksburg, Virginia

THE DEVELOPMENT OF A STOCHASTIC MODEL OF THE ATMOSPHERE BETWEEN 30 AND 90 KM TO BE USED IN DETERMINING THE EFFECT OF ATMOSPHERIC VARIABILITY ON SPACE SHUTTLE ENTRY PARAMETERS

by

Janet W. Campbell

(ABSTRACT)

A stochastic model of the atmosphere between 30 and 90 km was developed for use in Monte Carlo Space Shuttle entry studies. The model is actually a family of models, one for each latitude-season category as defined in the 1966 U. S. Standard Atmosphere Supplements. Each latitude-season model generates a pseudo-random temperature profile whose mean is the appropriate temperature profile from the Standard Atmosphere Supplements. The standard deviation of temperature at each altitude for a given latitude-season model is estimated from sounding-rocket data. Departures from the mean temperature at each altitude are produced by assuming a linear regression of temperature on the solar heating rate of ozone. A profile of random ozone concentrations is first generated using an auxiliary stochastic ozone model, also developed as a part of this study, and then solar heating rates are computed for the random ozone concentrations.

Pressure and density profiles are calculated from each temperature profile by solving simultaneously the hydrostatic equation and the

equation of state. Isopynic layers, regions where atmospheric density is almost constant, are created at 24 and 90 km altitudes by using these two altitudes as boundary points in integrating the hydrostatic equation.

A computer tape of 442 sounding-rocket measurements of the atmosphere above 35 km was used to estimate parameters in the temperature distribution, and to compare the data's statistical characteristics with those of the model. The rocket soundings were sorted according to latitude-season categories and adjustments were made to assure independence of profiles. Because the resultant sample sizes were small, confidence intervals associated with the sample statistics were so wide that comparisons of these statistics with model statistics were inconclusive.

The model was used in Monte Carlo simulations of Shuttle entries to study the effect of atmospheric variability on the Shuttle entry parameters: maximum dynamic pressure, maximum stagnation-point heating rate, maximum g-load, final down-range distance, and final cross-range distance. A sample of 1000 entries was generated for each of the four seasons in the 30° latitude band, and the resultant parameter distributions were analyzed to determine parameter values. In general, autumn and winter parameter distributions showed more dispersion than spring and summer distributions, because the autumn and winter atmosphere models were more variable than the spring and summer models. Pearson distributions were fitted to the empirical distributions, and design values obtained in this manner were compared with the traditional "three-sigma" design values.

ACKNOWLEDGMENTS

For their approval and support of her graduate program, the author wishes to thank the management staff of the National Aeronautics and Space Administration's Langley Research Center, and, in particular, the Graduate Studies Committee, the Training Office, and her supervisors in the Space Systems Division.

Individuals who deserve specific acknowledgments are:

- Dr. Richard G. Krutchkoff, the author's major advisor, for his assistance with the stochastic modeling and simulation techniques,
- Mr. Paul F. Holloway, NASA - Langley, for suggesting the topic and for his assistance with the Shuttle trajectory portion,
- Dr. Walter B. Olstad, NASA - Langley, for his review of the dissertation, particularly the material relating to atmospheric physics,
- Dr. O. E. Smith and his associates at NASA's Marshall Space Flight Center for their advice concerning atmospheric modeling,
- Dr. James M. Russell, NASA - Langley, for suggesting the use of Green's ozone formula,
- Dr. Robert E. Boughner, NASA - Langley, for his assistance with the radiative heating model, and
- Dr. James F. Campbell, the author's husband, for believing in Women's Liberation.

TABLE OF CONTENTS

Page

Title Page i

Acknowledgments ii

Table of Contents iii

Chapter

I. Introduction 1

II. Atmospheric Models and Modeling Techniques 7

A general description of the atmosphere 7

Physical laws relating atmospheric temperature, pressure and density 12

Deterministic empirical models 13

Deterministic theoretical models 16

Stochastic models 19

III. The Atmospheric Temperature Model 25

The source of temperature variation 25

Radiative heating rates 30

Model linking temperatures to solar heating rates 33

IV. The Ozone Model 39

The ozone model below 50 km 40

The ozone model above 50 km 48

V. Comparison of the Model with Data 59

The MRN data tape 59

Comparison of model temperatures with data 61

Comparison of model densities and pressures with data 74

TABLE OF CONTENTS (continued)

Chapter	Page
Conclusions	83
VI. The Effect of Atmospheric Variability on Five Important Space Shuttle Entry Parameters: An Application of the Model	85
A two-dimensional random density model	86
Procedure	90
Results and discussion	92
Conclusions	104
VII. Summary and Conclusions	106
Summary	106
Concluding observations	110
References	113
Appendix A. Equations for Calculating Atmospheric Properties	117
Governing equations	117
Solving for ρ and P given a temperature-altitude profile	118
Solving for z and ρ given a temperature-pressure profile	120
Appendix B. Equations for Calculating Solar Heating Rates	122
Ozone absorption coefficients	123
Solar heating rates	125
Calculating optical thicknesses	127
Appendix C. Estimating the Parameters in Green's Formula Using Ozonagrams	130
Criteria for a good fit	131

TABLE OF CONTENTS (concluded)

Page

Calculating the shaping parameter A 131

Calculating PO_3^* and P* 132

Appendix D. Equations for Fitting Pearson Distributions to Data 135

The Pearson Type I distribution 139

The Pearson Type II distribution 140

The Pearson Type III distribution 141

The Pearson Type IV distribution 141

The Pearson Type V distribution 142

The Pearson Type VI distribution 143

The Pearson Type VII distribution 144

The Normal distribution 144

I. INTRODUCTION

In evaluating the performance of various aerospace entry vehicle designs, a major tool has been the use of entry trajectory computer programs. The majority of these programs use the U. S. Standard Atmosphere, [1], to furnish atmospheric temperatures, densities, and pressures as a function of altitude. These tables, published in 1962 by the Committee on Extension to the Standard Atmosphere (COESA) representing 29 U. S. scientific and engineering organizations, were developed as a means of standardizing aircraft and spacecraft engineering calculations. The basis of the tables is an annual mean temperature profile located at 45° N. latitude. Thus, the atmospheric properties furnished by the U. S. Standard Atmosphere are reasonably close to conditions during the spring and fall months at 45° N. latitude but are not representative of winter and summer properties nor those at different latitudes. In 1966, COESA published the U. S. Standard Atmosphere Supplements, [2], which contains seasonal atmospheric tables for 30°, 45°, 60°, and 75° N. latitudes and a set of annual mean profiles for 15° N. latitude.

Although these standard atmospheric tables are valuable for calculating nominal trajectories and for providing a basis of comparison for engineering calculations made by different individuals, they are inadequate for determining the impact of extreme atmospheres on a vehicle's performance. In designing a spacecraft it is necessary to establish a performance envelope within which all flight parameters are expected

to lie with high probability regardless of environmental extremes. Once this envelope is determined, one can establish a set of design criteria stating the extreme loads or stresses which an entry vehicle must be able to withstand.

In past design studies on atmospheric entry vehicles, a common method for obtaining a performance envelope (e.g., [3] and [4]), was to calculate trajectories using both maximum and minimum atmospheric density profiles as shown in Figure 1.1. Generally these are profiles in which atmospheric density is three standard deviations above or below its mean at all altitudes simultaneously. This method has two major disadvantages. One is that since density profiles such as these never occur in any real atmosphere, a design parameter based on this method might be overly conservative and, thereby, require unnecessary expense. A second disadvantage, more critical than the first, is that these extreme density profiles do not produce extremes in all entry parameters. For example, with some spacecraft a more severe total heat load is produced when atmospheric density is extremely low during the initial phase of entry and suddenly becomes extremely high at lower altitudes [5]. The reason for this severity is that the initial low density causes less deceleration than is normal, and thus the spacecraft encounters an extremely dense atmosphere while traveling at an unusually high velocity.

To account for the fact that extremes in the various entry parameters are produced by different atmospheric situations, an alternate deterministic approach, [6], has been to determine analytically for each performance parameter the atmospheric profile which produces an extreme in

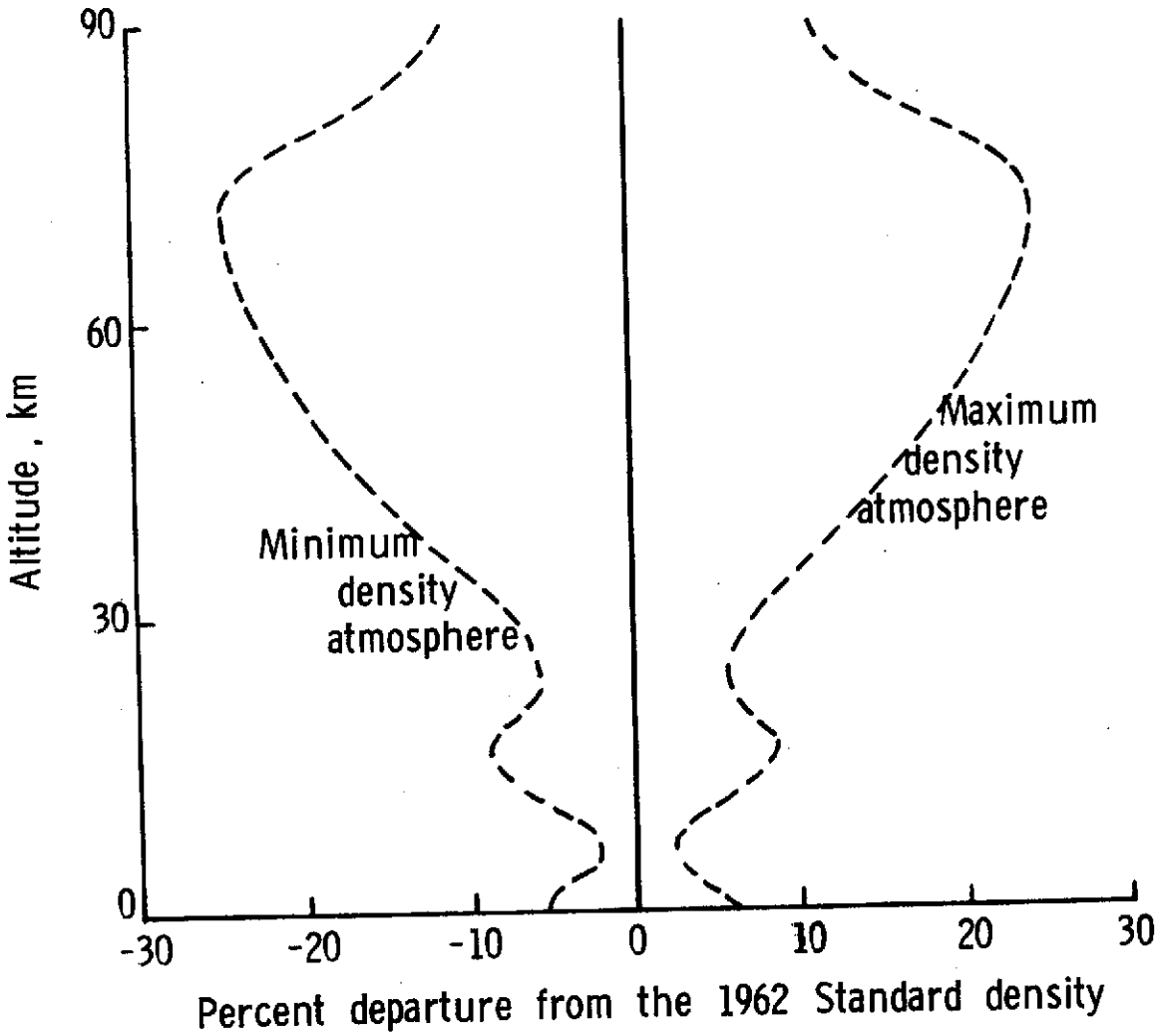

Figure 1.1 - "Extreme" atmospheres used in entry vehicle design studies.

that parameter, and then design the vehicle to withstand that extreme. As with any deterministic approach, however, this has the disadvantage that any specific atmospheric profile has a zero probability of occurrence, and thus the design may be overly conservative. Furthermore, the degree of conservatism cannot be ascertained since no knowledge is provided as to the probability of encountering atmospheric profiles similar to the design atmosphere.

The disadvantages associated with deterministic methods are strong justification for using statistical methods in establishing design criteria. A Monte Carlo entry study based on realistic random atmospheres can be used to estimate the statistical distribution of any entry parameter. Then a parameter's design value can be selected for any desired risk or exceedance probability. The optimum design criterion is one in which the risk associated with its design value is a compromise between safety and cost. That is, its risk should be low enough to provide a high measure of safety but not so low as to make the design impossible or unnecessarily expensive.

The next major space transportation system of the future, the Space Shuttle, is currently in the design stage. One major innovation in this new system is that the Shuttle will be capable of returning from orbit and landing much like today's conventional aircraft. Thus, the Shuttle can be reused, and the waste of disposing with spacecraft will be eliminated. With the advent of this reusable spacecraft, however, it has become much more important to have a good estimate of the probability of exceeding any design value. For example, when a spacecraft

was used only once it was not so critical to distinguish between a failure probability of .005 and one of .001. With the Shuttle having an expected lifetime of 100 missions, however, the difference between single-flight failure probabilities of .005 and .001 makes the difference between a 40 percent and a 10 percent chance of at least one failure during the lifetime of the Shuttle. This, therefore, is further justification for using the best available statistical techniques in design studies to acquire as much confidence as possible in reliability estimates.

In order to do Monte Carlo simulations of Shuttle entries, it was necessary to develop a stochastic atmosphere model capable of rapidly generating realistic atmospheric profiles. The author has accomplished this for the altitude region between 30 and 90 km, the region of greatest impact on Shuttle entry design considerations. This model uses a combination of empirical and theoretical techniques to derive a pseudo-random altitude profile of atmospheric temperature. The mean temperature at each altitude is defined empirically, and variations about the mean are explained, in part, by theoretical considerations. An auxiliary stochastic model of atmospheric ozone concentrations, also developed as a part of this study, is used to produce variations in solar heating rates, which are then linked to temperature variations via a linear regression model. Since the three thermodynamic properties of the atmosphere, temperature, density, and pressure, are related by two physical equations, it is possible to calculate any two quantities given an altitude profile of the third. Therefore, this model is fundamentally a stochastic model of atmospheric temperature, and pressure and

density profiles are obtained by using the pseudo-random temperature profiles provided by the model to solve two deterministic equations.

A review of atmospheric modeling techniques and current models is presented in Chapter II. Chapter III describes the development of the temperature model, and Chapter IV presents the auxiliary stochastic ozone model mentioned above. Chapter V presents the statistical characteristics of all three atmospheric profiles generated by the model (i.e., temperature, density, and pressure), and compares these with data obtained from Meteorological Rocket Network soundings. Chapter VI describes a Monte Carlo Shuttle entry study based on the present model. The model was used to furnish one pseudo-random density profile at the beginning of each entry simulation. In order to be realistic, since the Shuttle follows a long shallow entry path, it was necessary to add a horizontal variation to atmospheric density. This is also discussed in Chapter VI. Chapter VII begins with a summary of what has been accomplished, points out directions for improvement and future work, and states several conclusions regarding the overall approach.

II. ATMOSPHERIC MODELS AND MODELING TECHNIQUES SURVEY OF LITERATURE

A general description of the atmosphere

For the purposes of entry studies it will be assumed that the atmosphere extends to an altitude of 90 km (~300,000 ft). Aside from the fact that only .0001 percent of the atmosphere lies outside this radius, 90 km is a convenient upper limit for the atmosphere because at that altitude the relative proportions of the various constituents begin to vary, making it more complicated to relate temperature, density, and pressure. Below 90 km the molecular weight of air is essentially constant (28.964 kg), reflecting a constancy in the relative proportions of its principal constituents (see Table 2.1). As the molecular weight of air begins to vary above 90 km, this quantity becomes a fourth variable in the equation of state. Furthermore, the hydrostatic equation relating pressure and density begins to fail, and, therefore, the mathematical relationships between temperature, density and pressure used below 90 km become invalid above that altitude.

Figure 2.1 shows a general schematic diagram of the atmosphere and its various layers. The temperature profile shown here is that which forms the basis of the U. S. Standard Atmosphere, [1]. It is a piecewise linear approximation to a mean temperature profile obtained by averaging over temperatures from all seasons and latitudes. The various layers of the atmosphere indicated in Figure 2.1 are distinguished according to whether the rate of change of temperature with height is

Table 2.1 - Composition of Dry Air
Below 90 km

Constituent gas and formula	Content, percent by volume	Content variable relative to its normal	Molecular weight*
Nitrogen (N_2)	78.084	-	28.0134
Oxygen (O_2)	20.9476	-	31.9988
Argon (Ar)	0.934	-	39.948
Carbon dioxide (CO_2)	0.314	†	44.00995
Neon (Ne)	0.001818	-	20.183
Helium (He)	0.000524	-	4.0026
Krypton (Kr)	0.000114	-	83.80
Xenon (Xe)	0.0000087	-	131.30
Hydrogen (H_2)	0.00005	?	2.01594
Methane (CH_4)	0.0002	†	16.04303
Nitrous oxide (N_2O)	0.0005	-	44.0128
Ozone (O_3)	0 to .00002	†	47.9982
Sulfur dioxide (SO_2)	0 to 0.0001	†	64.0628
Nitrogen dioxide (NO_2)	0 to 0.000002	†	46.0055
Ammonia (NH_3)	0 to trace	†	17.03061
Carbon monoxide (CO)	0 to trace	†	28.01055
Iodine (I_2)	0 to 0.000001	†	253.8088

*On basis of carbon-12 isotope scale for which $C^{12} = 12$.

†The content of the gases marked with a dagger may undergo significant variations from time to time or from place to place relative to the normal indicated for those gases.

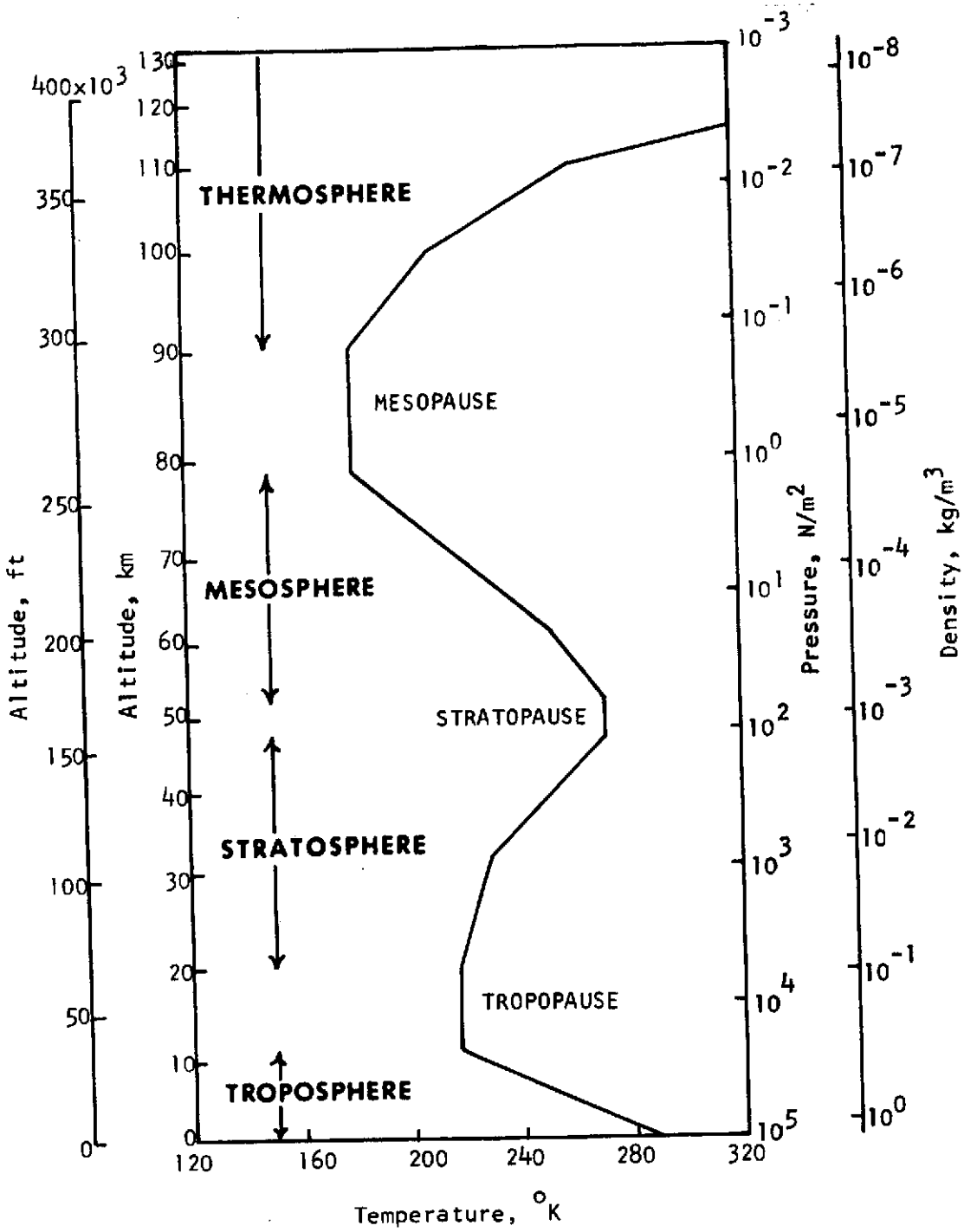

Figure 2.1 - Atmospheric layers based on 1962 U. S. Standard Atmosphere.

negative or positive.

The troposphere is the region beginning at the earth's surface in which temperatures decrease as altitude increases. This region contains approximately 99.8 percent of the atmosphere's precipitable water and, accordingly, contains the weather systems which affect surface conditions. The stratosphere is the region of increasing temperatures between ~10 km (the tropopause) and ~50 km (the stratopause), and the mesosphere, extending to ~90 km (the mesopause), is a second region of decreasing temperatures. The lowest temperatures in the atmosphere occur at the mesopause. Up to an altitude of about 65 km, summer temperatures exceed winter temperatures. However, between 65 and 110 km summer temperatures are lower than winter temperatures with an annual difference of as much as 60° K occurring at the mesopause.

The isothermal tropopause, stratopause and mesopause regions depicted on Figure 2.1 do not represent the shape of real temperature profiles. They result from the averaging of temperature profiles in which the tropopause, stratopause and mesopause occur at distinct variable altitudes.

The thermosphere begins at the mesopause and extends upward to an undefined height. Here temperatures increase exponentially with altitude until they reach an asymptotic value, known as the exospheric temperature, which ranges between 600 and 2000° K depending on the amount of solar activity.

This partioning of the atmosphere into a troposphere, stratosphere, mesosphere, and thermosphere is based on the temperature structure.

Another classification dividing the atmosphere into an ionosphere and a neutrosphere, above and below 80 km, respectively, is based on the fact that above ~80 km the air is highly ionized by high-frequency solar radiation. Another dual system divides the atmosphere at 90 km according to whether the molecular weight of air is constant (homosphere) or variable (heterosphere). In this study, the temperature-based system will be used.

The shape of the temperature profile can be explained in terms of the various heating and cooling mechanisms which exist at different altitudes. The temperature "bulge" in the stratosphere and mesosphere results from the absorption of solar radiation by ozone, a gas which is formed by photochemical processes in that region of the atmosphere. Although ozone is a minor constituent, in terms of its relative concentration, it plays a vital role in controlling the nature of our atmosphere. It absorbs virtually all of the sun's extremely high frequency radiation, wavelengths less than ~3000 $\mathring{A}$, and thereby shields the earth's surface from potentially harmful ultraviolet radiation, X-rays, and gamma rays.

Mechanisms which create the tropospheric temperature structure are more complicated than those in the stratosphere and mesosphere. Approximately 50 percent of all solar radiation reaches the earth's surface, and 90 percent of this incident radiation is absorbed. Heat from the surface is then transfered to the air adjacent to the surface, and water at the surface evaporates. As this moist heated air rises, it cools, becomes saturated, and eventually its moisture condenses, thus releasing heat into the atmosphere. These vertically moving air masses, together

with horizontal winds and radiative processes, govern the temperatures in the troposphere.

This combination of conductive, convective, and radiative processes, plus the heat exchanges resulting from evaporation and condensation, make the troposphere an extremely difficult region to model. Fortunately, however, the region of most importance for Shuttle entry considerations is the region between 30 and 90 km, the upper stratosphere and mesosphere, where maximum heating rates, g-loads, and dynamic pressures occur. The present discussion of modeling techniques and current models will be limited to those which pertain, at least partially, to this region.

Physical laws relating atmospheric temperature, pressure, and density

There are two well-established laws relating the thermodynamic properties of temperature, T, pressure, P, and density, ρ. The equation of state of an ideal gas (Perfect Gas Law) is given by

$$\rho = \frac{MP}{KT} \tag{2.1}$$

where K is the universal gas constant and M is the molecular weight of air. The hydrostatic equation, relating the rate of change in atmospheric pressure to density, is expressed as

$$dP = -g\rho\, dz \tag{2.2}$$

where z is altitude and g is the acceleration due to gravity, a deterministic quantity which depends on the distance from its point of application to the center of the earth. The hydrostatic equation

expresses the fact that the difference in pressure between two altitudes is equal to the weight of air in a vertical column of unit cross-sectional area contained between those altitudes. This relationship assumes that the atmosphere is static relative to the earth, an assumption which may be made below ~90 km.

Appendix A gives the simultaneous solution of (2.1) and (2.2) which is used to derive the pressure and density profiles corresponding to a given temperature profile. It also contains an equation used in this study for calculating g as a function of latitude and altitude.

Most atmospheric models either assume or derive one atmospheric profile (e.g., temperature, density, or pressure) and then calculate the remaining two using the equation of state, (2.1), and the hydrostatic equation, (2.2). The models vary according to which profile is the one used as a basis and according to whether that profile is empirically constructed from experimental data or is derived from a set of theoretical laws. The two latter classifications, empirical versus theoretical, will be discussed separately.

Deterministic empirical models

Probably the best known empirical atmosphere models are the 1962 U. S. Standard Atmosphere, [1], and the 1966 U. S. Standard Atmosphere Supplements, [2]. These are temperature-based models which assume piecewise linear temperature profiles approximating the means of experimental data. These assumed temperature profiles are then used to tabulate values of pressure, density, speed of sound, coefficient of viscosity,

thermal conductivity and other gas properties for altitudes at one-kilometer intervals between 0 and 120 km. These tables are used for general engineering purposes. For more specialized applications such as trajectory analyses of launches from Cape Kennedy, Vandenburg, Wallops Island, etc., reference atmospheres for these and other sites have been tabulated, (e.g., [7], [8], and [9]).

Empirical models are sometimes called "statistical" models when, in addition to including means of the various properties, they also include standard deviations and other sample statistics. An example of such a "statistical" model is reference [10] where Theon, et al., present a summary of statistics based on 208 temperature soundings made between 1960 and 1968.

Many so-called "models" are actually data summaries such as reference [11]. This is an example of the monthly data reports on Meteorological Rocket Network soundings at selected sites around the world. Besides giving the individual profiles measured during the month, they also list, for each site, the means and standard deviations of all the accumulated data taken during that month since 1961. The various Meteorological Rocket Network sites are shown in Figure 2.2.

As the quantity of data increases each year, global atmosphere models are being developed which account not only for seasonal and latitudinal variations, but also for longitudinal or time-of-day variations. The model presented by Weidner, Chambers and Lou, [12] is a preliminary one resulting from a study initiated in 1968 to develop a global model of the atmosphere above 25 km for NASA design criteria

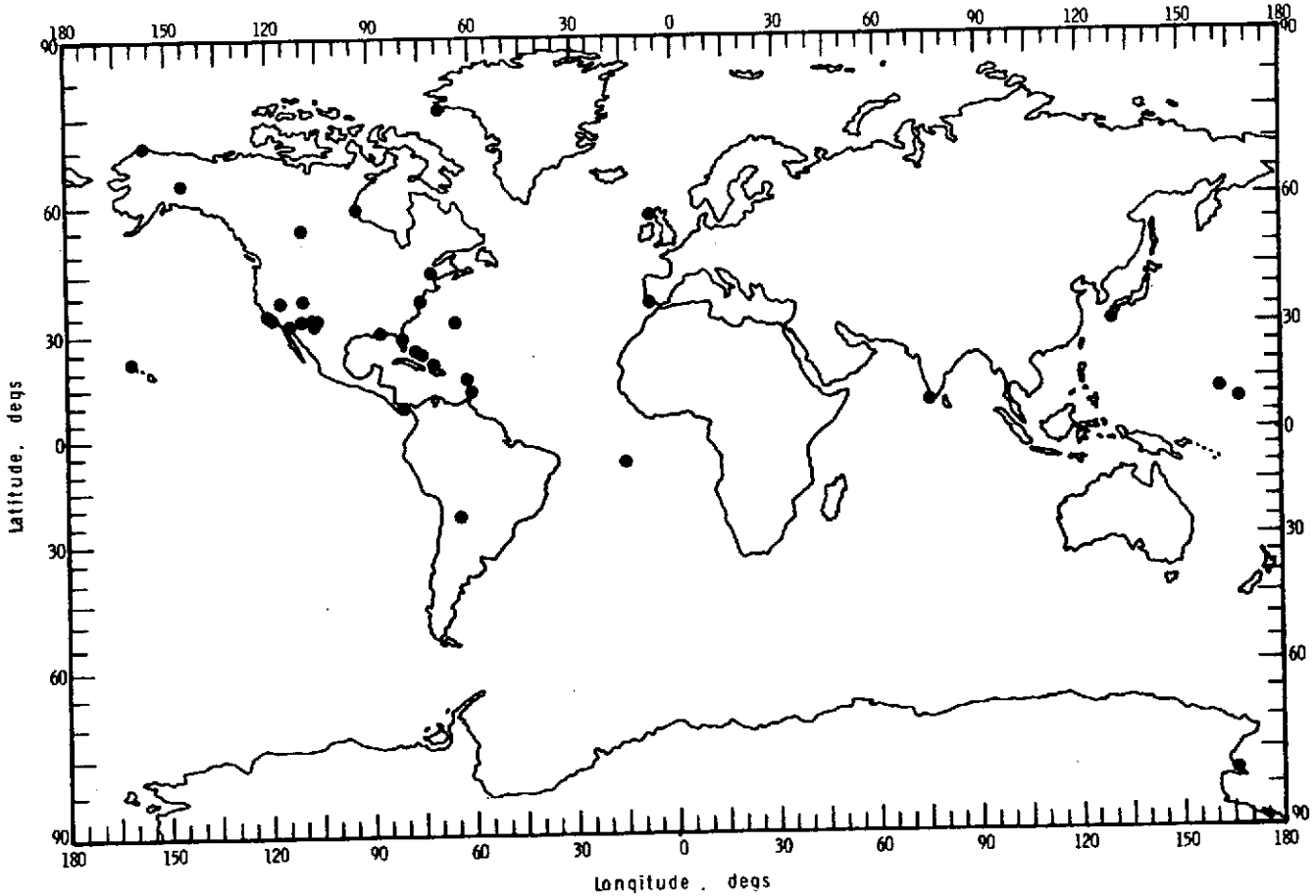

Figure 2.2 - Location of Meteorological Rocket Network launch sites.

purposes. This can be used with another global model developed by Spiegler and Fowler, [13], for the first 25 km. Another model developed specifically to provide a three-dimensional atmosphere for long horizontal Shuttle trajectories is that of Bowman [14].

Deterministic theoretical models

The models described above were classified as "empirical" because they rely largely on experimental data to provide values of temperature, density and pressure as a function of height. In some cases, [11], they are simple tabulations of data, whereas in other cases, [14], polynomials or other such curves have been fitted to the data to give mathematical representations of the atmospheric profiles. Such empirical models are valuable as engineering tools in that they provide the best estimate of atmospheric conditions. Theoretical models, on the other hand, such as those of Goody, [15], Harris and Priester, [16], and Kuhn, [17], attempt to explain observed properties using physical laws and hypotheses. Although good representations of the atmosphere are achieved, these models never completely reproduce the atmosphere's structure, many characteristics of which are not yet fully understood. Such models are important to the physicist as they enable him to explain observed phenomena, but as engineering tools, theoretical models are, in general, computationally too cumbersome, and the properties they predict are not as accurate as those of empirical models. Only those theoretical techniques and models which influenced this development will be discussed here. For an excellent general history of atmospheric temperature

modeling techniques, the reader is referred to Kuhn, [17].

Probably the most common approach to describing the atmosphere theoretically has been to calculate a temperature profile using the assumption that the atmosphere is in radiative equilibrium (e.g., Manabe and Möller, [18], and Manabe and Strickler, [19]). Although equilibrium temperature profiles of this type approximate observed temperature profiles, (see Figure 2.3), they cannot agree perfectly because the atmosphere is not actually in radiative equilibrium. In reality, there are regions which act as heat sources and sinks thus accounting for known global circulation patterns. The atmosphere is, however, close to radiative equilibrium, particularly in the stratosphere [15], and thus radiative processes explain, to a great extent, the temperature structure.

Instead of calculating equilibrium temperatures, an alternate approach was that used by Kuhn, [17]. He assumed a mean temperature profile and then calculated the corresponding infrared heating and cooling rates in the upper stratosphere and mesosphere. His infrared heating and cooling rates added to the solar heating rates of Murgatroyd and Goody, [20], give a net heat balance for the atmosphere which agrees well with known circulation patterns.

One major characteristic of any modeling technique based on radiation theory is its computational difficulty. The radiative transfer equation is a multiple integral equation requiring a numerical solution. Seemingly minor simplifying assumptions can often have disastrous effects on the predicted temperature profile or heating and cooling rates, [17].

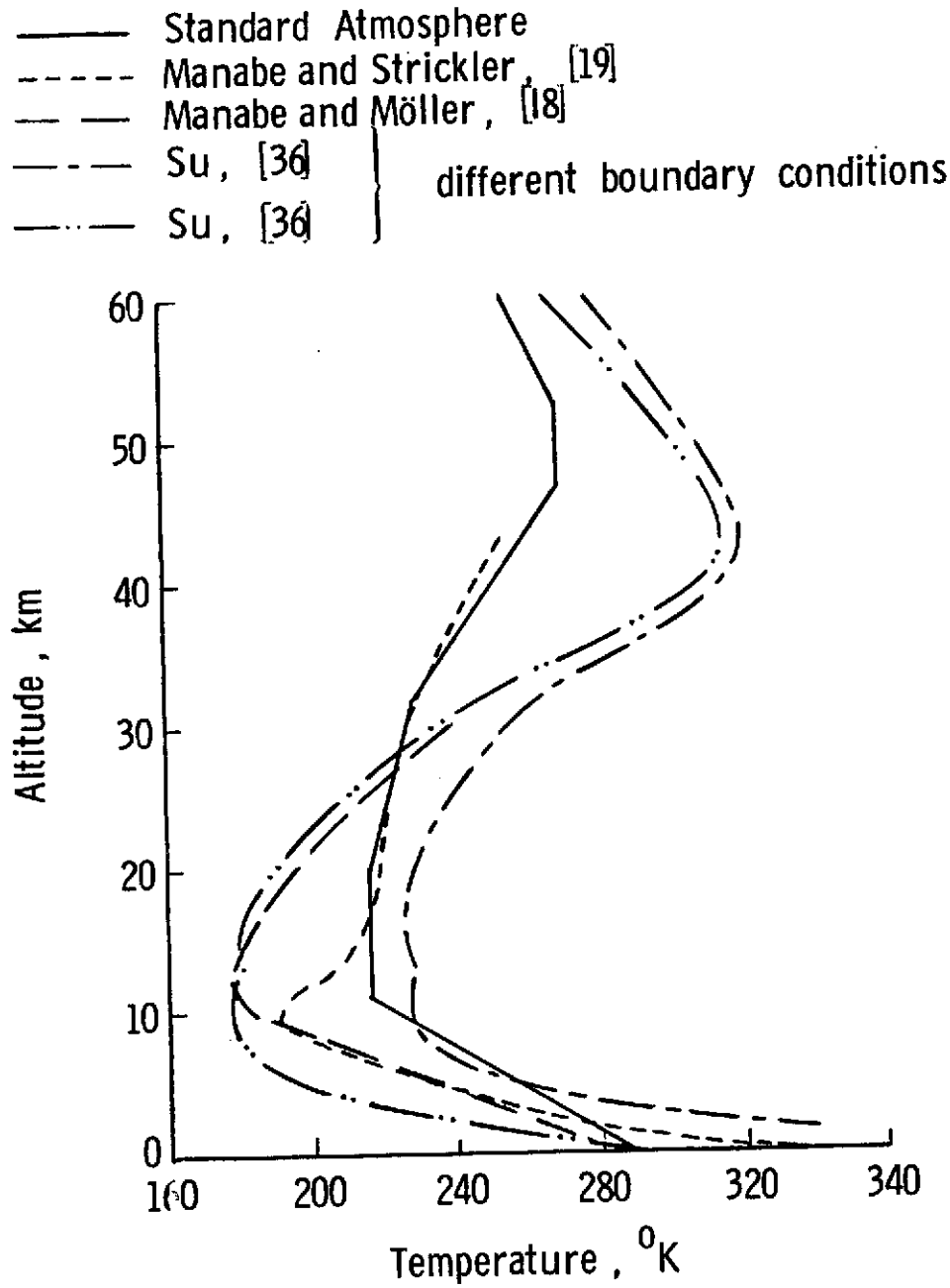

Figure 2.3 - Comparison of radiative equilibrium temperature profiles with 1962 Standard temperature profile.

Thus, radiative transfer calculations, in general, are not suitable for use in a stochastic model required to generate large numbers of temperature profiles rapidly. However, energy transfer calculations involving only solar radiation are much simpler, and these have been incorporated into the present stochastic model.

Stochastic models

Historically one of the first statistical treatments of atmospheric properties was made by Dines, [21], in 1919. Using the equation of state of an ideal gas, (2.1), and the assumption that in the atmosphere departures from the mean temperature, density and pressure are small in comparison with these means, Dines derived the approximate relations

$$\begin{aligned} C_\rho &= C_P r(P\rho) - C_T r(\rho T) \\ C_T &= C_P r(PT) - C_\rho r(\rho T) \\ C_P &= C_\rho r(P\rho) + C_T r(PT) \end{aligned} \tag{2.3}$$

where C_ρ , C_T , and C_P are the coefficients of variation of ρ , T , and P , respectively, and $r(\cdot\,\cdot)$ denotes a correlation coefficient between the two indicated quantities.

In 1954, Buell, [22], used these relationships in conjunction with the hydrostatic equation to derive an expression for the vertical gradient of $\sigma(P)$, the standard deviation of pressure. His expression is given by

$$\frac{d\sigma(P)}{dz} = -g\,\sigma(\rho)\,r\,(P\rho) \tag{2.4}$$

where $\sigma(\rho)$ is the standard deviation of density. According to this relationship, $\sigma(P)$ should be maximum or minimum at altitudes where $r(P\rho) = 0$.

Dine's work has recently been applied by Smith, et al., [23], to a modern problem relating to aerospace vehicle design criteria. Smith and his associates solved equations (2.3) for the correlation coefficients $r(\rho T)$, $r(P\rho)$, and $r(PT)$, using experimental measurements of C_ρ, C_T, and C_P at different altitudes. Their results are shown in Figure 2.4. They propose that these correlation coefficients be used to determine the appropriate combination of P, ρ, and T when one of these properties is taken to be extreme. For example, $r(PT)$ can be used to determine the appropriate value of temperature to accompany an extreme pressure. This approach is valuable in design problems where atmospheric properties are needed at a fixed altitude, e.g., along horizontal flight paths. In such cases, vertical atmospheric profiles are not known, and hence the hydrostatic equation is not applicable.

A number of authors have fitted polynomials to various atmospheric profiles and, by estimating the statistical distributions of the coefficients in their polynomials, they are able to generate random profiles. One example of this is the work of Essenwanger, [24], in which he approximates temperature and wind profiles below 25 km using Fourier series and density profiles below 25 km using Tchebycheff polynomials. He uses only one random coefficient in each approximation and assumes a Weibull distribution for that coefficient.

Another example of this approach is the recent work of Engler and

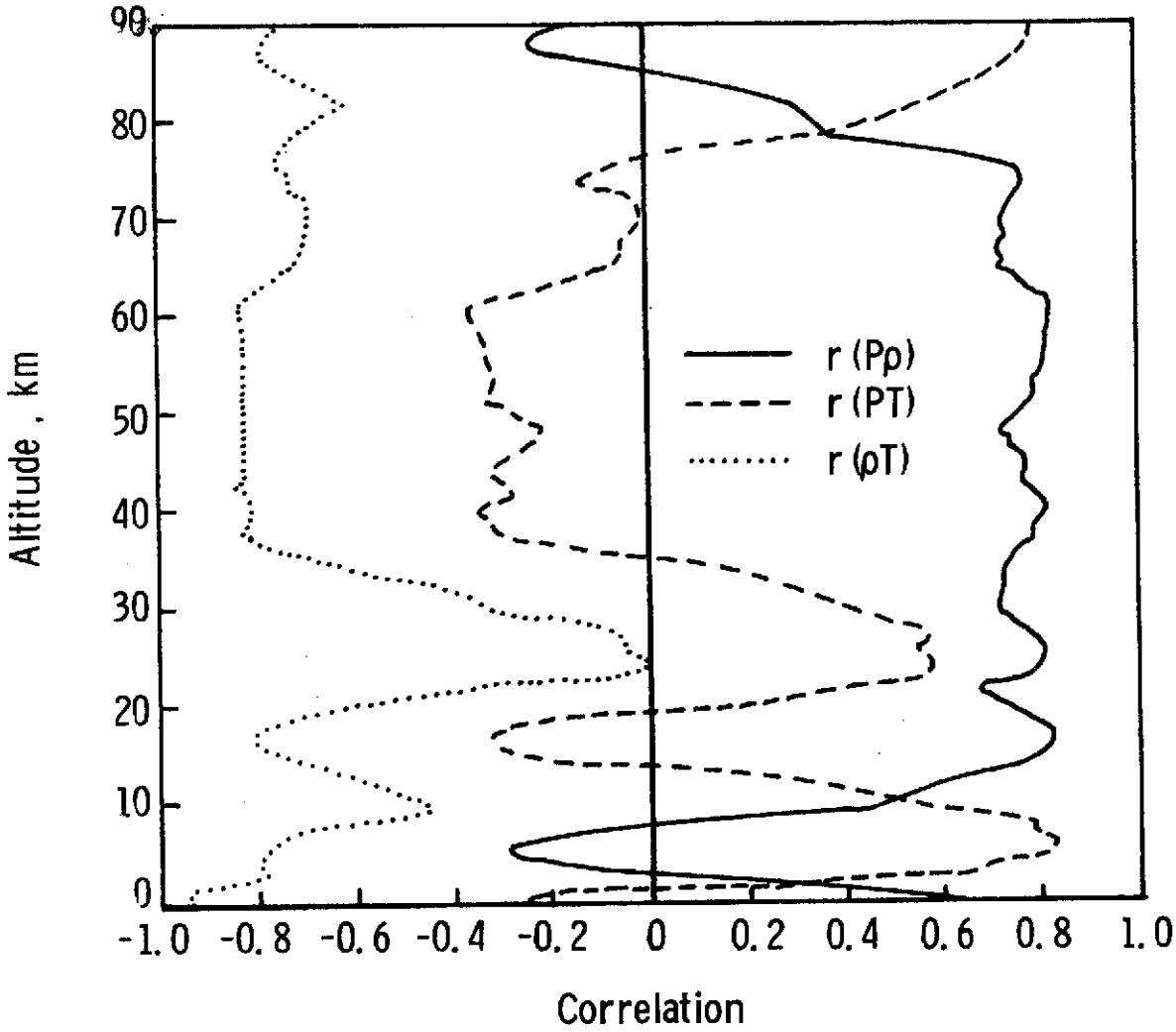

Figure 2.4 - Coefficients of correlation between atmospheric properties as calculated by Smith et al, [23].

Goldschmidt, [25]. Using a set of 67 experimentally measured pressure profiles, they fitted polynomials of order $k = 2,\ldots,6$ to profiles of $\log(P)$ and found that for most profiles a third-order fit was adequate. They then determined that the four coefficients, β_0, β_1, β_2 and β_3, used in their third-order polynomials were highly correlated, and so they expressed β_0, β_1 and β_2 as linear functions of β_3. The distribution of β_3 was estimated to be normal. Using their third-order polynomial for $\log(P)$, Engler and Goldschmidt were able to express the pressure at altitude z as

$$P = P_1(\beta_3, z)\, P_2(z) \tag{2.5}$$

where they call the factor $P_2(z)$ the steady-state pressure, since it is independent of β_3, and they called $P_1(\beta_3, z)$ the perturbation factor.

As Engler and Goldschmidt point out, one limitation of their model is that the 67 profiles used as their data base were for different seasons and locations. They speculate that if the data were for a single season and location, the correlations between the coefficients β_0, β_1, β_2, and β_3 would increase. However, this author believes that just the opposite would be true. That is, high correlations among the β_i's reflect a systematic variation in the shape of the $\log(P)$ profiles which may be due to season and latitude effects. If that is the case, then in a single season and latitude the variation in $\log(P)$ would be smaller and more irregular (i.e., less systematic). Hence, the β_i's would be less correlated. Nevertheless, the necessity of using as many

as four random variables instead of one would not be a serious disadvantage, and this model appears to be quite attractive for Monte Carlo simulations.

Justus and Woodrum, [26], have estimated the statistical distribution of "irregular" variations in atmospheric properties. They assumed that an atmospheric parameter such as density or pressure can be expressed as

$$F(z) = F_o(z) + f(z) \tag{2.6}$$

where the term $F_o(z)$ is made up of diurnally repeating components and steady-state components persisting over a period of several days. That is, two values of $F_o(z)$ measured 24 hours apart would be identical. The component $f(z)$ is called the irregular variation, and measurements of this were obtained by differencing profiles made at the same time of day on consecutive days. Knowing the distribution of $f(z)$, a random $F(z)$ profile could then be generated for any fixed $F_o(z)$. However, the variation in $f(z)$ is not sufficient to account for all the variation in $F(z)$ even within the same season and location. One would also need a model to provide the temporal and spacial variation in $F_o(z)$.

A final stochastic model of interest is a multiple regression model for atmospheric density between 30 and 110 km developed by Morgenstern and Orner, [27]. A stepwise regression procedure was used in selecting the optimum set of independent variables which significantly affect density. It has been shown by Jacchia, [28], that a number of variables have a strong influence on atmospheric density above 200 km. Using the

variables in Jacchia's model as a starting point, Morgenstern and Orner determined a set of 14 independent variables which have a significant correlation with density in the 30 - 110 km region. These are various measurements of solar flux, latitude, annual and semi-annual cycles. They divided the atmosphere into three quasi-homogeneous regions and used a different subset of these 14 parameters in their regression equation for each region. Their low altitude density model (30 - 50 km) required five independent variables; their middle region model (50 - 65 km) required six, and their high region model (65 - 110 km) required two parameters. They claim that their model accounts for 50 percent of the variability in density data between 30 and 75 km.

This model is not complete enough, as given, for generating pseudo-random density profiles. It is of interest, however, because, unlike the stochastic models discussed above, it is an effort to account for atmospheric variation by identifying the major causes of that variation. This was the approach taken in the development of the present stochastic temperature model.

III. THE ATMOSPHERIC TEMPERATURE MODEL

The single most dominant feature of the altitude region between 30 and 90 km is the temperature "bulge" caused by the absorption of solar energy by ozone. Thus, the temperature profile appears to be a logical starting point in attempting to model this region. It is for this reason, primarily, that the author has chosen to use temperature as the basis of the present atmosphere model. Another reason is that it is difficult to perturb a standard pressure or density profile and still have the associated temperature profile retain its characteristic shape as shown in Figure 2.1.

The source of temperature variation

To begin modeling variations in atmospheric temperature in the 30 - 90 km region, the first step is to identify the underlying processes which cause that variation and determine which ones are random. Any variable which can readily be ascertained without error at the time of the spacecraft's entry will be considered nonrandom. Variables which can only be estimated statistically at the time of entry will be considered random.

Among the nonrandom causes of temperature variation, a major one is nearness to the sun as determined by season and latitude. The present model accounts for this source of variation by requiring that season and latitude be fixed before estimating the various model parameters. That is, the model furnishes pseudo-random temperature profiles

characteristic of a specified season and latitude range.

Another nonrandom source of variation is time of day. The temperature model is based on rates of absorption of solar radiation; therefore, it is only representative of profiles during daylight hours. At the present time there is insufficient data to estimate model parameters for specific times of day. However, the standard deviation of atmospheric temperature at each altitude level is specified by the user of the model, and thus the model includes all observed variability in daylight temperatures for a given season and latitude band.

There are two major sources of temperature variation which are considered random. One is the creation and destruction of constituents which absorb and/or emit radiation, and the other is the random movement of air masses. Since the atmosphere is not in radiative equilibrium there are regions which act as heat sources (have a positive radiative heating rate) and other regions which act as heat sinks (have a negative radiative heating rate). Figure 3.1 shows the heating and cooling rates, in degrees per day, in the 30 - 100 km region as calculated by Kuhn, [17]. These gradients set up global circulation patterns which maintain an overall balance in the atmosphere's heat budget. Superimposed on these steady-state circulation patterns are winds or small-scale random air movements. A great amount of attention has been focused on random wind modeling, (e.g., [29], [30], [31], and [32]). The present temperature model does not include the effects of winds explicitly, although there is a random error term which might be considered as resulting from winds. It may be possible to include winds more directly by combining the present

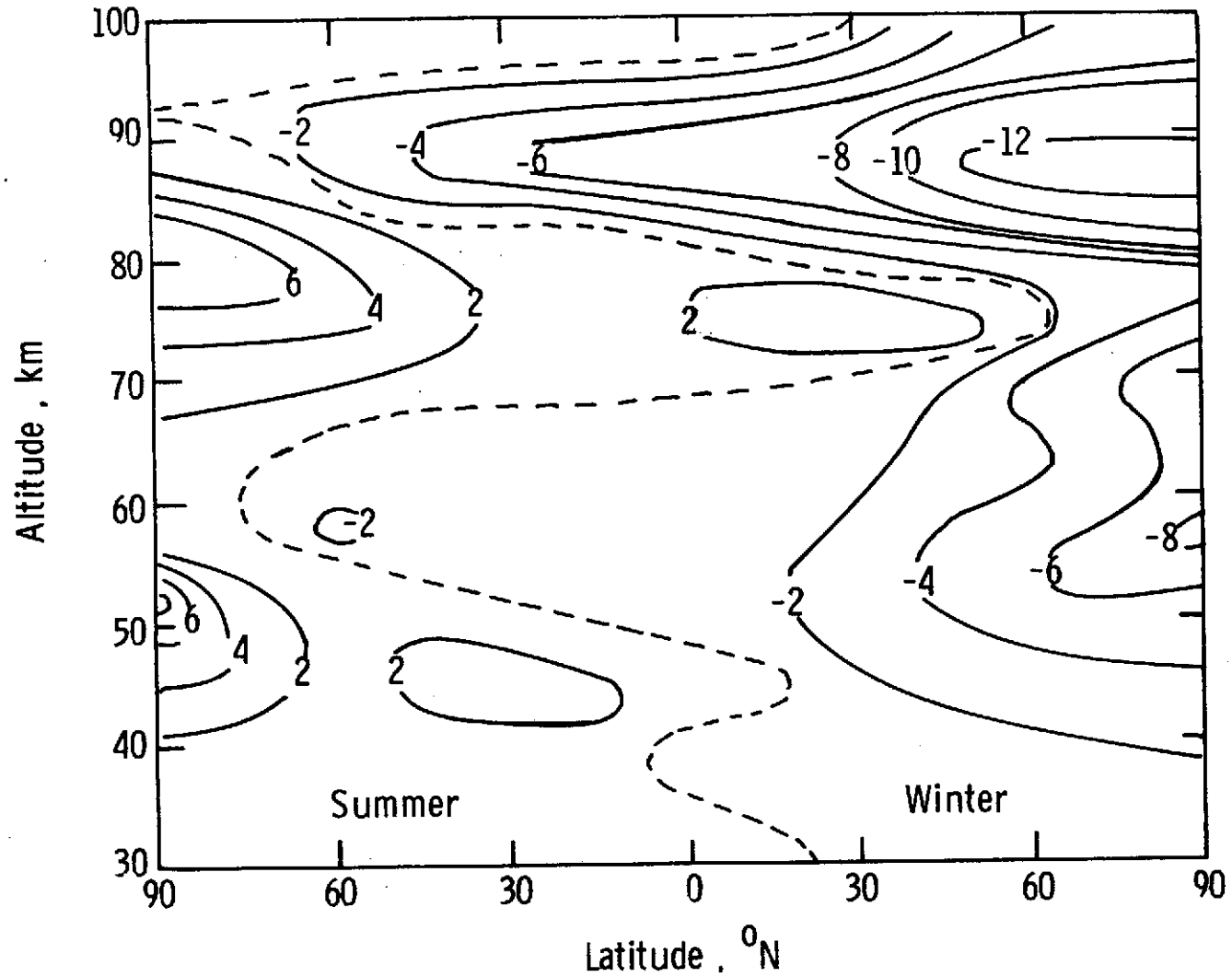

Figure 3.1 - Radiative heating and cooling rates in degrees Kelvin per day, as calculated by Kuhn, [17].

model with the random wind model described in [29].

The radiative heating rate at any point is a function of the radiant energy being absorbed and emitted at that point. These absorptions and emissions depend largely on the amounts of various radiatively active gases present. Electromagnetic radiation in the atmosphere has two major sources as illustrated in Figure 3.2. Radiation from the sun, with almost all wavelengths less than 4 μ, lies primarily in the optical spectral region, whereas radiation from the earth and its atmosphere, with most wavelengths greater than 4 μ, lies in the infrared spectral region. The two types of radiation are generally treated separately.

Solar energy is absorbed primarily by oxygen in the thermosphere, ozone in the stratosphere and mesosphere, and water vapor in the troposphere. Terrestrial radiation (including that from the atmosphere) is absorbed by water vapor, carbon dioxide, and ozone. Of these four radiatively active gases only water vapor and ozone have concentrations which vary significantly from day to day, and of these ozone is the major influence in the upper stratosphere and mesosphere. Thus, it was decided to model the variations in ozone and use these to produce variations in temperature between 30 and 90 km.

One advantage in linking atmospheric temperatures to radiative processes is that radiation, particularly solar radiation, is the only obvious means by which temperatures in two widely separated altitude regions can be correlated. For example, suppose the ozone in a high altitude region absorbs more solar energy than is normal. This means that less radiation reaches the ozone below that altitude and, as a

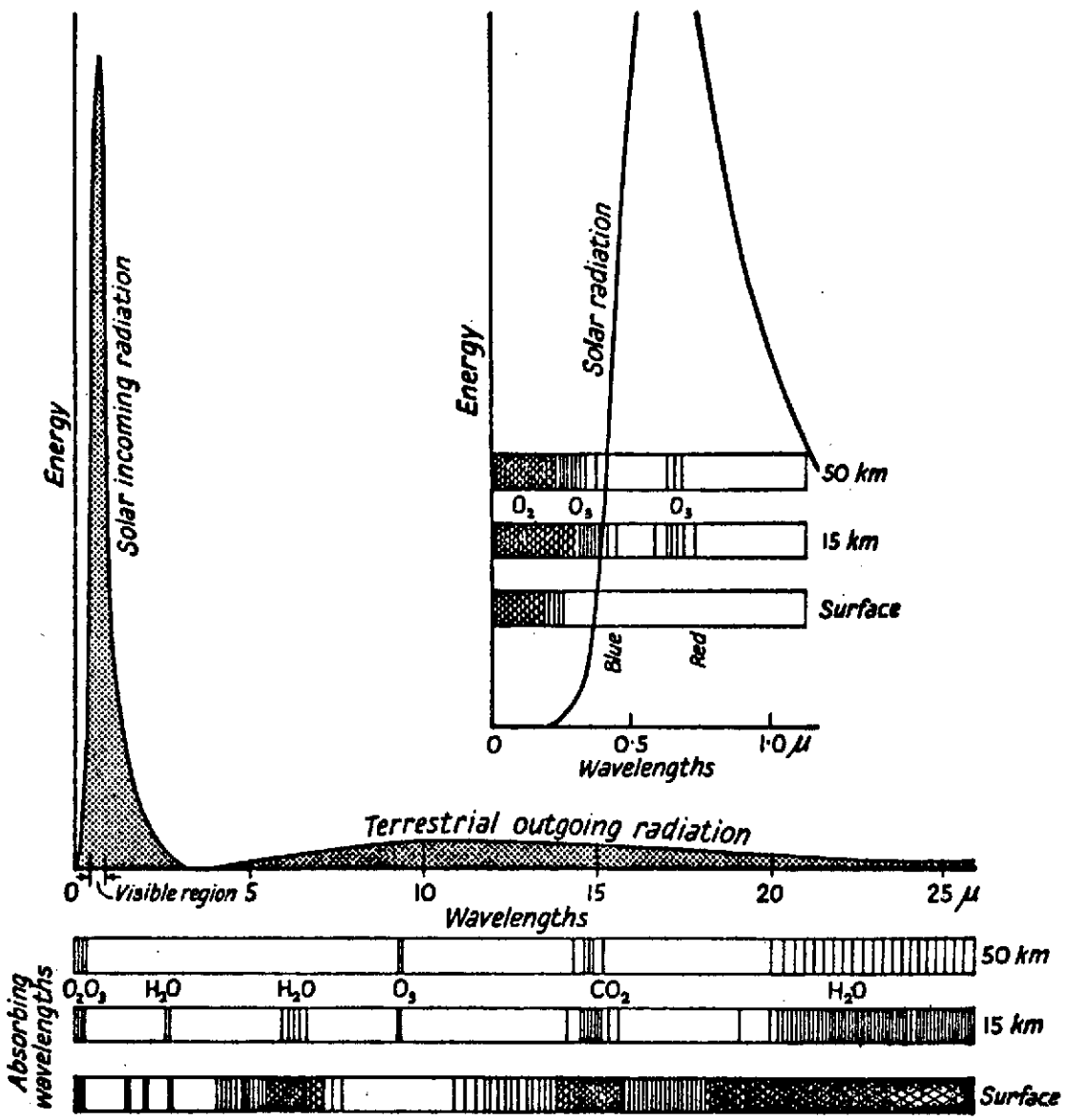

Figure 3.2 - Spectral distribution of solar and terrestrial (infrared) radiation.

consequence, less is absorbed. Since temperatures vary according to the amount of energy absorbed, then an increase in temperature (high absorption) at a high altitude would tend to be associated with a decrease in temperatures (low absorption) at some lower altitude, and vice versa.

The difficulty in modeling temperature profiles, or any other atmospheric profile, lies in modeling these interlayer correlations. Since pressures and densities are obtained by integrating over the temperature profile, it is important to generate temperature profiles with realistic shapes, i.e., temperature profiles whose deviations from the mean in one region are realistic relative to those in other regions. Otherwise, it is possible, for example, to construct a temperature model having a correct temperature distribution at each individual altitude which, at the same time, produces a very unrealistic distribution for the integrated temperature profile (i.e., temperature integrated over altitude). Since pressure and density depend on this integral, their distributions would be adversely affected.

Radiative heating rates

A basic premise underlying the development of the present model is that there is a strong positive linear correlation between the temperature at altitude z, $T(z)$, and the radiative heating rate at that altitude, $\dot{T}(z)$. The heating rate, in degrees per unit time, is given by

$$\dot{T}(z) = -\frac{1}{\rho c_p}\frac{dF}{dz} \qquad (3.1)$$

where ρ is atmospheric density, c_p is the specific heat at constant pressure (a constant), and F is the energy flux (the amount of energy per unit time passing through a unit area perpendicular to the z direction).

The change in F across a layer of incremental depth dz is

$$dF = \text{rate of emission} - \text{rate of absorption} \qquad (3.2)$$

The total flux F can be separated into two disjoint spectral terms, the flux of optical or solar radiation S and that of infrared radiation R. Thus, one can write $F = S + R$ or $dF = dS + dR$. Since the optical energy is basically solar radiation and the atmosphere, for most practical purposes, does not emit energy at those wavelengths, one can write

$$dS = - \text{rate of absorption of solar energy} \qquad (3.3)$$

The solar energy absorbed by a layer depends on the quantity of any absorbing gases in that layer (e.g., oxygen, ozone, water vapor) and on the amount of direct and reflected solar radiation which is incident on that layer. This latter dependency means that dS at altitude z depends not only on the quantity of an absorbing gas at altitude z, but also on the amounts of that gas at other altitudes, particularly at altitudes above z. Thus, in the 30 - 90 km region, variations in dS can be determined largely by modeling variations in the ozone profile.

The change in infrared (IR) flux is given by

$$dR = \text{rate of IR emission} - \text{rate of IR absorption} \qquad (3.4)$$

The infrared emission rate depends on both the temperature and pressure of the emitting gas as well as on its relative concentration. The absorption rate depends not only on these properties for the absorbing gas, but also on these properties for the surrounding gases. Thus, dR at one altitude is a function of the temperature profile, the pressure profile, and the appropriate constituent density profiles.

For a given ozone profile, a calculation of dS is reasonably straight-forward. One reason for this is that absorption coefficients needed in the calculation are well-behaved functions of wavelength in the visible and ultraviolet spectral regions and are virtually independent of atmospheric temperatures and pressures. An average absorption coefficient can be assumed to apply over a fairly wide wavelength band without sacrificing much accuracy in the resulting calculations. In the infrared region of the spectrum, on the other hand, calculations are very difficult. Thousands of overlapping absorption lines, each with its own absorption coefficient, are contained in any small spectral band. As it is impossible to treat each line separately, a number of band models representing various levels of approximation are used, (e.g., [33], [34], and [35]). Besides being mathematically formidable, these models involve parameters which are dependent on pressure and temperature. As a consequence, calculations involving the infrared radiative flux in the atmosphere are highly complex, time consuming, and poorly suited for the present purposes.

Fortunately, it is possible to concentrate on correlating temperatures to the solar heating rate

$$\dot{T}_s(z) = -\frac{1}{\rho c_p}\frac{dS}{dz} \tag{3.5}$$

and ignore the effect of the infrared processes on the variation of temperature. Theoretically, such an omission is justifiable provided that either dR is insignificant relative to dS, or dR is closely correlated to dS so that the partial correlation of T on dR, given dS, is small. The former justification is not valid, in general, since the atmosphere is close to radiative equilibrium so that $dR \approx -dS$. However, according to Kuhn's calculations, an increase in ozone produces a decrease in dR above 40 km and an increase in dR between 30 and 40 km. Calculations made in the present investigation indicate that the same is true of dS. That is, when ozone is increased, dS decreases above 40 km and increases between 30 and 40 km. Thus, it appears that changes in dS and dR resulting from ozone variations are positively correlated in the regions between 30 and 90 km.

Calculations of $\dot{T}_s$ in the present study are based on a three-step non-gray radiative model of the atmosphere used by F. Y. Su, [36]. Details of these calculations are presented in Appendix B.

Model linking temperatures to solar heating rates

The decision to relate variations in atmospheric temperature to variations in the solar heating rate of ozone required first the development of a stochastic model for ozone. Details of this development are described in the next chapter. By using this model to

generate pseudo-random ozone profiles, it is possible to vary the heating rates $\dot{T}_s(z)$, and thus effect changes in the temperature profile $T(z)$.

To relate $T(z)$ and $\dot{T}_s(z)$, a linear regression model is assumed. That is, it is assumed that the temperature at altitude z is given by a linear function of the general form

$$T(z) = \beta_0(z) + \beta_1(z)\dot{T}_s(z) + \varepsilon(z) \tag{3.6}$$

where $\beta_0(z)$ and $\beta_1(z)$ are regression coefficients and $\varepsilon(z)$ is a random component representing unmodeled variation (error).

Equation (3.6) can be written in a more definitive form as

$$T(z) = \mu_T(z) + \lambda\sigma_T(z)\frac{[\dot{T}_s(z) - \mu_s(z)]}{\sigma_s(z)} + \varepsilon(z) \tag{3.7}$$

where $\mu_T(z)$ and $\sigma_T(z)$ are the mean and standard deviation of $T(z)$, respectively; $\mu_s(z)$ and $\sigma_s(z)$ are the mean and standard deviation of $\dot{T}_s(z)$; λ is the coefficient of correlation between $T(z)$ and $\dot{T}_s(z)$, and $\varepsilon(z)$ is a normal random number with zero mean and variance given by

$$\sigma_\varepsilon^2(z) = (1 - \lambda^2)\sigma_T^2(z) \tag{3.8}$$

There are no data available which provide simultaneous measurements of $T(z)$ and $\dot{T}_s(z)$, or of $T(z)$ and ozone, in the 30 - 90 km region. Thus, it is not possible to use the usual least-squares methods for

estimating the regression coefficients. Instead, $\mu_T(z)$ and $\sigma_T(z)$ were estimated from sounding-rocket temperature data. A large volume of data is available, [37], on ozone concentrations in the troposphere and stratosphere. These data were utilized to develop a random ozone model which was then programmed to generate a large sample of $\dot{T}_s(z)$ profiles from which $\mu_s(z)$ and $\sigma_s(z)$ could be estimated.

The choice of $\lambda = .9$ in the present model was based on two considerations. First, a qualitative comparison was made between real measured profiles and model-generated profiles using a range of λ values between 0 and 1. As seen in Figure 3.3, the choice of λ determines the amount of small scale random scatter in modeled temperature profiles. A value of $\lambda = 1$ eliminates $\varepsilon(z)$ in equation (3.7) and, therefore, results in smooth temperature profiles influenced only by changes in $\dot{T}_s$. A value of $\lambda = 0$, on the other hand, eliminates the dependence of T on $\dot{T}_s$ and accounts for all temperature variation with $\varepsilon(z)$, thus producing a "white noise" type of variation. That is, with $\lambda = 0$, temperatures at any two altitudes would be uncorrelated regardless of how close the altitudes are. This comparison of model with data indicated that a choice of λ between .7 and .9 gave the model an amount of small-scale random fluctuation resembling that in the data.

A second consideration in the choice of λ was based on the need for a sufficiently high correlation between temperatures at adjacent altitudes. In the present model pseudo-random temperatures are generated at one-kilometer intervals; thus, "adjacent" altitudes are one kilometer apart. It follows from equation (3.7) that the correlation between

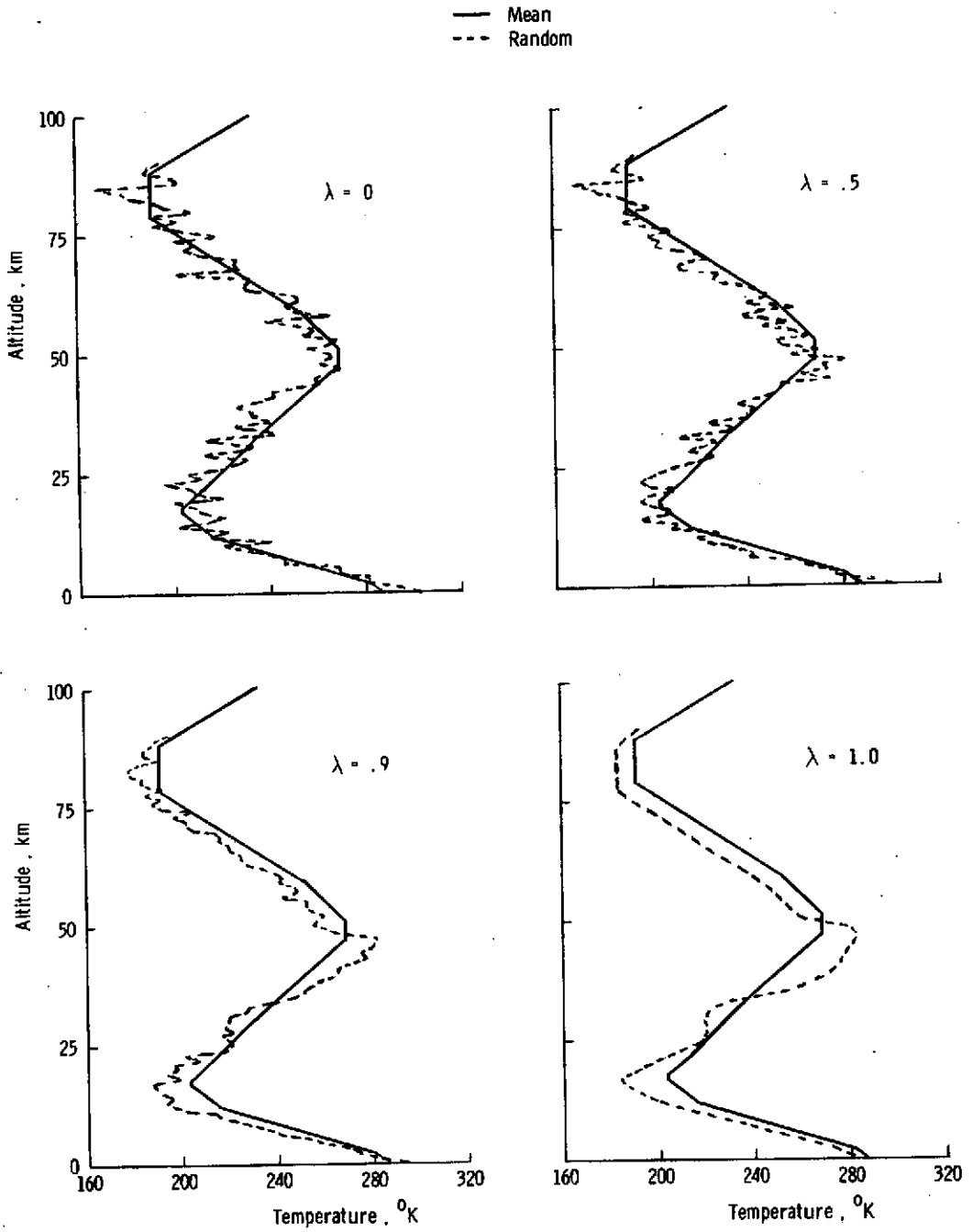

Figure 3.3 - Model-generated temperature profiles using different values of λ .

temperatures at any two altitudes cannot exceed λ^2 . In the data, temperatures at adjacent altitudes generally had very high correlations. Thus, to maximize these correlations in the model within the constraint $.7 \leq \lambda \leq .9$, the value $\lambda = .9$ was selected. Figure 3.4 shows a comparison of two measured profiles with two pseudo-random temperature profiles using $\lambda = .9$. Statistical characteristics of the model are compared with those of experimental data in Chapter V.

Before proceeding to a description of the ozone model, one further word of explanation is in order. It will be noticed in the next chapter that the ozone model gives ozone concentrations as a function of atmospheric pressure, P . Quite often atmospheric pressure instead of altitude is used as a vertical scale. This is possible because P is a strictly monotonic (decreasing) function of altitude. In the present model, it was found to be more convenient to use P or, more exactly, $\log(P)$ as the independent variable instead of altitude z . This is because the ozone model is based on $\log(P)$. Thus, all the quantities dependent on z in equation (3.7) were transformed so as to be functions of $\log(P)$ so that the model gives a temperature-log(P) profile. Using the equation of state and the hydrostatic equation, it is possible to solve for z and ρ as functions of the T-log(P) profile. Details are explained in Appendix A.

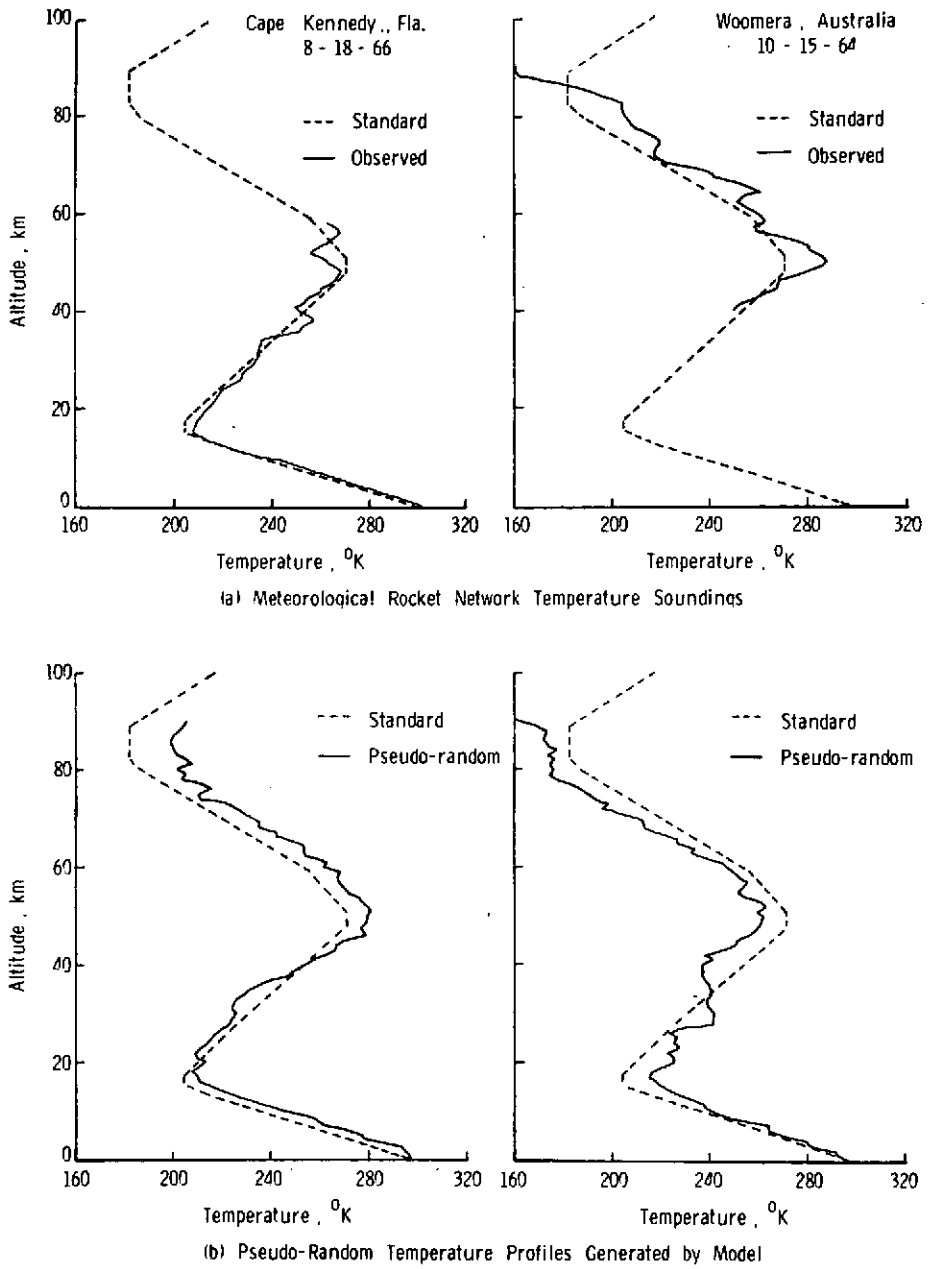

Figure 3.4 - Comparison of experimentally measured temperature profiles with model-generated temperature profiles.

IV. THE OZONE MODEL

Atmospheric ozone has been the subject of much scientific scrutiny since its existence was first hypothesized by Schobein in 1840, (see historical discussion in [38]). Ozone is formed by photochemical processes at altitudes where molecular oxygen O_2 and atomic oxygen O exist simultaneously. Atomic oxygen is formed in the upper atmosphere by the dissociation of O_2 when the latter is exposed to high-frequency solar radiation. Collisions between O_2 and O produce ozone, O_3. Ozone is subsequently destroyed when either O_3 and O collide, forming two O_2 molecules, or when O_3 is dissociated into O and O_2 by solar radiation.

In the mesosphere and upper stratosphere, the rates by which ozone is produced and destroyed through these processes balance one another so that it should be possible to predict concentrations using photochemical equilibrium theory. Unfortunately, however, very few measurements of ozone have been made in this region, and consequently the necessary reaction rates have not been clearly established.

Beginning at the stratopause and extending downward, photochemical equilibrium gradually disappears, and hence theoretical prediction methods become less applicable for modeling these ozone concentrations. In this region the best predictions of ozone appear to be empirical ones based on measured profiles.

In the present statistical model of ozone, it has been assumed that ozone profiles can be described by empirical expressions requiring

only a small set of parameters to define any specific profile. It is further assumed that the statistical distributions of these parameters can be estimated from data. Pseudo-random ozone profiles can then be generated by randomly sampling parameters from their respective distributions.

The ozone model below 50 km

In 1963 a network of observation stations was established by the Air Force Cambridge Research Laboratories (AFCRL) to systematically measure the vertical distribution of ozone in the troposphere and stratosphere. Figure 4.1 shows the stations making up this "ozonesonde" network.

Figure 4.2 is a typical "ozonagram" published by the AFCRL in a four-volume series entitled "Ozonesonde Measurements over North America", [37]. The partial pressure of ozone, PO_3, is plotted on the left as a function of total atmospheric pressure P. PO_3 reaches a maximum between approximately 20 and 25 km. Above that point the PO_3 profile decreases smoothly as it approaches a photochemical equilibrium profile. Below its maximum the PO_3 profile is characterized by large irregular fluctuations in the lower stratosphere and by a constancy or sometimes a slight increase in the troposphere. The curve on the right in Figure 4.2 is a simultaneous reading of atmospheric temperature. Unfortunately these curves usually end somewhere between 30 and 35 km, and, thus cannot be used for estimating the regression coefficients in equation (3.6) where the region of interest is $30 \leq z \leq 90$ km.

Station	Lat. (Deg.N)	Long. (Deg.W)
Albrook Field, Canal Zone	9.0	79.6
Colorado State University, Fort Collins	40.6	105.1
Eielson AFB, Fairbanks, Alaska	64.8	147.9
Florida State University, Tallahassee	30.4	84.3
Fort Churchill, Manitoba, Canada	58.8	94.1
Goose Bay, Labrador	53.3	60.4
L. G. Hanscom Field, Bedford, Mass.	42.5	71.3
Thule AFB, Greenland	76.5	68.8
University of New Mexico, Albuquerque	35.0	106.6
University of Washington, Seattle	47.4	122.3
University of Wisconsin, Madison	43.1	89.4

Figure 4.1 - Location of Ozonesonde Network stations.

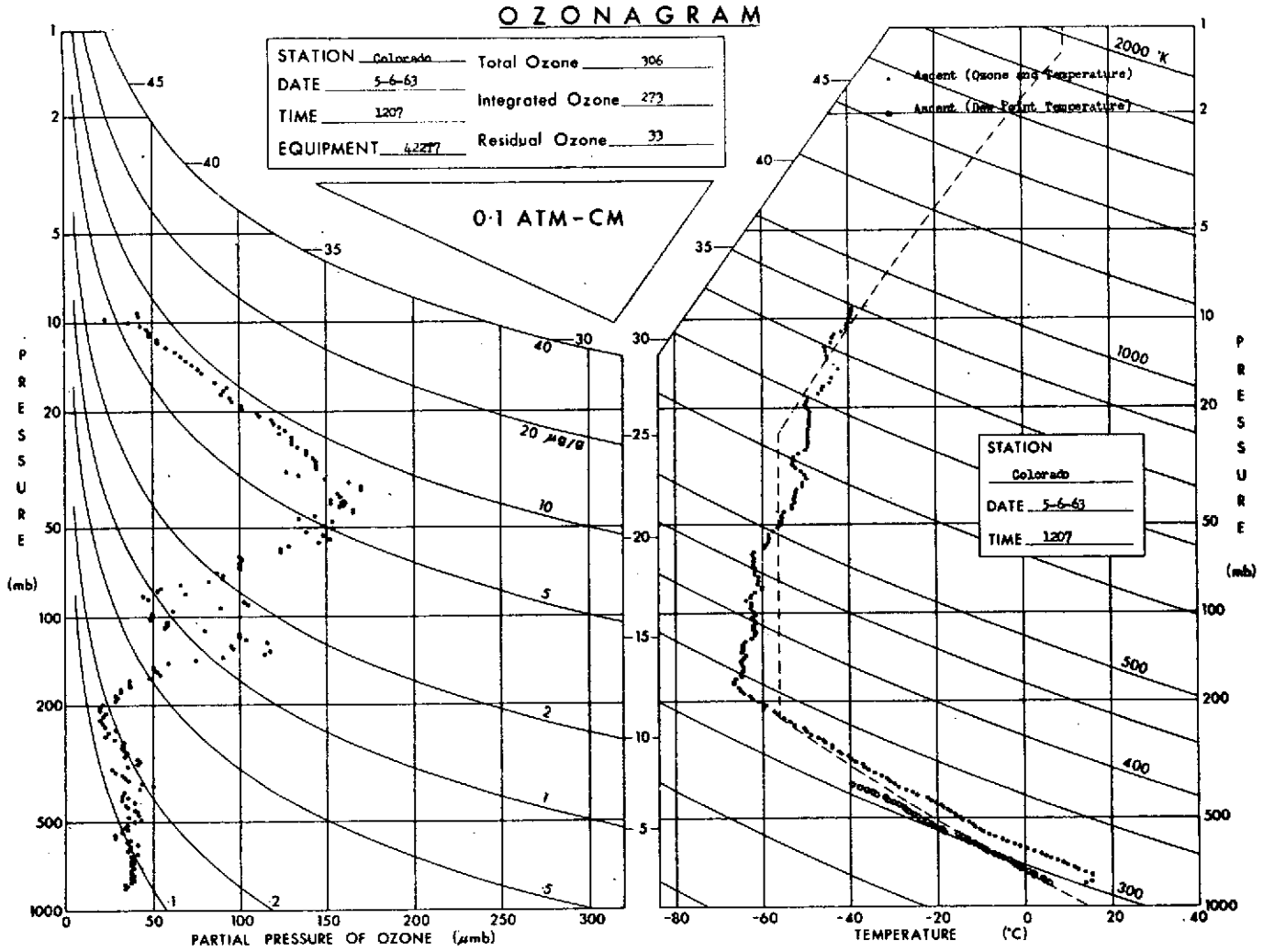

Figure 4.2 - Typical "Ozonagram" published by the Ozonesonde Network, [37].

Although ozone concentrations below 25 km do have some effect on solar heating rates above that altitude, because of reflected solar radiation passing upwards through the atmosphere, emphasis in the present investigation is placed on modeling the ozone profile above 25 km. For this reason it was not considered necessary to include the large irregular variations below the maximum PO_3 level.

An excellent empirical formula was used by Green, [39], for approximating PO_3 profiles such as the one in Figure 4.2. The formula, expressing PO_3 as a function of P, is given by

$$PO_3 = 4\, PO_3^* \frac{e^x}{(1+e^x)^2} \tag{4.1}$$

where

$$x = A \log (P/P^*) \quad ; \tag{4.2}$$

PO_3^* is the maximum partial pressure of ozone; P^* is the total atmospheric pressure at the altitude where PO_3 is maximum, and A is a shaping parameter. Equation 4.1 will hereafter be referred to as Green's formula. Examples of how well Green's formula fits ozonagram data are shown in Figure 4.3. In each case the parameters PO_3^* and P^* were selected so as to match the data above the ozone maximum as closely as possible. The four ozonagram shapes are typical of their respective stations. In general, both PO_3^* and P^* increase with latitude.

By integrating over the ozone profile, it is possible to derive an approximate expression for total ozone, TO_3, as a function of PO_3^*

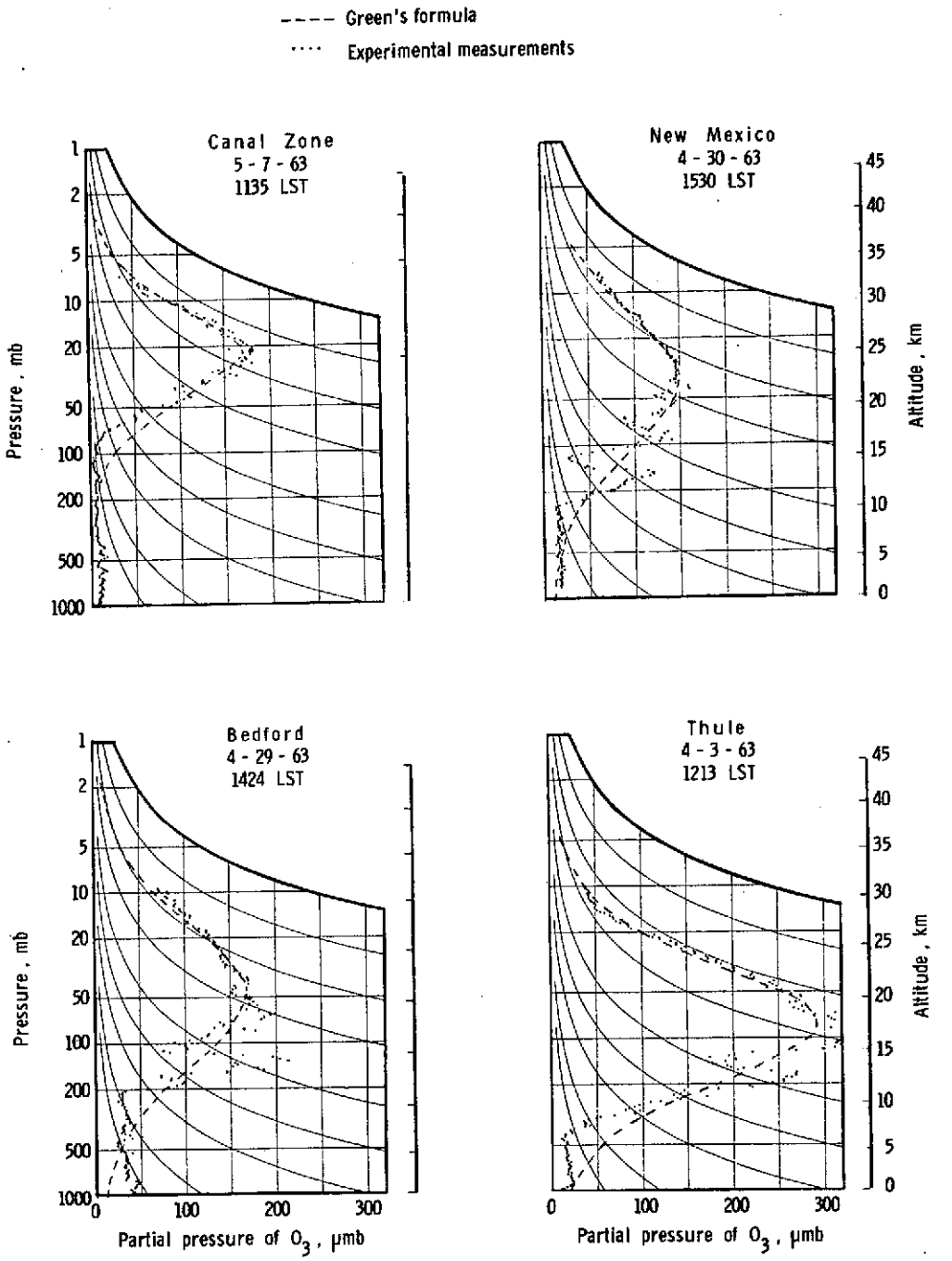

Figure 4.3 - Examples of Green's formula fitted to Ozonagram data.

and the shaping parameter A . Setting this expression equal to the measured total ozone indicated on each ozonagram, one can solve for A in terms of PO_3^* and TO_3 . Details as to how PO_3^* , P* , and A are calculated for each ozonagram are contained in Appendix C.

The statistical distributions of PO_3^* and P* were estimated from the ozonesondenetwork data in volumes 2 and 3 of reference [37]. Each ozone network station was assigned to one of five latitude bands, and within each latitude band (except the 15° band), the ozonagrams were divided into four seasonal groups. These season-latitude definitions conform to those established by the Meteorological Rocket Network and are shown in Table 4.1. This classification results in 17 latitude-season categories, and the parameter distributions for each must be estimated. This is a tedious job, and, to date, has only been accomplished for the ozonagrams in the 30° latitude band, the band in which the Shuttle landing site (Cape Kennedy) is located. If the need arises it can be completed for all 17 categories, and the data in volumes 1 and 4, [37], can also be included.

The parameters PO_3^* and P* have been estimated for each ozonagram using the procedure outlined in Appendix C. Samples of these parameters and the TO_3 values read directly from the ozonagrams have been tabulated for the four season categories in the 30° latitude band, and their means, standard deviations and correlations have been estimated. These statistics are listed in Table 4.2.

Since most of the variation in total ozone results from large irregular fluctuations in the lower stratosphere, variations which are

Table 4.1 - Season - Latitude Definitions

Meteorological Rocket Network Latitude Band Definitions

15° Band	0.00° - 22.50°
30° Band	22.51° - 37.50°
45° Band	37.51° - 52.50°
60° Band	52.51° - 67.50°
75° Band	67.51° - 90.00°

Meteorological Rocket Network Season Definitions: Northern Latitudes

Spring	April - May
Summer	June - August
Autumn	September - October
Winter	November - March

Meteorological Rocket Network Season Definitions: Southern Latitudes

Spring	October - November
Summer	December - February
Autumn	March - April
Winter	May - September

Table 4.2 Ozone Statistics in 30° Latitude Band

Parameter	Mean †	Standard Deviation	Correlations				
			PO_3^*	P*	TO_3	$\log(PO_3^*)$	$\log(P^*)$
FLORIDA - SPRING (sample size = 19)							
PO_3^*	0.0167	0.001951	1.00	0.51	-0.04		0.53
P*	3386	726.4	0.51	1.00	0.12	0.53	
TO_3	0.315	0.0177	-0.04	0.12	1.00		
$\log(PO_3^*)$	-4.101	0.1176		0.53		1.00	0.55
$\log(P^*)$	8.106	0.2115	0.53			0.55	1.00
NEW MEXICO - SPRING (sample size = 25)							
PO_3^*	0.0146	0.001422	1.00	-0.01	0.04		0.04
P*	3224	660.6	-0.01	1.00	0.30	0.01	
TO_3	0.321	0.0206	0.04	0.30	1.00		
$\log(PO_3^*)$	-4.233	0.0952		0.01		1.00	0.05
$\log(P^*)$	8.058	0.2051	0.04			0.05	1.00
FLORIDA - SUMMER (sample size = 12)							
PO_3^*	0.0144	0.001537	1.00	-0.12	0.28		-0.12
P*	3248	398.6	-0.12	1.00	0.68	-0.14	
TO_3	0.305	0.0135	0.28	0.68	1.00		
$\log(PO_3^*)$	-4.243	0.1070		-0.14		1.00	-0.14
$\log(P^*)$	8.079	0.1256		-0.12		-0.14	1.00
NEW MEXICO - SUMMER (sample size = 24)							
PO_3^*	0.0136	0.001234	1.00	0.46	0.31		0.50
P*	2935	595.4	0.46	1.00	0.24	0.47	
TO_3	0.292	0.0154	0.31	0.24	1.00		
$\log(PO_3^*)$	-4.304	0.0886		0.47		1.00	0.51
$\log(P^*)$	7.968	0.1747	0.50			0.51	1.00

Parameter	Mean	Standard Deviation	Correlations				
			PO_3^*	P*	TO_3	$\log(PO_3^*)$	$\log(P^*)$
FLORIDA - AUTUMN (sample size = 6)							
PO_3^*	0.0136	0.001519	1.00	0.13	-0.51		0.14
P*	3258	164.3	0.13	1.00	-0.45	0.19	
TO_3	0.283	0.0194	-0.51	-0.45	1.00		
$\log(PO_3^*)$	-4.306	0.1121		0.19		1.00	0.20
$\log(P^*)$	8.088	0.0510	0.14			0.20	1.00
NEW MEXICO - AUTUMN (sample size = 7)							
PO_3^*	0.0132	0.001463	1.00	0.13	0.39		0.14
P*	2661	164.4	0.13	1.00	0.11	0.16	
TO_3	0.259	0.0119	0.39	0.11	1.00		
$\log(PO_3^*)$	-4.329	0.1102		0.16		1.00	0.17
$\log(P^*)$	7.885	0.0597	0.14			0.17	1.00
FLORIDA - WINTER (sample size = 14)							
PO_3^*	0.0155	0.002146	1.00	0.46	0.60		0.48
P*	3151	419.6	0.46	1.00	0.39	0.48	
TO_3	0.303	0.0286	0.60	0.39	1.00		
$\log(PO_3^*)$	-4.175	0.1426		0.48		1.00	0.49
$\log(P^*)$	8.047	0.1354	0.48			0.49	1.00
NEW MEXICO - WINTER (sample size = 22)							
PO_3^*	0.153	0.002519	1.00	0.48	0.55		0.51
P*	3349	812.6	0.48	1.00	0.81	0.48	
TO_3	0.316	0.0443	0.55	0.81	1.00		
$\log(PO_3^*)$	-4.191	0.1778		0.48		1.00	0.52
$\log(P^*)$	8.091	0.2255	0.51			0.52	1.00

† Units for PO_3^* and P* are N/m^2: units for TO_3 are atm-cm.

not accounted for by Green's formula, it was decided to use a fixed value for TO_3 in our model. Accordingly, TO_3 was set equal to its latitude-season average and was not allowed to vary.

The empirical cumulative frequencies of both PO_3^* and P^* were compared with normal and log-normal cumulative distribution functions. This was done by plotting both the parameter and its natural logarithm on normal probability paper, obtaining a least-squares fit, and then comparing the sums of squared errors (errors being defined as differences between empirical cumulative frequencies and the normal cumulative distribution function). Neither the normal nor the log-normal distribution emerged as a clear choice, although the log-normal fit appeared to be slightly better in most cases for both PO_3^* and P^*. Furthermore, the log-normal distributions for both PO_3^* and P^* produced smaller, more realistic, variances for PO_3 at each altitude than did normal distributions for either or both parameters. Thus, log-normal distributions for PO_3^* and P^* were used. In most cases there was insufficient data to warrant fitting a Pearson distribution or attempting a more sophisticated estimate of the parameter distribution.

The ozone model above 50 km

Six hundred pseudo-random ozone profiles were generated by sampling from the P^* and PO_3^* distributions as described above. Solar heating rate profiles $\dot{T}_s(z)$ corresponding to each ozone profile were calculated, and the mean and standard deviation of $\dot{T}_s$ were estimated at each altitude. It was found that the profiles of heating rate averages agreed

quite well with deterministic $\dot{T}_s$ profiles predicted by Su, [36], and Manabe and Strickler, [19]. Comparisons are shown in Figure 4.4. On the other hand, Green's formula and the above parameter distributions produced unrealistically large variations in $\dot{T}_s$ at altitudes above approximately 50 km. At these altitudes, the heating rate is almost directly proportional to PO_3, and although the latter is quite small in magnitude, the variations in PO_3^* and P^* caused PO_3 to vary by several orders of magnitude. For example, using Green's formula at an altitude of 75 km, the parameter variations result in a range of PO_3/PO_3^* ratios between 10^{-2} and 10^{-5}. This is sufficient to produce a three-order-of-magnitude variation in heating rates at that altitude resulting in heating rates as high as 30° per day, a physically unrealistic value.

In reality, ozone in the mesosphere (above 50 km) is in photochemical equilibrium, for most practical purposes, and its concentrations are not as variable as those in the stratosphere. In fact, it is unrealistic to allow variations in PO_3^* and P^* to cause appreciable changes in PO_3 above 50 km. For this reason, it was decided to modify the ozone model in the mesosphere so as to reduce the variation in PO_3 in that region.

In Green's formula, (4.1), the term e^x approaches 0 as altitude increases such that $e^x << 1$ above 50 km. Hence,

$$PO_3 \simeq 4PO_3^* e^x \qquad (4.3)$$

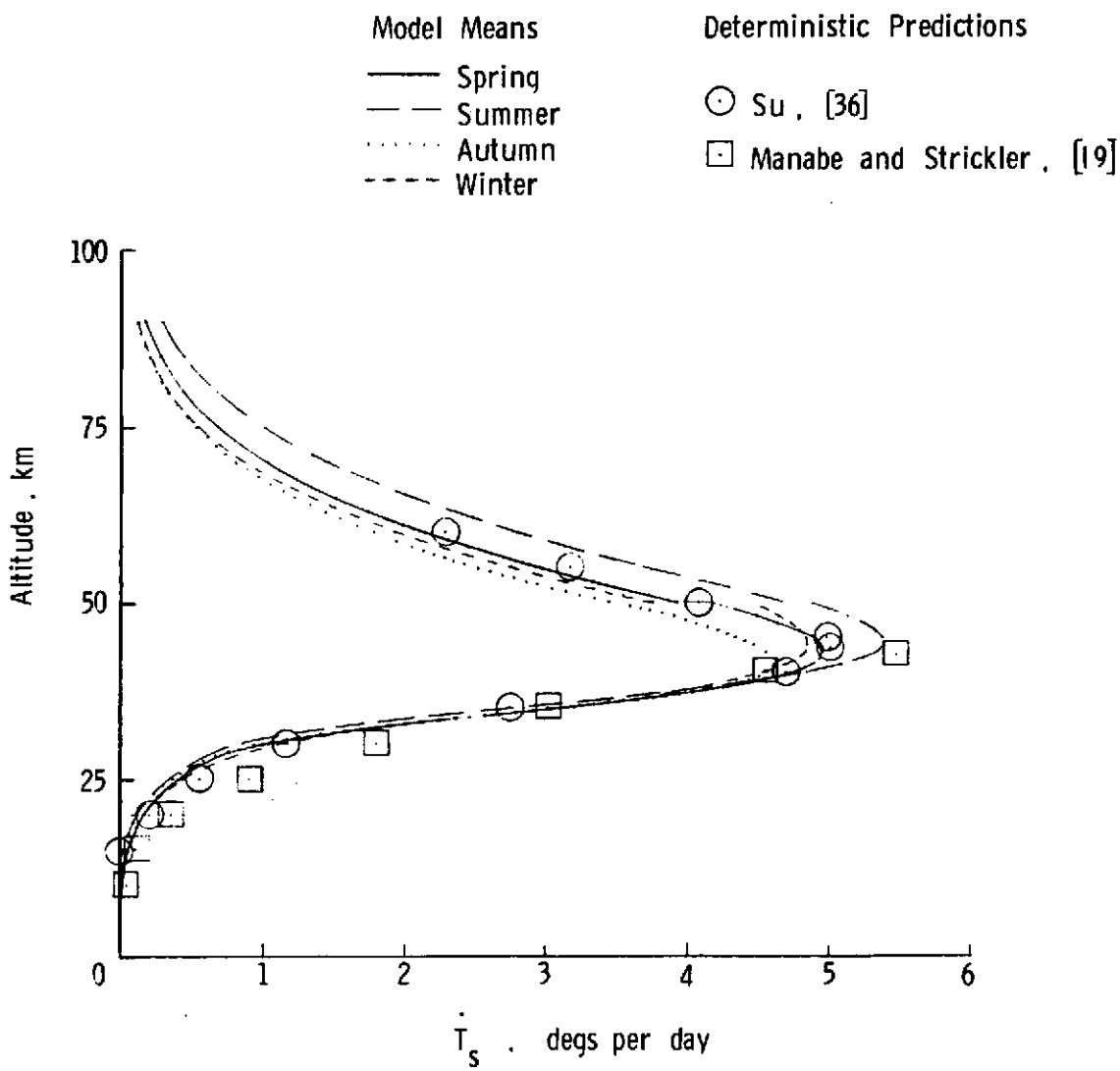

Figure 4.4 - Comparison of model-generated mean $\dot{T}_s$ profiles with deterministic predictions of $\dot{T}_s$.

Substituting from equations (4.1) and (4.2), this becomes

$$PO_3 \approx \exp [A \log (P/P^*) + B] \tag{4.4}$$

where A is the shaping parameter given in Appendix C as

$$A = A_o \, PO_3^*/TO_3 \tag{4.5}$$

(for constants A_o and TO_3), and

$$B = \log (4PO_3^*) \tag{4.6}$$

The ozone model above 50 km was modified as follows: The partial pressure of ozone above 50 km is given by

$$PO_3 = \exp [A \log (P/P^*) + B] \tag{4.7}$$

where now P^* is assumed to be constant and serves strictly as a non-dimensionalizing factor. Furthermore, it is now assumed that

$$A \sim N (\mu_A , \sigma_A^2) \tag{4.8}$$

and

$$B \sim N (\mu_B , \sigma_B^2) \tag{4.9}$$

Thus, PO_3 has a log-normal distribution with mean

$$E(PO_3) = \exp\left[\mu_A \log (P/P^*) + \frac{\sigma_A^2}{2} \log^2 (P/P^*) + \mu_B + \frac{\sigma_B^2}{2} \right] \tag{4.10}$$

and variance

$$\mathrm{Var}(PO_3) = E(PO_3)^2 \left\{ \exp\left[\sigma_A^2 \log^2 (P/P^*) + \sigma_B^2\right] - 1 \right\} \qquad (4.11)$$

The quantity $\log(P^*)$, which is a normal random number below 50 km, is set equal to its expected value above 50 km.

To maintain continuity with Green's forumula below 50 km, the means of A and B are, respectively,

$$\mu_A = A_o \, E\,(PO_3^*)/TO_3 \qquad (4.12)$$

and

$$\mu_B = \log(4) + E\,[\log\,(PO_3^*)] \qquad (4.13)$$

Since P/P^* approaches 0 as altitude increases, $\log(P/P^*) \to -\infty$, and, therefore, the coefficient of variation of PO_3,

$$CV(PO_3) = \left\{ \exp\left[\sigma_A^2 \log^2 (P/P^*) + \sigma_B^2\right] - 1 \right\}^{1/2} \times 100\% \qquad (4.14)$$

increases monotonically with altitude. The rate by which this coefficient of variation increases is controlled by the selection of σ_A^2 and σ_B^2. Accordingly, σ_A^2 and σ_B^2 were selected so as to satisfy two boundary conditions placed on $CV\ (PO_3)$. At the 50 km boundary the coefficient of variation was set equal to the coefficient of variation produced by Green's formula, a value which varied between 48% and 83% depending on the season-latitude model. At the upper boundary, $z = 90$ km, PO_3 was assumed to have a coefficient of variation of 100%. These two boundary

conditions resulted in a pair of simultaneous equations which were solved to give σ_A^2 and σ_B^2.

The four mean PO_3 profiles produced by this model for the 30° latitude band are shown in Figure 4.5. The dashed lines are loci of maxima and minima occurring in a pseudo-random sample of size 600. Figure 4.6 compares histograms of PO_3 values produced by the model at the pressure height of 1000 N/m^2 with corresponding histograms from the data in reference [37]. Four mean heating-rate profiles corresponding to the PO_3 means in Figure 4.5 are shown in Figure 4.7, again with loci of maxima and minima. Table 4.3 lists the mean and coefficient of variation of heating rate as a function of altitude for these four seasons.

It should be remembered that this ozone model was developed as a tool for modeling temperature variations in the stratosphere and mesosphere. For a large enough λ in equation (3.7), the shape of the temperature distribution at any altitude will essentially be that of the heating-rate distribution at that altitude. However, the actual magnitudes of the mean and standard deviation of heating rate will not affect the mean or standard deviation of temperature, since the two latter quantities are built into the model. Thus, further fine-tuning of the ozone model to reduce its variance was not considered necessary. The only type of modification which could significantly improve the model for its present purposes would be a change affecting the shape of the heating-rate distribution; this could only be accomplished by changing the distribution of PO_3. For example, if the distribution of P^* is estimated to be something other than log-normal, then the PO_3

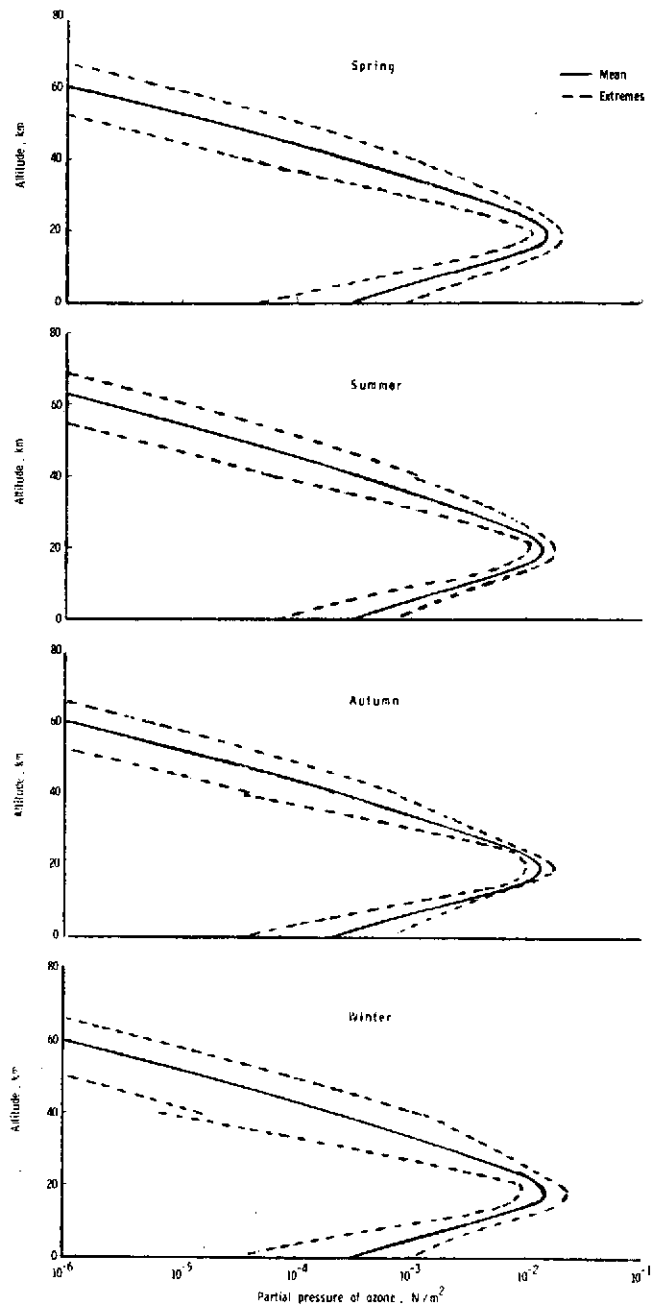

Figure 4.5 - Mean and extreme PO_3 profiles based on sample of 600 model-generated PO_3 profiles.

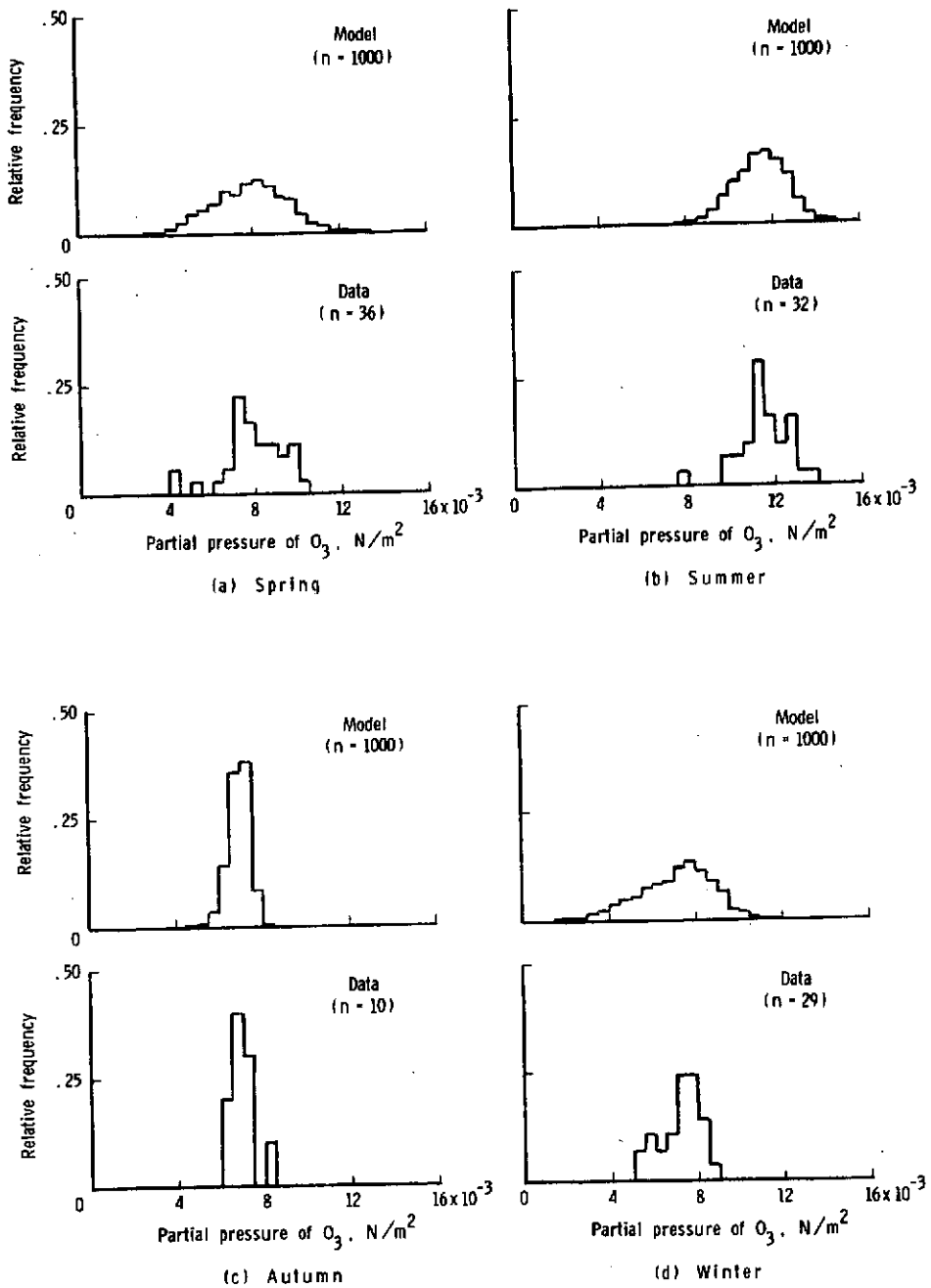

Figure 4.6 - Comparison of model and data histograms of PO_3 at a pressure height of 1000 N/m^2.

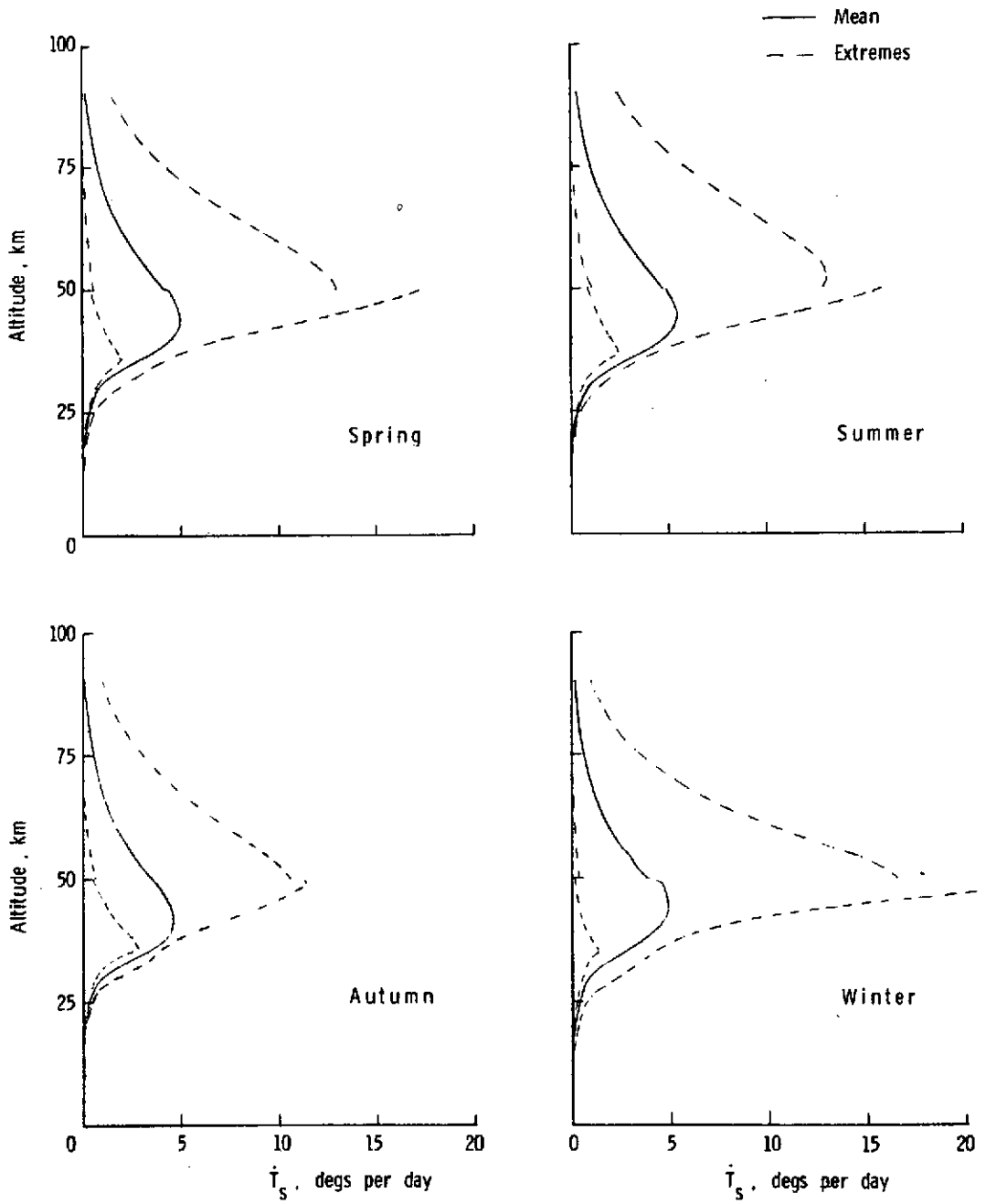

Figure 4.7 - Mean and extreme $\dot{T}_s$ profiles based on sample of 600 model-generated $\dot{T}_s$ profiles.

Table 4.3 - Means and Coefficients of Variation $\dot{T}_s$ at discrete altitudes

	Spring		Summer		Autumn		Winter			Spring		Summer		Autumn		Winter	
Altitude, km	Mean o/day	CV,%	Mean o/day	CV,%	Mean o/day	CV,%	Mean o/day	CV,%	Altitude, km	Mean o/day	CV,%	Mean o/day	CV,%	Mean o/day	CV,%	Mean o/day	CV,%
0	.000	48.038	.000	39.850	.000	48.359	.000	58.489	46	4.770	47.259	5.338	37.431	4.219	38.740	4.806	64.968
									47	4.649	50.571	5.256	40.394	4.069	41.822	4.744	70.067
1	.000	46.546	.000	38.515	.000	46.390	.000	55.959	48	4.511	53.754	5.147	43.229	3.910	44.793	4.666	75.139
2	.000	45.045	.000	37.156	.000	44.384	.000	53.421	49	4.361	56.830	5.019	45.957	3.746	47.677	4.574	80.208
3	.000	43.533	.000	35.780	.000	42.336	.000	50.880	50	3.940	52.963	4.683	42.806	3.447	45.886	3.756	71.653
4	.001	42.008	.001	34.388	.000	40.236	.001	48.282									
5	.001	40.469	.001	32.982	.001	38.079	.001	45.631	51	3.741	54.393	4.493	44.326	3.250	47.160	3.552	73.338
									52	3.543	55.696	4.299	45.742	3.059	48.355	3.348	74.799
6	.001	38.917	.001	31.562	.001	35.862	.001	42.970	53	3.348	56.896	4.103	47.073	2.873	49.489	3.148	76.069
7	.002	37.350	.001	30.127	.001	33.577	.002	40.286	54	3.157	58.009	3.907	48.335	2.693	50.574	2.953	77.177
8	.002	35.768	.002	28.675	.002	31.213	.002	37.592	55	2.972	59.051	3.713	49.538	2.521	51.622	2.764	78.145
9	.003	34.170	.003	27.210	.002	28.765	.003	34.906									
10	.005	32.559	.004	25.735	.003	26.227	.005	32.254	56	2.792	60.034	3.522	50.692	2.356	52.639	2.582	78.995
									57	2.620	60.969	3.336	51.807	2.200	53.634	2.408	79.745
11	.007	30.935	.006	24.258	.005	23.595	.007	29.678	58	2.455	61.866	3.156	52.890	2.051	54.613	2.243	80.413
12	.010	29.297	.008	22.785	.007	20.866	.010	27.236	59	2.298	62.733	2.981	53.949	1.911	55.582	2.086	81.012
13	.014	27.653	.011	21.330	.010	18.057	.014	25.029	60	2.129	63.578	2.813	54.991	1.778	56.547	1.938	81.555
14	.020	26.006	.016	19.906	.015	15.201	.020	23.163									
15	.029	24.350	.024	18.528	.021	12.347	.029	21.720	61	2.007	64.411	2.651	56.026	1.653	57.514	1.798	82.053
									62	1.871	65.238	2.495	57.060	1.535	58.491	1.666	82.517
16	.041	22.689	.034	17.233	.031	9.625	.042	20.745	63	1.743	66.064	2.346	58.099	1.423	59.479	1.541	82.954
17	.058	21.027	.048	16.056	.045	7.307	.060	20.213	64	1.622	66.893	2.202	59.146	1.318	60.482	1.425	83.370
18	.082	19.356	.067	14.995	.064	5.883	.084	19.998	65	1.507	67.730	2.065	60.206	1.219	61.503	1.315	83.770
19	.111	17.678	.092	14.031	.090	5.867	.116	19.893									
20	.148	16.002	.123	13.137	.122	6.987	.155	19.666	66	1.399	68.578	1.934	61.281	1.127	62.545	1.212	84.160
									67	1.297	69.441	1.810	62.375	1.040	63.610	1.115	84.542
21	.192	14.368	.161	12.286	.162	8.482	.201	19.145	68	1.201	70.320	1.691	63.492	.959	64.700	1.027	84.922
22	.241	12.861	.204	11.467	.208	9.834	.252	18.278	69	1.111	71.219	1.578	64.634	.883	65.818	.943	85.301
23	.295	11.611	.253	10.691	.260	10.777	.307	17.169	70	1.027	72.140	1.472	65.803	.812	66.966	.866	85.882
24	.351	10.726	.306	10.001	.316	11.205	.364	16.121									
25	.410	10.222	.362	9.447	.374	11.190	.425	15.604	71	.948	73.086	1.370	67.004	.746	68.146	.793	86.068
									72	.874	74.058	1.275	68.237	.685	69.360	.726	86.460
26	.475	10.254	.421	9.104	.438	11.094	.497	17.807	73	.804	75.059	1.184	69.507	.628	70.609	.664	86.860
27	.553	11.765	.488	9.318	.516	11.681	.592	22.441	74	.740	76.090	1.099	70.815	.575	71.896	.606	87.269
28	.660	15.552	.574	10.972	.625	13.756	.726	28.473	75	.679	77.155	1.018	72.164	.525	73.223	.553	87.690
29	.812	20.244	.692	14.380	.790	16.980	.913	32.753									
30	1.028	23.568	.863	18.175	1.033	19.715	1.165	33.801	76	.623	78.254	.942	73.557	.479	74.592	.504	88.122
									77	.571	79.389	.871	74.995	.437	76.004	.458	88.567
31	1.319	24.298	1.103	20.610	1.565	20.585	1.479	31.538	78	.522	80.563	.804	76.483	.398	77.462	.416	89.027
32	1.684	22.547	1.423	20.837	1.779	19.339	1.847	27.862	79	.477	81.778	.741	78.023	.362	78.969	.378	89.501
33	2.110	19.145	1.818	19.078	2.248	16.494	2.250	23.017	80	.435	83.035	.682	79.617	.328	80.525	.342	89.992
34	2.574	15.129	2.275	16.020	2.736	12.759	2.668	18.482									
35	3.046	11.704	2.767	12.487	3.207	8.869	3.080	15.624	81	.396	84.332	.637	81.269	.298	82.129	.310	90.498
									82	.360	85.665	.575	82.983	.270	83.775	.280	91.010
36	3.499	10.417	3.267	9.462	3.630	5.992	3.487	15.879	83	.328	87.029	.427	84.744	.244	85.455	.254	91.554
37	3.908	12.060	3.747	8.321	3.984	6.270	3.815	18.510	84	.298	88.416	.483	86.537	.221	87.163	.230	92.067
38	4.256	15.553	4.182	9.820	4.259	9.342	4.116	22.923	85	.272	89.927	.443	88.358	.200	88.897	.208	92.611
39	4.535	19.726	4.557	12.929	4.454	13.239	4.363	28.010									
40	4.741	24.047	4.863	16.594	4.572	17.259	4.557	33.337	86	.247	91.261	.406	90.207	.181	90.656	.188	93.164
									87	.225	92.718	.373	92.084	.164	92.442	.170	93.727
41	4.878	28.309	5.096	20.354	4.622	21.206	4.699	38.717	88	.205	94.199	.342	93.990	.149	94.253	.154	94.300
42	4.950	32.433	5.258	24.068	4.616	25.018	4.794	44.074	89	.187	95.702	.314	95.924	.135	96.091	.140	94.883
43	4.967	36.392	5.356	27.641	4.582	28.675	4.847	49.381	90	.170	97.224	.288	97.887	.123	97.949	.127	95.473
44	4.937	40.179	5.396	31.061	4.473	32.176	4.663	54.830									
45	4.869	43.798	5.387	34.323	4.358	35.528	4.847	59.824									

distribution, and, consequently, the temperature distribution, would be changed. This approach could be a fruitful area for additional investigation when more data are available.

V. COMPARISON OF THE MODEL WITH DATA

The MRN data tape

In order to estimate the various statistical parameters of the temperature distribution at each altitude as required in the temperature model, a computer tape containing experimentally measured temperature profiles was obtained from the Aero-Astrodynamics Laboratory at the NASA Marshall Space Flight Center. The tape consists of 442 sounding-rocket measurements of atmospheric temperature, pressure and density made at altitudes above 35 km by 25 Meteorological Rocket Network stations in different parts of the world. Of the 25 stations, seven are in the 30° latitude band, but only five of these had temperature profiles. (A number of stations reported only density or pressure profiles.) These five stations and their longitudes are listed in Table 5.1. The columns under the heading "number of useable profiles" give the total number of independent daylight profiles at each site in the season indicated. In order to have even the small numbers listed here, "daylight" was defined as being between 5 a.m. and 7 p.m. If, for example, the winter daylight hours were redefined to be between 7 a.m. and 5 p.m., six of the 20 winter measurements would have been disqualified.

In several instances two or more firings from a single station were made on the same day, sometimes only minutes apart. Since measurements cannot be considered independent in such circumstances, all temperature profiles made on the same day, at the same site, were first averaged to give a single profile which was then counted as a part of the sample of

Table 5.1 - Meteorological Rocket Network Stations in 30° Latitude Band

Site	Latitude	Longitude	Number of Useable Profiles			
			Spring	Summer	Autumn	Winter
Holloman AFB, New Mexico	32.85° N	106.10° N	1	0	1	2
Eglin AFB, F Florida	30.38° N	86.70° W	6	5	10	4
Point Mugu, California	34.12° N	119.12° W	0	0	0	1
Woomera, Australia	31.11° S	136.97° E	2	0	5	9
Carnarvon, Australia	24.82° S	113.87° E	0	0	0	4
TOTALS			9	5	16	20

independent profiles.

Each profile consisted of a set of measurements made at one-kilometer intervals, but the range of altitudes covered varied from one profile to the next. Consequently, the number of observations at each altitude level varied as shown in Table 5.2.

In addition to their use in estimating statistical parameters of the temperature distribution, the MRN data were used for comparison with model-generated temperatures, pressures and densities in an effort to evaluate the model. For each of the four seasons in the 30° latitude band, a sample of 500 pseudo-random atmospheres was generated (i.e., 500 consistent sets of temperature, density and pressure profiles). The means and standard deviations of each property were computed at one-kilometer altitude intervals between 0 and 90 km. In addition, histograms of temperatures were constructed at various altitudes, and interlayer correlations among temperatures were computed. These model characteristics were then compared with corresponding characteristics of the MRN data.

Comparison of model temperatures with data

In order to compare trajectories computed using the present model with those based on the 1966 Standard Atmosphere Supplements, [2], it was decided to use temperatures prescribed by the latter as mean temperatures in the model. That is, the mean temperature at altitude z, for a particular season and latitude band, is defined as

Table 5.2 - Number of MRN measurements at each altitude, $36 \leq z \leq 90$

Altitude	Spring	Summer	Autumn	Winter	Altitude	Spring	Summer	Autumn	Winter
36	0	0	0	2	64	9	5	10	15
37	0	0	0	2	65	9	4	9	15
38	0	0	0	3					
39	1	0	1	4	66	9	4	9	14
40	4	0	3	6	67	7	3	10	14
					68	7	2	8	13
41	4	1	4	6	69	5	1	8	12
42	6	2	6	9	70	5	0	7	11
43	8	2	9	12					
44	8	2	10	13	71	5	0	6	11
45	8	3	10	15	72	4	0	6	12
					73	3	0	6	12
46	8	3	13	15	74	3	0	6	12
47	8	4	13	15	75	2	0	6	12
48	9	4	13	15					
49	9	4	13	17	76	2	0	6	12
50	9	4	13	17	77	2	0	6	12
					78	2	0	6	12
51	9	5	13	17	79	2	0	6	12
52	9	5	13	17	80	2	0	6	11
53	9	5	13	17					
54	9	5	13	18	81	2	0	6	11
55	9	5	13	17	82	2	0	6	11
					83	2	0	6	10
56	9	5	13	17	84	2	0	6	9
57	9	5	13	17	85	2	0	6	9
58	9	5	13	18					
59	9	5	13	18	86	2	0	6	9
60	9	5	13	18	87	2	0	6	9
					88	2	0	6	9
61	9	5	12	17	89	2	0	6	7
62	9	5	12	17	90	2	0	5	7
63	9	5	11	15					

$$\mu_T(z) = T_{66}\ (z;\ \text{season, latitude}) \qquad (5.1)$$

where $T_{66}\ (z;\ \text{season, latitude})$ is the temperature at altitude z given by the 1966 Standard Atmosphere Supplements, [2], for the season and latitude indicated. For the 30°, 60°, and 75° latitude bands, reference [2] provides only summer and winter models. In these cases, the spring/fall temperature profile is defined as the average of summer and winter profiles.

Figure 5.1 compares model temperature means (solid curve) with the means of temperatures in the MRN data sample (circles). Ninety-five percent confidence intervals are drawn for each data point. The dashed curve on each plot is the temperature profile from the 1962 Standard Atmosphere, [1], drawn here as a fixed reference to aid in comparing the four seasonal means. Seasonal variations are not as pronounced in the 30° latitude band as they are in more northern latitudes.

The standard deviation of temperature at each altitude was estimated from the MRN data. As one might suspect from Figure 5.2, the amount of variation in the data estimates of $\sigma_T(z)$ (circles) over the altitude range is within the amount expected for such small samples if one were sampling from populations with the same standard deviation. In other words, there is no significant difference between the standard deviations of temperatures at different altitudes in the MRN data. Therefore, it was assumed that, for a particular season-latitude model, the standard deviation of temperature is the same at all altitudes. Its value was

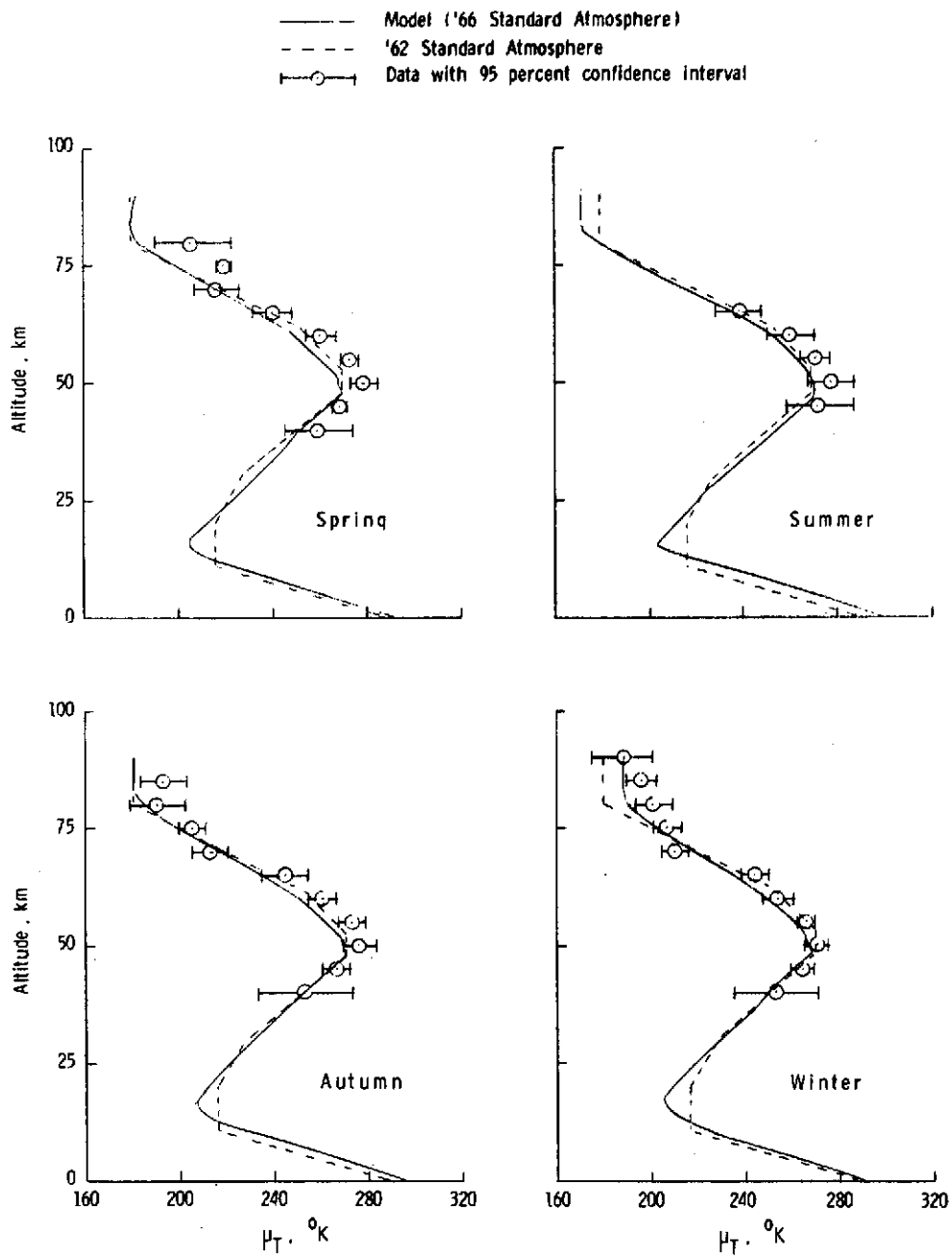

Figure 5.1 - Comparison of mean temperature profiles from model with mean temperatures in MRN data.

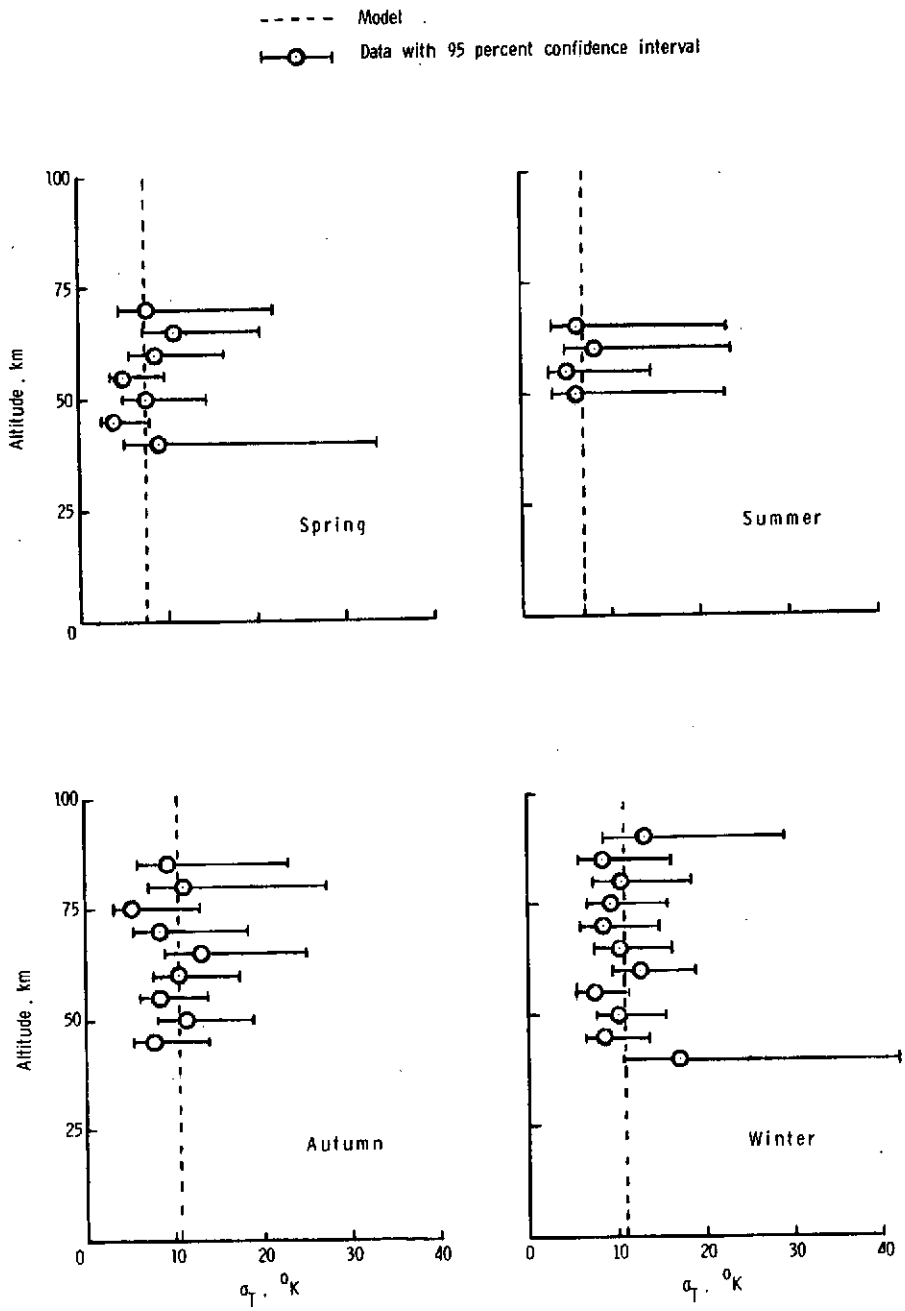

Figure 5.2 - Comparison of model standard deviations of temperature with MRN data standard deviations of temperature.

estimated by s_p, the usual pooled estimate of a standard deviation, given by

$$s_p = \left[\frac{\sum_i (n_i - 1)\, s_i^2}{\sum_i (n_i - 1)} \right]^{\frac{1}{2}} \qquad (5.2)$$

where n_i is the number of data points at altitude z_i (see Table 5.2); s_i is the standard deviation of sample temperatures at altitude z_i based on the MRN data, and the summation is only over i's where $n_i \neq 0$. The four values of s_p used in the 30° latitude model (dashed lines on Figure 5.2) are $s_p(\text{spring}) = 7.45°$ K, $s_p(\text{summer}) = 6.82°$ K, $s_p(\text{autumn}) = 10.44°$ K, and $s_p(\text{winter}) = 10.89°$ K.

Figures 5.3 - 5.6 show histograms of model-generated temperatures at 10-km altitude intervals between 40 and 90 km. Each histogram represents a sample of 500 temperatures, and within each histogram class or subdivision, the circles represent data points lying in that interval.

Perhaps the most important feature of the current temperature model - that which distinguishes it from any other model - is its inter-layer correlation structure (i.e., the correlations between temperatures at different altitudes). This correlation structure is linked directly to the behavior of the heating-rate profile $\dot{T}_s(z)$ as affected by the ozone variation. Letting $r_T(z_1, z_2)$ be the coefficient of correlation between $T(z_1)$ and $T(z_2)$, then in the present model

$$r_T(z_1, z_2) = \lambda^2\, r_s(z_1, z_2) \qquad (5.3)$$

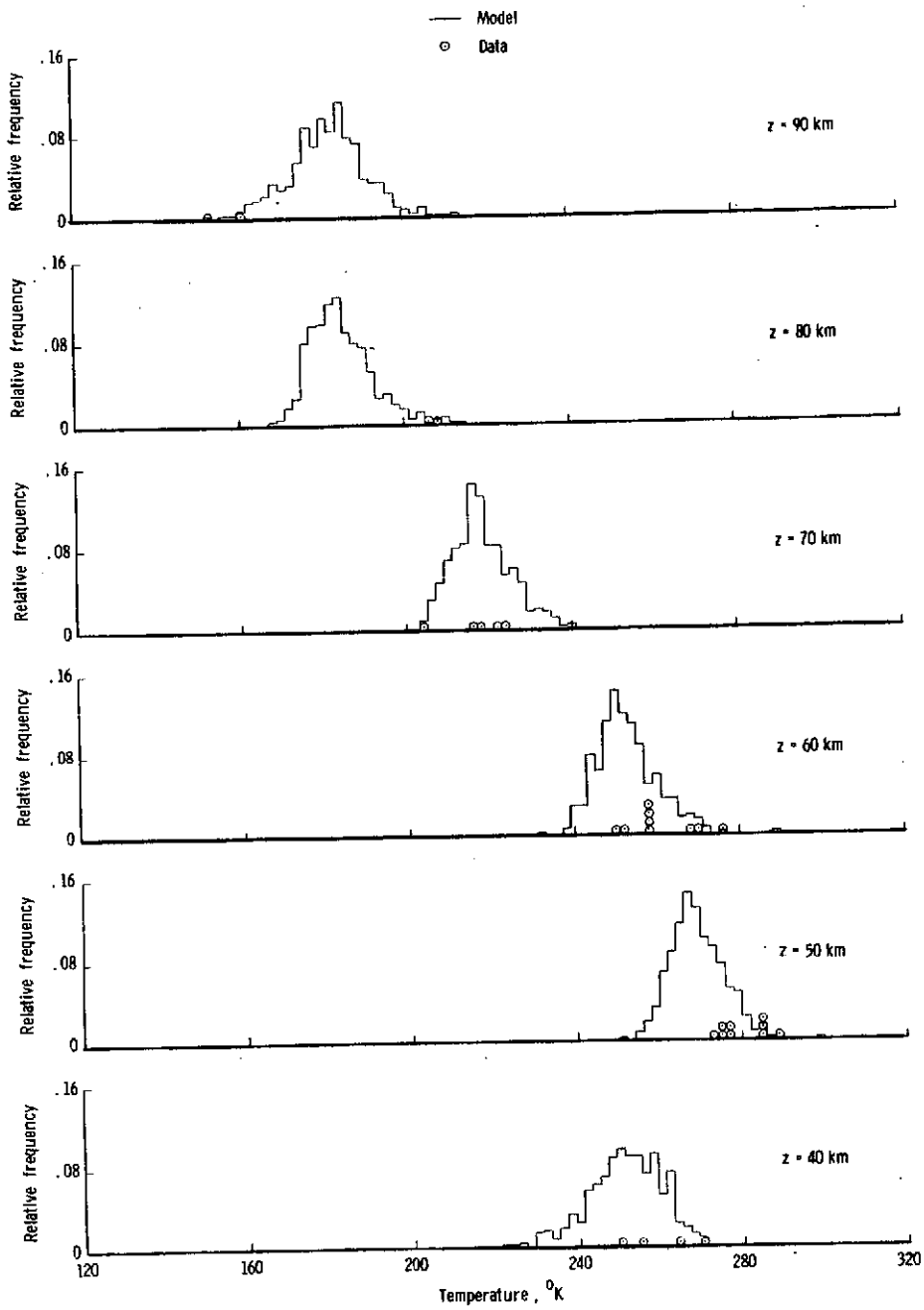

Figure 5.3 - Distribution of spring temperatures in model and data at discrete altitude levels between 40 and 90 km.

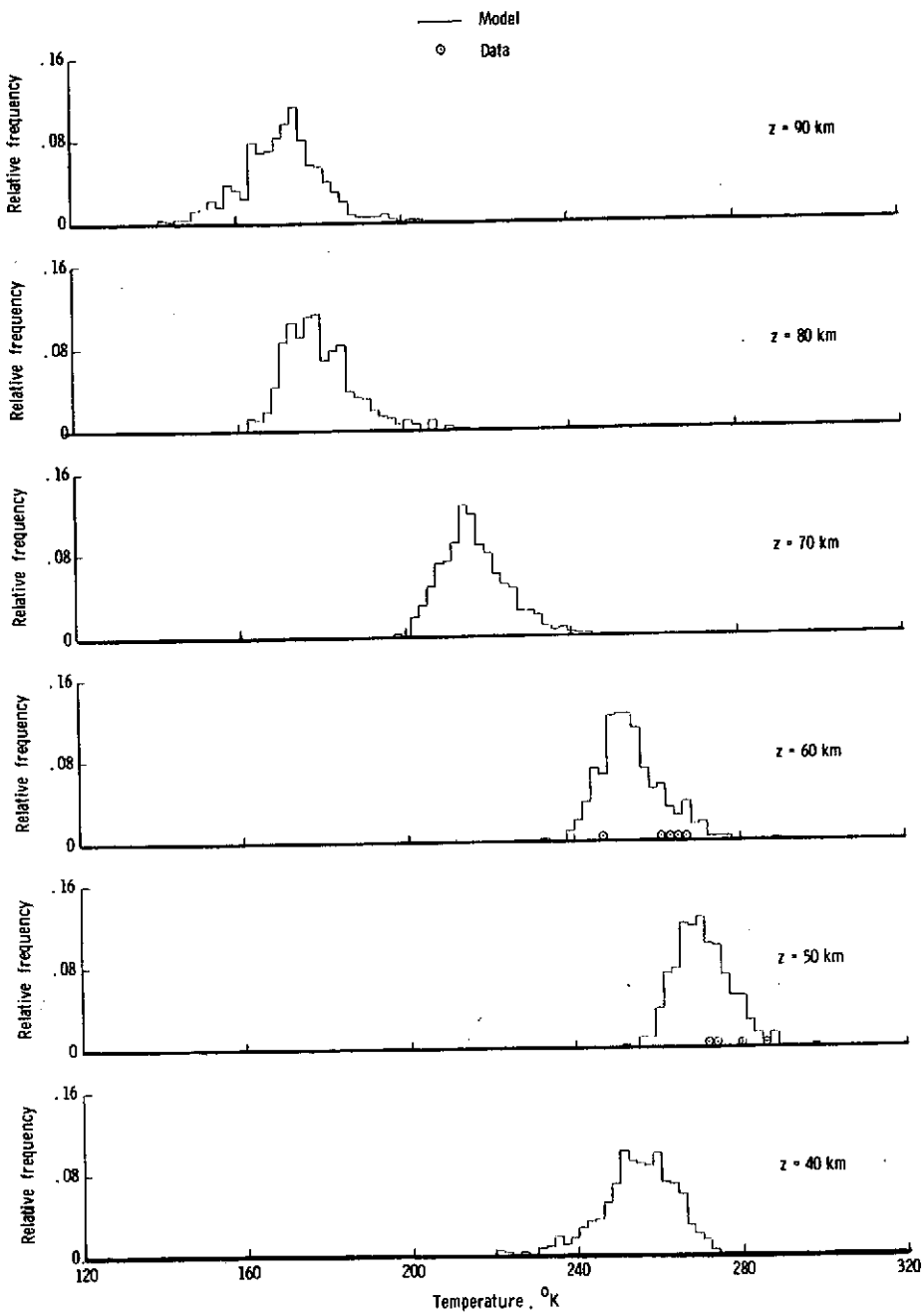

Figure 5.4 - Distribution of summer temperatures in model and data at discrete altitude levels between 40 and 90 km.

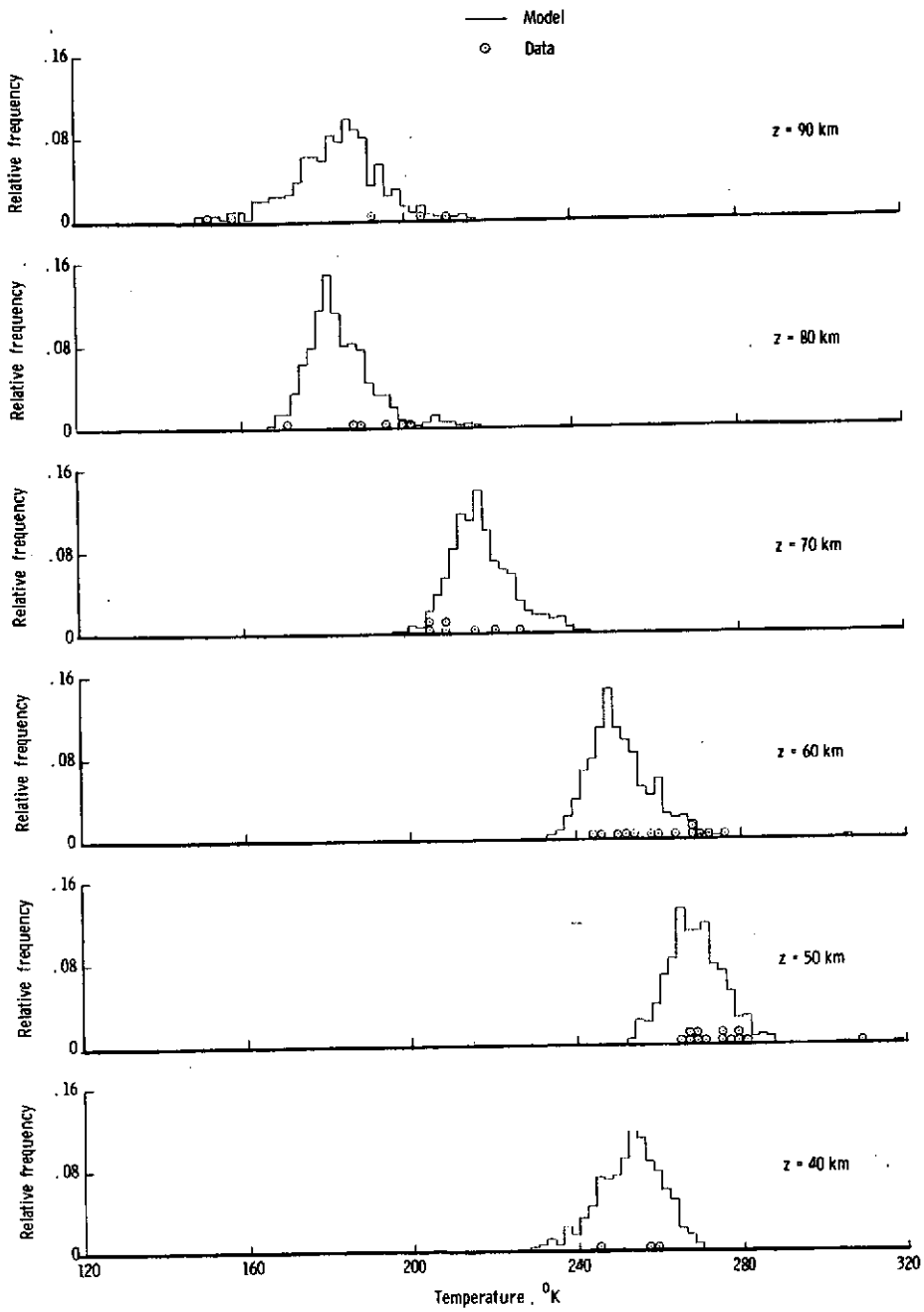

Figure 5.5 - Distribution of autumn temperatures in model and data at discrete altitude levels between 40 and 90 km.

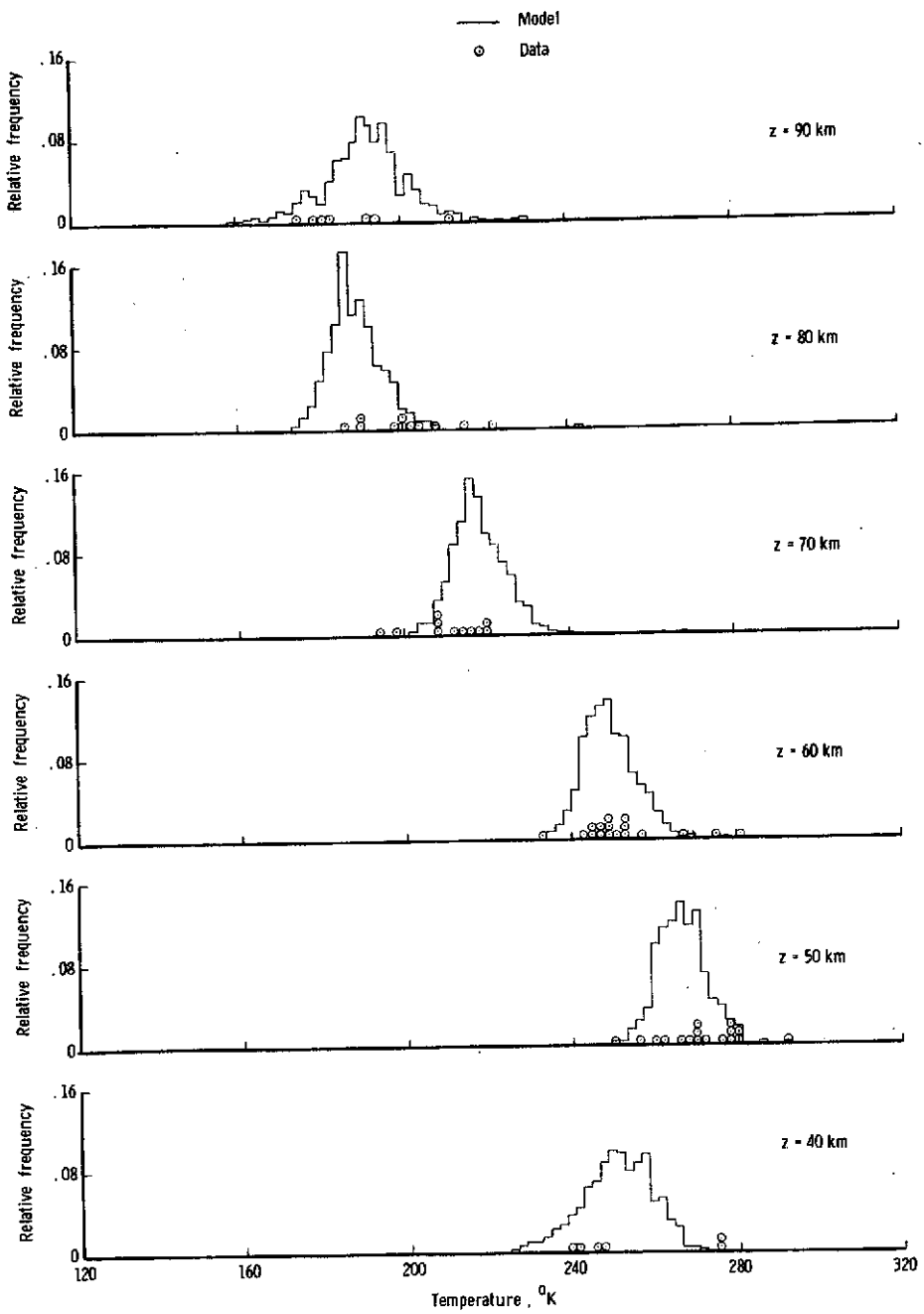

Figure 5.6 - Distribution of winter temperatures in model and data at discrete altitude levels between 40 and 90 km.

where $r_s(z_1, z_2)$ is the correlation between heating rates $\dot{T}_s(z_1)$ and $\dot{T}_s(z_2)$, and λ is the correlation between $T(z)$ and $\dot{T}_s(z)$, (see equation (3.7)). As atmospheric ozone varies according to its distribution, the $\dot{T}_s$ profile follows a distinct pattern. The segment of the $\dot{T}_s$ curve above its maximum at ~50 km altitude, (see Figure 4.7), shifts to the right and left in such a manner that it produces either a simultaneous increase or a simultaneous decrease in all $\dot{T}_s$ values above 50 km. Thus, if z_1 and z_2 are both greater than 50 km, $r_s(z_1, z_2)$ is approximately equal to +1, and hence $r_T(z_1, z_2)$ is approximately equal to λ^2.

The solid curves in Figure 5.7 are plots based on the winter model, of $r_T(z_1, z_2)$ versus z_2 for nine values of z_1 between 35 and 90 km. The winter model was chosen for comparison purposes because there are more MRN data for this season; plots of $r_T(z_1, z_2)$ for the other three seasons are quite similar. In the plots for z_1 = 60, 70, and 80 km, note that $r_T(z_1, z_2)$, $50 < z_2 < 90$, is approximately equal to $\lambda^2 = .81$.

Below the stratopause, ~50 km, the behavior of $\dot{T}_s$ is more irregular. In the upper stratosphere (40 - 50 km), $\dot{T}_s$ values are virtually uncorrelated to those above 50 km but have a strong negative correlation with heating rates in the lower stratosphere (20 - 30 km). This structure is reflected in the temperature correlations for z_1 = 40 and 45 km in Figure 5.7.

The data symbols (circles) in Figure 5.7 are estimates of $r_T(z_1, z_2)$ based on the MRN data. The solid circles are those whose 95 percent

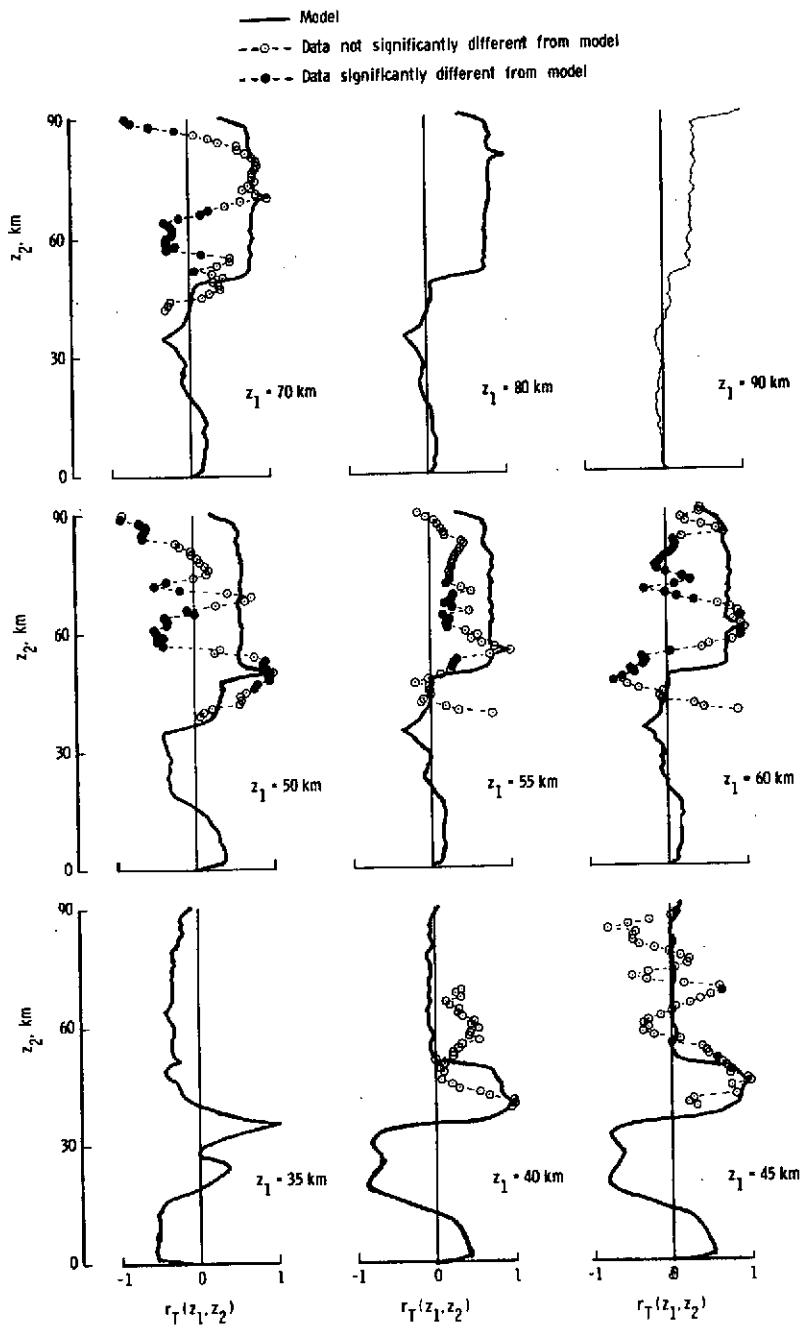

Figure 5.7 - Comparison of model and data interlayer temperature correlations.

confidence intervals do not cover the model value of $r_T(z_1, z_2)$. Because of the small sample sizes involved, it is difficult to make meaningful statements about the true nature of $r_T(z_1, z_2)$ based on the data; nevertheless, there is reason for disappointment in the poor agreement seen in Figure 5.7. In contradicting the model, these data estimates of $r_T(z_1, z_2)$ tend to imply that there is no strong linear correlation between T and $\dot{T}_s$. One possible explanation for this is that 10 of the 20 MRN profiles used to estimate $r_T(z_1, z_2)$ were measured either before 9 a.m. or after 4 p.m., times of day when the heating effects of the sun (particularly in winter) are not as pronounced as they are nearer to midday. Furthermore, the data represent varying sun zenith angles whereas the model-generated sample used a fixed zenith angle. Allowing this angle to vary in the model might produce a different statistical distribution for the $\dot{T}_s$ profile, thus affecting the distribution of temperatures. For these reasons, the comparison of model with data in Figure 5.7 is believed to be inconclusive. More data will be necessary in order to either validate or invalidate the model.

The value of $\lambda = .9$ used in this model determines the location of the model $r_T(z_1, z_2)$ curves at points where z_1 and z_2 are between 50 and 90 km. A smaller value of λ, say $\lambda = .7$, gives better agreement with data points (circles) to the left of the curve where $r_T(z_1, z_2) \approx \lambda^2$, but it also results in significant differences between model and data at virtually all points where $|z_1 - z_2|$ is small.

Comparisons of model densities and pressures with data

As explained in Chapter III, the natural logarithm of atmospheric pressure, log(P) , is the independent variable used as a vertical scale in the model. The reason for this is that the ozone model gives the partial pressure of ozone as a function of log(P) , and , hence, the solar heating rate profiles are based on this scale.

To be more exact, the vertical scale used in the model is

$$U \equiv \log(P/P_o) \tag{5.4}$$

where P_o is sea-level pressure. A set of fixed U values $\{U_0, U_1, \ldots, U_{90}\}$ is defined by

$$U_i = \log(P_{66}(z_i)/P_{66}(z_o)) \tag{5.5}$$

where $P_{66}(z_i)$ is the pressure at altitude z_i , (z_i = 0, 1,..., 90 km), as defined by the 1966 Standard Atmosphere Supplements, [2], for the appropriate season and latitude. Then at each U_i a pseudo-random temperature is given by

$$T(U_i) = \mu_T(U_i) + \lambda\sigma_T(U_i) \frac{[T_s(U_i) - \mu_s(U_i)]}{\sigma_s(U_i)} + \varepsilon(U_i) \tag{5.6}$$

where $\mu_T(U_i)$ is the mean temperature at U_i defined by

$$\mu_T(U_i) = T_{66}(z_i) \tag{5.7}$$

and $\sigma_T(U_i) = \sigma_T$ is a constant estimated from the MRN data, as explained

above.

From the $T(U_i)$ profile, one can then compute the geometric altitude $z(U_i)$ as

$$z(U_i) = \frac{\int_{U_i}^{0} T(u)\, du}{\left[\frac{Mg_o}{K} - \frac{1}{R_o}\int_{U_i}^{0} T(u)\, du\right]} \tag{5.8}$$

where M, g_o, K, and R_o are constants. (See Appendix A for derivation of 5.8).

Next, using linear interpolation, the profile $\{T(U_i), z(U_i)\}$ is converted to $\{T(z_i), z_i\}$ where the z_i's are even altitude increments $\{0, 1, \ldots, 90 \text{ km}\}$.

Pressure and density profiles are then calculated for the even altitude increments as

$$P(z_i) = P_b \exp\left[-\int_{z_b}^{z_i} \frac{Mg}{KT}\, dz\right] \tag{5.9}$$

and

$$\rho(z_i) = \frac{M\, P(z_i)}{K\, T(z_i)},$$

where P_b and z_b in equation (5.9) are pressure and altitude, respectively, at some boundary point. It is customary to take $z_b = 0$ and, hence, P_b is sea-level pressure. However, since this is a statistical model, one must specify the statistical distribution of P_b at the boundary altitude z_b, and then sample a value of P_b from that

distribution. It was found that, provided the same mean was used for P_b, the variance and shape of the P_b distribution had negligible effects on the means of pressures and densities. These choices did, however, have a fairly sizable impact on the variances of pressure and density. The selection of z_b and its associated P_b distribution will be discussed in more detail shortly.

Figure 5.8 shows mean density profiles (solid curves) corresponding to the four 30° latitude models. The actual quantity plotted here is the percent departure from the 1962 Standard density $\rho_{62}(z)$ as defined by

$$\delta_\rho(z) = \left[\frac{\bar{\rho}(z) - \rho_{62}(z)}{\rho_{62}(z)}\right] \times 100\% \qquad (5.11)$$

where $\bar{\rho}(z)$ is the average of 500 pseudo-random density values generated by the model at altitude z. Since densities and pressures vary by about six orders of magnitude between sea level and 90 km, pressures and densities are customarily plotted as a percent departure from the 1962 Standard pressures and densities, thus avoiding the use of 6-cycle log paper.

The dashed lines on Figure 5.8 represent the 1966 Standard densities for the four seasons, the density profiles which correspond to the mean temperature profiles used in the model. As one can see, there is close agreement between the 1966 Standard and the model's mean densities. However, perfect agreement between the Standard density and the model's mean density should not be expected. Indeed, such agreement would be surprising, since, in general, if F is a function of a random variable

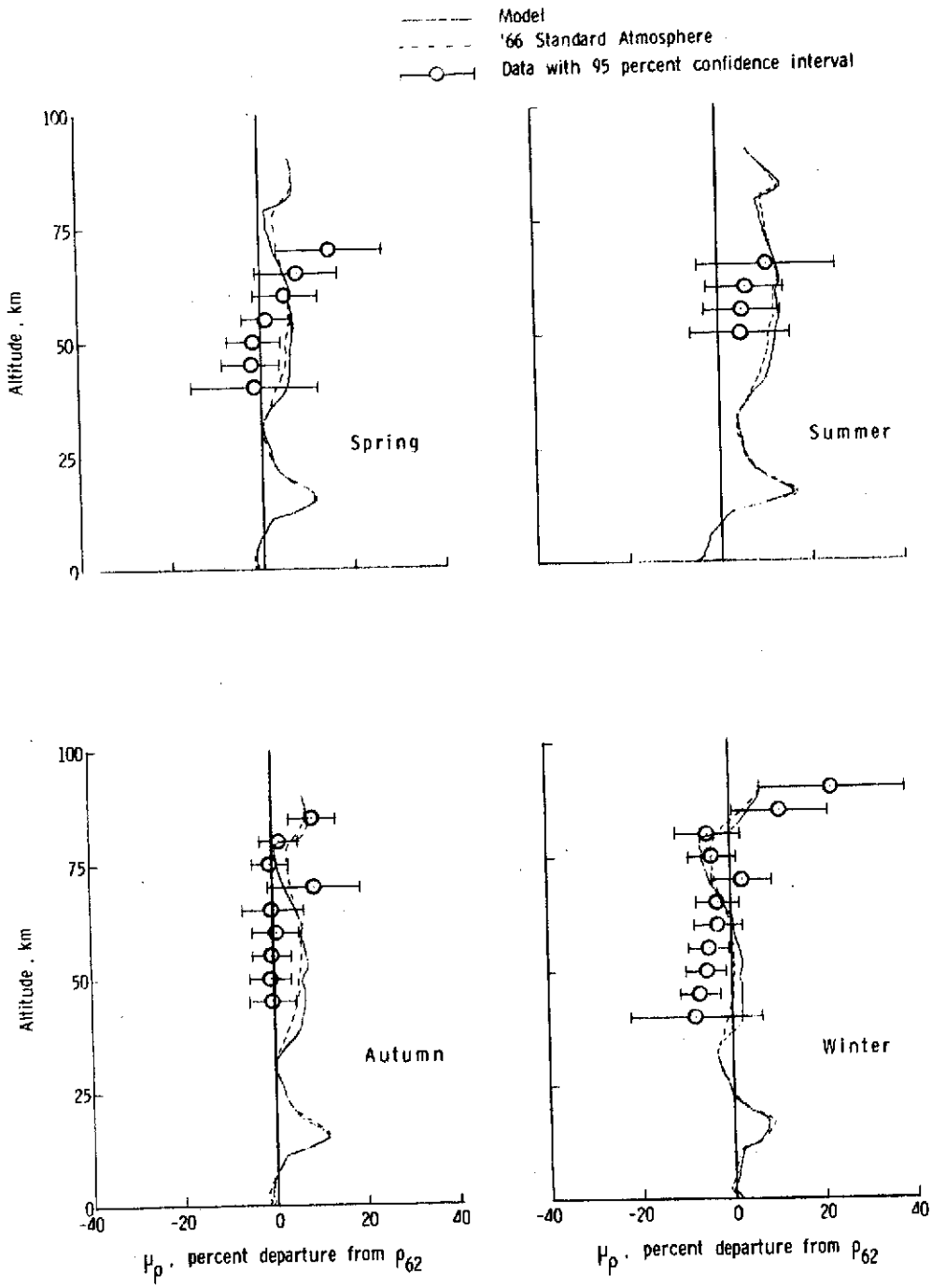

Figure 5.8 - Comparison of mean density profiles from model with mean densities in MRN data.

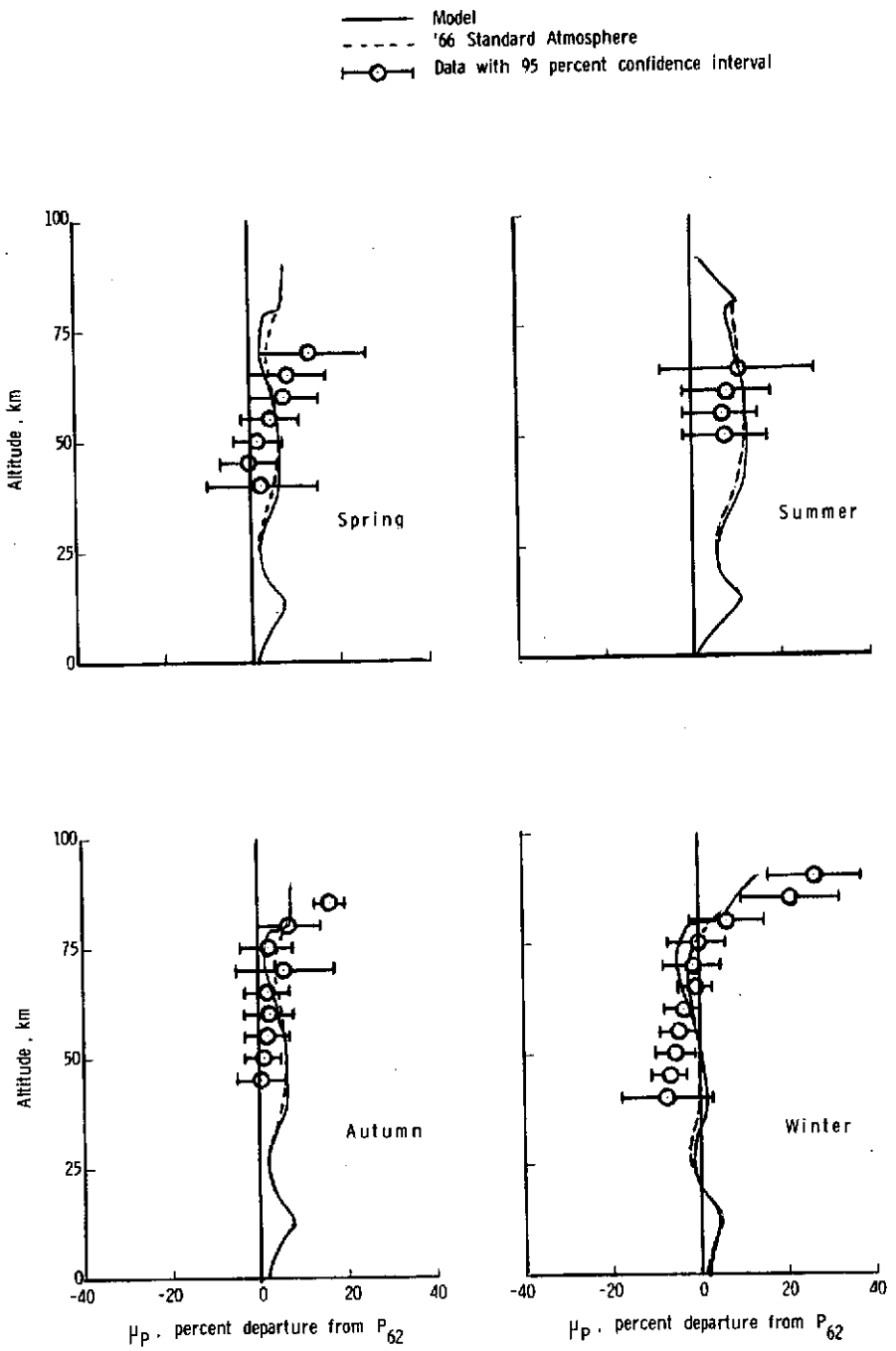

Figure 5.9 - Comparison of mean pressure profiles from model with mean pressures in MRN data.

X , the mean of which is μ_X , the mean of $F(X)$ is not necessarily equal to $F(\mu_X)$.

The data symbols (circles) on Figure 5.8 show the percent departures of the MRN density averages from the 1962 Standard density. Again 95 percent confidence intervals are drawn. At best one can say that the data averages and model averages exhibit the same seasonal trends. Figure 5.9, similar to Figure 5.8, is a comparison of the percent departures of pressure means from the 1962 Standard Pressure.

As stated earlier, the choice of the P_b distribution at the boundary point z_b has a significant impact on the variances of pressures and densities. Consequently, this choice could not be arbitrary, but had to be justifiable in terms of physical reality. Accordingly, it was decided to select as a boundary point an altitude where density variation is minimal. There are certain altitudes, called isopynic layers, [40], where atmospheric density is almost constant throughout the year. These isopynic layers lie at altitudes of approximately 8, 24, and 90 km. By taking z_b to be one of these altitudes and by letting ρ_b , atmospheric density at altitude z_b , be a constant, then the distribution of P_b is determined by the distribution of $T(z_b)$ since the equation of state gives

$$P_b = \frac{K \rho_b T(z_b)}{M} \tag{5.12}$$

Two boundary points, $z_b = 24$ km and $z_b = 90$ km , were used in the present model. When $z_i < 80$ km, in equation (5.9), the boundary

point $z_b = 24$ km is used, and when $z_i \geq 80$ km, $z_b = 90$ km is used. The selection of 80 km as a dividing point was made because at $z_i = 80$ km the variance of atmospheric density is the same using either $z_b = 24$ or $z_b = 90$ km.

Although it was only necessary to select one boundary point, the two were chosen here to force the existence of isopynic layers at those altitudes. The 8 km isopynic layer, on the other hand, has been omitted since it does not affect the 30 - 90 km region of primary interest. If the model were perfect, then isopynic layers would be created naturally at 8, 24, and 90 km even if only one of these is used as the boundary point. However, in the present model, the use of only one boundary point resulted in the disappearance of isopynic layers at non-boundary points.

In Figure 5.10 the ratio of the standard deviation of density to the 1962 Standard density is plotted for each season. The solid curves represent standard deviations calculated from samples of 500 model-generated density profiles. The data symbols are the corresponding standard deviations in the MRN samples, and 95 percent confidence intervals are drawn. Note the isopynic layers at $z = 24$ km and 90 km. The peak in standard deviations at 80 km is a result of using this altitude as a dividing point, as explained above, but the peak at around 30 km results solely from the way the temperatures vary and is not related to the integration boundaries.

Figure 5.11 is analogous to Figure 5.10 except that here standard deviations of pressure are plotted. The solid curves, representing the

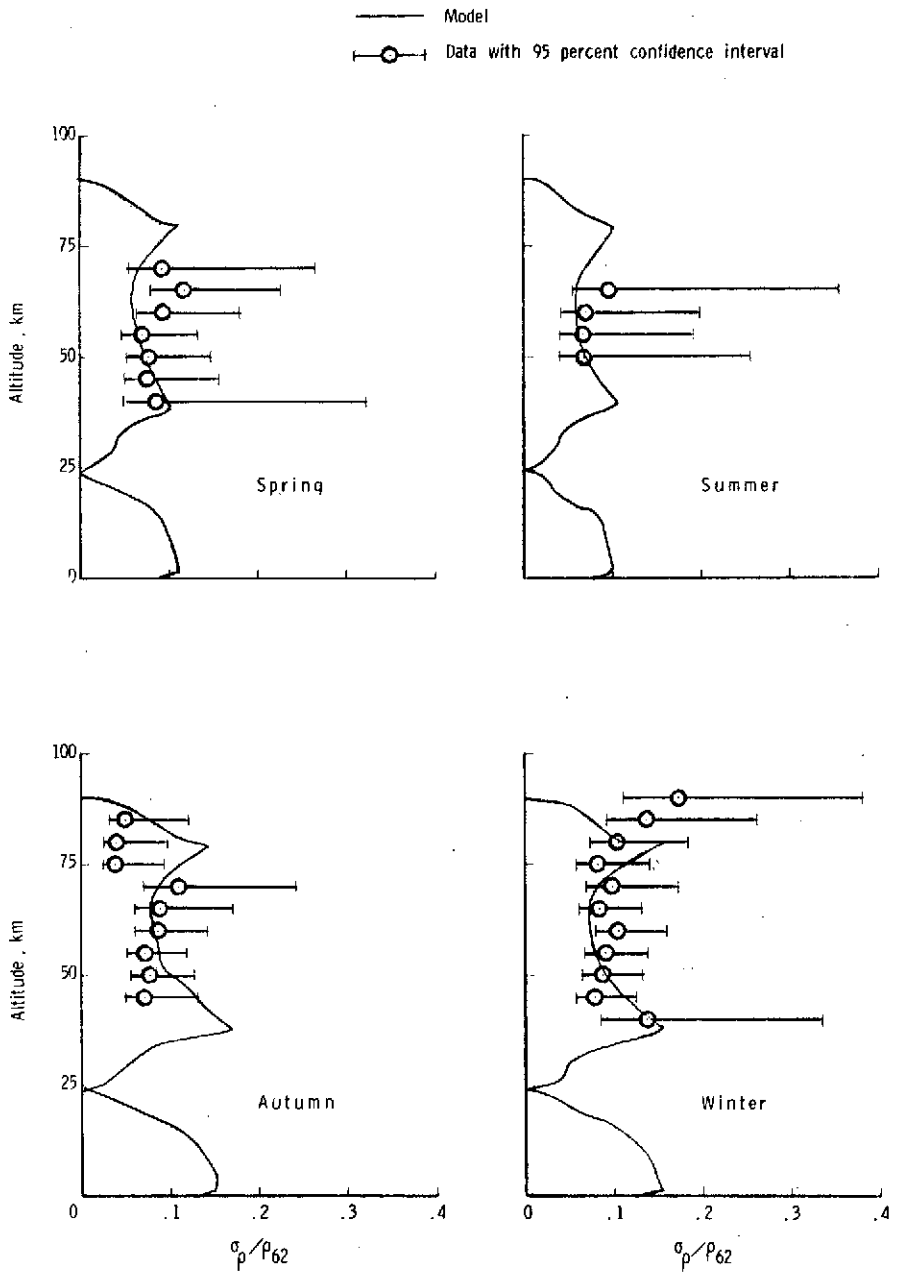

Figure 5.10 - Comparison of model standard deviations of density with MRN data standard deviations of density.

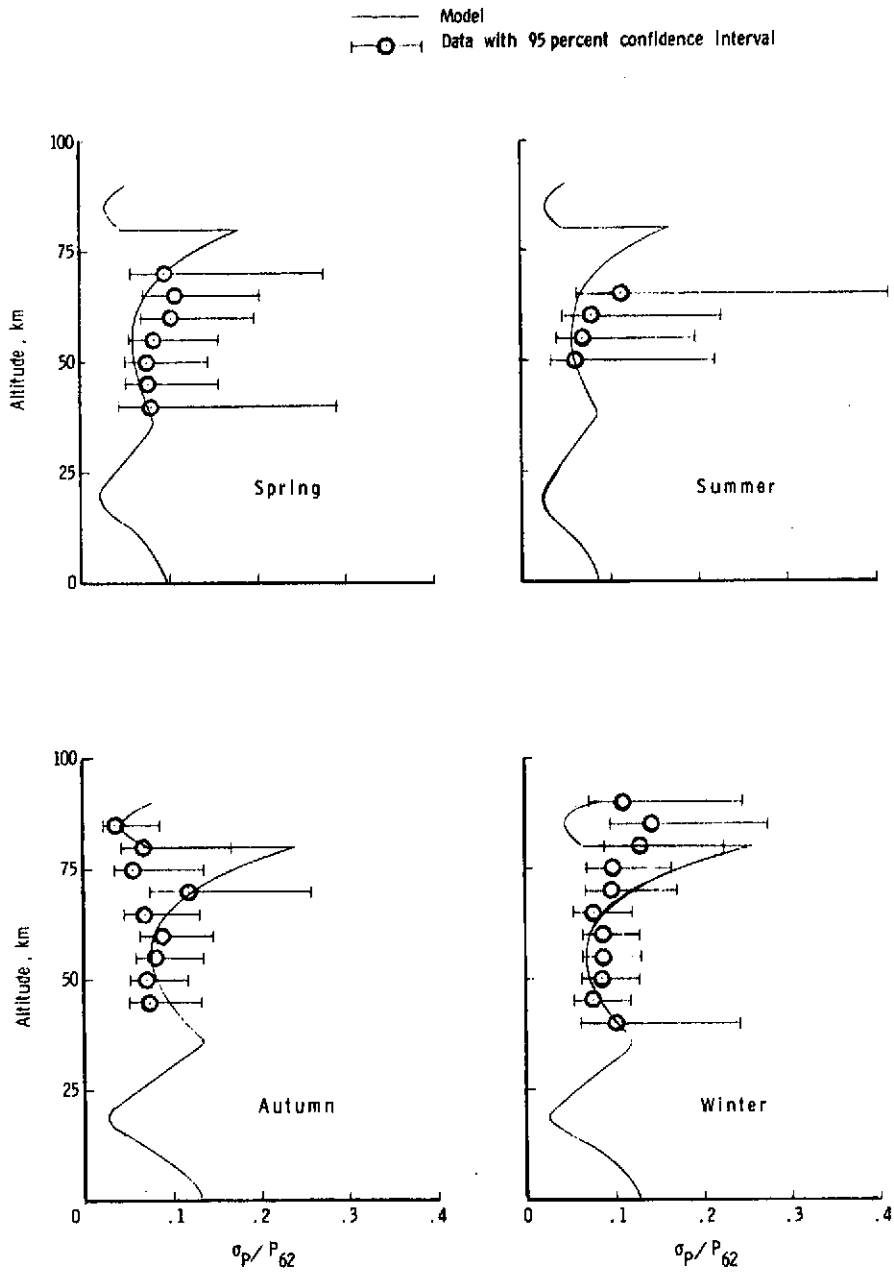

Figure 5.11 - Comparison of model standard deviations of pressure with MRN data standard deviations of pressure.

model standard deviations, resemble those on Figure 5.10. However, the minimum points appear to be approximately 5 km below the isopynic levels, and the peak at approximately 35 km is less pronounced. There is a discontinuity in the standard deviations of model pressures at 80 km, which is caused by the use of 80 km as an integration boundary.

Conclusions

In comparing the model with data, a distinction should be drawn between model characteristics which are estimated from the data and those which are not. Temperature means and standard deviations are examples of the former, whereas, the statistical properties of pressure and density are of the latter type.

Since temperature means and standard deviations are selected by the model user, the amount of disagreement between these and their counterparts in the data is a matter of choice. It was decided, for example, to use the 1966 Standard Atmosphere temperatures as model means instead of estimating means from the data. In the case of temperature standard deviations, a constant standard deviation was used for all altitudes, and this value was obtained by pooling standard deviations in the MRN data sample. Thus, any differences between model and data seen in Figures 5.1 and 5.2 do not constitute errors in the model.

The means of model pressures and densities agree well with their corresponding 1966 Standard Atmosphere values even though such agreement was not guaranteed a priori. As in the case of temperature, the data estimates of pressure and density means differ from the 1966

Standard and, therefore, cannot be expected to match model means.

The standard deviations of model pressures and densities, which ideally should agree with data about as well as do temperature standard deviations, instead show slightly poorer agreement. If the integration scheme could be modified so as to remove the artificial peak at 80 km, agreement between model and data standard deviations would be significantly improved.

The most serious discrepancy between model and data lies in the interlayer temperature correlations, $r_T(z_1, z_2)$. Although some of this error can perhaps be explained in terms of zenith-angle differences, it still may be necessary to alter the model. One possible solution would be to extract from the unmodeled error term a source of variation which correlates temperatures at adjacent altitudes. Winds would be such a source, for example. Thus, λ could be reduced and most model $r_T(z_1, z_2)$ values made smaller without decreasing the correlation between temperatures at adjacent altitudes.

Another possible method of improving the agreement between the data and model $r_T(z_1, z_2)$ values would be to allow λ to vary as a function of altitude. There is physical justification for this since λ, the correlation between temperature and the solar heating rate of ozone, is smaller at altitudes where there is absorption by other gases (e.g., water vapor) than where O_3 is the only absorber. Before attempting to improve the agreement between model and data, however, the data base should be enlarged so as to increase the confidence in estimates of $r_T(z_1, z_2)$.

VI. THE EFFECT OF ATMOSPHERIC VARIABILITY ON FIVE IMPORTANT SPACE SHUTTLE ENTRY PARAMETERS: AN APPLICATION OF THE MODEL

A Monte Carlo entry trajectory program was developed by modifying a rapid, three-dimensional point-mass entry program to use pseudo-random atmospheric density profiles instead of the 1962 U. S. Standard density profile, [1]. Large samples of entry trajectories were then generated, and the statistical behavior of five major performance indicators was studied.

The five entry parameters selected for study were:

(1) maximum dynamic pressure

(2) maximum stagnation-point heating rate

(3) maximum g-load

(4) final down-range distance

(5) final cross-range distance

The objective of the study was to analyze the statistical distributions of these five parameters and, thereby, determine "three-sigma" design values for each. The adjective "three-sigma" is used here to refer to a value which will be exceeded with a probability of .0013. If the statistical distribution of the parameter is normal (Gaussian), then this design value will, in fact, lie a distance of three standard deviations (three sigma's) away from the mean. In general, however, this .0013-probability design value is not three standard deviations from the mean, and hence, the quotation marks on "three-sigma".

A two-dimensional random density model

Instead of entering along a steep trajectory easily described by one atmospheric profile, the Space Shuttle will actually fly back from orbit along a shallow trajectory which takes it a distance of several thousand kilometers down range. (See Figure 6.1.) Thus, a stochastic atmosphere model used to simulate Shuttle entries should provide variation in atmospheric properties along horizontal flight paths; one random atmospheric profile per entry assigning a single set of properties at each altitude is not adequate.

In the present simulation the model described in the preceeding chapters was used to generate one pseudo-random atmospheric density profile at the location where entry began. Density profiles at locations down-range differ from this initial profile but are not completely uncorrelated. Therefore, at a location 110 km down range from the initial entry point, it would have been wrong to generate a new independent atmospheric density profile using the same model. Instead, the initial profile was perturbed slightly to give a new profile 110 km down range. An explanation will be given below as to how this was done and why the 110 km increment was used. At a point 220 km down range a new density profile was obtained by perturbing the previous profile, (i.e., the one at 110 km down range), and this was continued until a sequence of density profiles spaced 110 km apart was generated. The Shuttle orbiter was then flown through this array of densities, and the value of atmospheric density at any point along its trajectory was found by linear interpolation

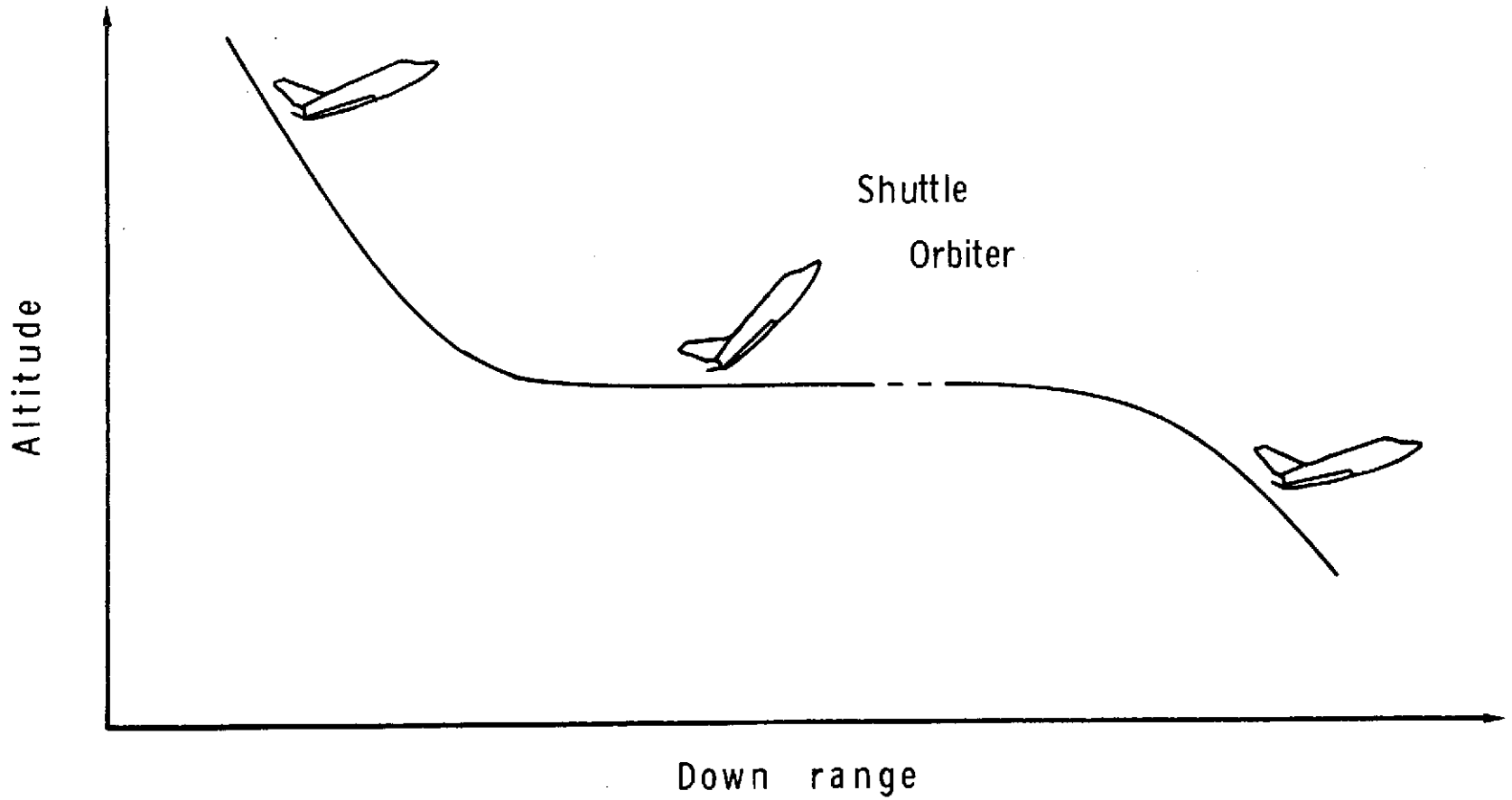

Figure 6.1 - Illustration of shallow entry path of Space Shuttle Orbiter.

between nearby density profiles.

Let $\rho_o(z)$ denote a pseudo-random value of atmospheric density at altitude z ($z = 0, 1, \ldots, 90$ km) generated by the stochastic atmosphere model described in the preceeding chapters. The profile $\{\rho_o(z): z = 0, \ldots, 90 \text{ km}\}$ is located at the point where down-range distance DR is 0. Let $\{\rho_1(z)\}$ be the density profile located where DR = 110 km, and in general, let $\{\rho_j(z)\}$ be located where DR = $j \times 110$ km. Then the density $\rho_{j+1}(z)$ was given by

$$\rho_{j+1}(z) = \rho_j(z) + \delta(z) \qquad j = 0, 1, 2, \ldots \tag{6.1}$$

where

$$\delta(z) \sim N(0, \sigma_\delta^2(z)) \tag{6.2}$$

The variance of $\delta(z)$, $\sigma_\delta^2(z)$, was based on a set of maximum horizontal density gradients given in reference [23]. This reference places an upper limit on the horizontal change in atmospheric density between two locations 110 km apart (hence the use of 110 km intervals). Since $\rho_j(z)$ and $\rho_{j+1}(z)$, as defined above, are two densities at altitude z located 110 km apart, then according to [23] the following must hold:

$$-\gamma(z)\rho_{62}(z) \leq \rho_{j+1}(z) - \rho_j(z) \leq \gamma(z)\rho_{62}(z) \tag{6.3}$$

where $\rho_{62}(z)$ is the 1962 Standard atmospheric density at altitude z, and $\gamma(z)$ is obtained by linear interpolation from Table 6.1.

In the present situation $\rho_{j+1}(z) - \rho_j(z) = \delta(z)$ is a normal

Table 6.1 - Design Horizontal Density Gradients

30° Latitude Band

Altitude	Spring/Autumn	Summer	Winter
0	0.35	0.20	0.50
30	0.35	0.20	0.50
40	0.70	0.30	1.10
50	0.95	0.40	1.50
60	1.25	0.50	2.00
70	1.40	0.60	2.20
80	1.25	0.50	2.00
90	0.20	0.10	0.30

If ρ_1 and ρ_2 are two values of density at the same altitude z but 110 km apart, then $|\rho_1 - \rho_2|$ must be less than $\gamma\rho_{62}$, where γ is interpolated from this table, and ρ_{62} is the 1962 Standard Atmosphere density at altitude z.

Table 6.2 - Shuttle Characteristics used in Simulations

Orbiter weight	=	870000 N (196000 lbs)
Reference area	=	268 m^2 (2890 ft^2)
Angle of attack	=	34 deg
Lift-to-drag ratio	=	1.25
Drag coefficient	=	0.572
Lift coefficient	=	0.457

random variable and, hence, does not have strict upper and lower limits as required by reference [23], equation (6.3). However, by chosing $\sigma_\delta(z)$ such that

$$\gamma(z)\rho_{62}(z) = 3\sigma_\delta(z) \tag{6.4}$$

the absolute limit in equation (6.3) was replaced by

$$\Pr\left[-\gamma(z)\rho_{62}(z) \leq \rho_{j+1}(z) - \rho_j(z) \leq \gamma(z)\rho_{62}(z)\right] = .997 \tag{6.5}$$

a probabilistic limit. The design horizontal density gradients of reference [23] then became "three-sigma" design values.

Procedure

The vehicle and aerodynamic characteristics used in this study (see Table 6.2) are based on the current Shuttle design, [41]. Four samples of 1000 pseudo-random entries were generated, each sample representing a different season in the 30° latitude band. Within each sample, the only difference between any two entry trajectories was their respective atmospheres. The five entry parameters listed above were recorded for each entry. Sample means and standard deviations were calculated; histograms were constructed, and empirical cumulative frequencies were plotted on normal probability paper. The first four moments of each parameter were used to fit a Pearson distribution, [42], to the empirical distributions (see Appendix D).

For comparison purposes, a number of different methods were used

to determine "three-sigma" design values. The methods used were the following:

Method A (Traditional Method). The parameter was assumed to have a normal distribution, and its design value was given by

$$\text{(A) design value} = \bar{X} \pm 3s \tag{6.6}$$

where $\bar{X}$ and s are the sample mean and sample standard deviation, respectively. A plus or minus sign was chosen depending on the nature of the parameter.

Method B (Probability Paper Method). Again, the parameter was assumed to have a normal distribution. However, by this method, a normal cumulative frequency curve $F(x)$ was fitted to the empirical cumulative frequencies, using probability paper, and the design value was the parameter value, x = (B) design value, satisfying $F(x) = .9987$ (or .0013 if it is a minimum).

Method C (Non-parametric Method). The "three-sigma" design value, as defined above, is a value which will be exceeded approximately once in a sample of size 1000. Letting x_n and x_{n-1} denote the largest and next largest values, respectively, in the parameter sample of size 1000, then any value between x_{n-1} and x_n has been exceeded once in that sample and could justifiably be chosen as the "three-sigma" design value. Method C took the design value to be

$$\text{(C) design value} = x_n \tag{6.7}$$

the most conservative choice between x_{n-1} and x_n. (In the case where a design value was a minimum the smallest sample value was used).

Method D (Pearson Distribution Method). By this method, the first four sample moments were used to fit one of the Pearson distributions to the observed distribution. Then the "three-sigma" design value was that value which satisfied $F_p(x) = .9987$ (or .0013) where $F_p(\cdot)$ was the cumulative distribution function of the Pearson distribution which best fitted the data.

Results and Discussion

Table 6.3 lists various sample statistics computed from the four entry samples. Values in the "Deterministic Prediction" column are values of the parameters obtained from non-random trajectories using the appropriate atmosphere from the 1966 Standard Atmosphere Supplements, [2].

The coefficients of variation, defined by,

$$CV = \left(\frac{s}{\bar{X}}\right) \times 100\% \tag{6.8}$$

can be used to estimate confidence intervals for the means. A 95 percent confidence interval for any mean in Table 6.3 is

$$\bar{X}\ (1 \pm .0006\ CV) \tag{6.9}$$

For example, since the coefficient of variation of autumn down-range distances is 3%, one can state with 95 percent confidence, that the

Table 6.3 - Entry Parameter Statistics Based on 1000 Entries

Parameter	Deterministic Prediction	Mean	Standard Deviation	Coefficient of Variation, %
(a) Maximum dynamic pressure, N/m^2				
Spring	5305	5505	104.1	1.9
Summer	5296	5431	86.4	1.6
Autumn	5305	5592	158.3	2.8
Winter	5307	5674	168.5	2.9
(b) Maximum stagnation-point heating rate, $\times 10^{-5}$, W/m^2				
Spring	9.910	9.897	0.353	3.6
Summer	10.059	10.069	0.375	3.7
Autumn	9.910	9.915	0.462	4.7
Winter	9.749	9.863	0.414	4.2
(c) Maximum g-load				
Spring	1.165	1.206	0.0251	2.1
Summer	1.150	1.185	0.0180	1.5
Autumn	1.165	1.223	0.0346	2.8
Winter	1.152	1.247	0.0412	3.3
(d) Down range, km				
Spring	13610	13630	294.1	2.2
Summer	13450	13470	396.3	2.9
Autumn	13610	13650	415.2	3.0
Winter	13790	13760	394.1	2.9
(e) Cross range, km				
Spring	1290	1288	22.46	1.7
Summer	1295	1297	26.80	2.1
Autumn	1290	1286	32.87	2.6
Winter	1283	1279	31.56	2.5

estimated mean down-range distance in autumn, $\bar{X}$ = 13650 km, is accurate to within ± .0018 $\bar{X}$ (i.e., to within ± .18%).

Figures 6.2 - 6.6 show histograms of the five entry parameters. The dashed lines are the Pearson probability density functions fitted to each distribution. One general characteristic of each parameter is that its autumn and winter distributions have more dispersion (greater variance) than its spring and summer distributions. This reflects the fact that the variances of temperature, density and pressure in the autumn and winter atmosphere models were greater than those of the spring and summer models. The down-range distributions appear to be skewed to the left, whereas all other distributions appear to be skewed to the right.

In the cases of the summer maximum dynamic pressure, down-range, and cross-range distributions, it was not possible to find Pearson distributions using the usual moments fit. This is because β_1 and β_2 were inadmissible (see definitions in Appendix D). It was possible to modify the β_1 and β_2 values for maximum dynamic pressure to get the "closest" Pearson fit. (See Appendix D). This is the dashed curve in Figure 6.2 (summer). The same modification when applied to the summer down-range and cross-range distributions resulted in J-shaped Pearson Type VI distributions which did not resemble the sample distributions at all. Therefore, no Pearson fits were obtained for the summer down-range and cross-range distributions.

Table 6.4 lists the various "three-sigma" design values obtained by Methods A, B, C, and D, as described above. If a design value lies

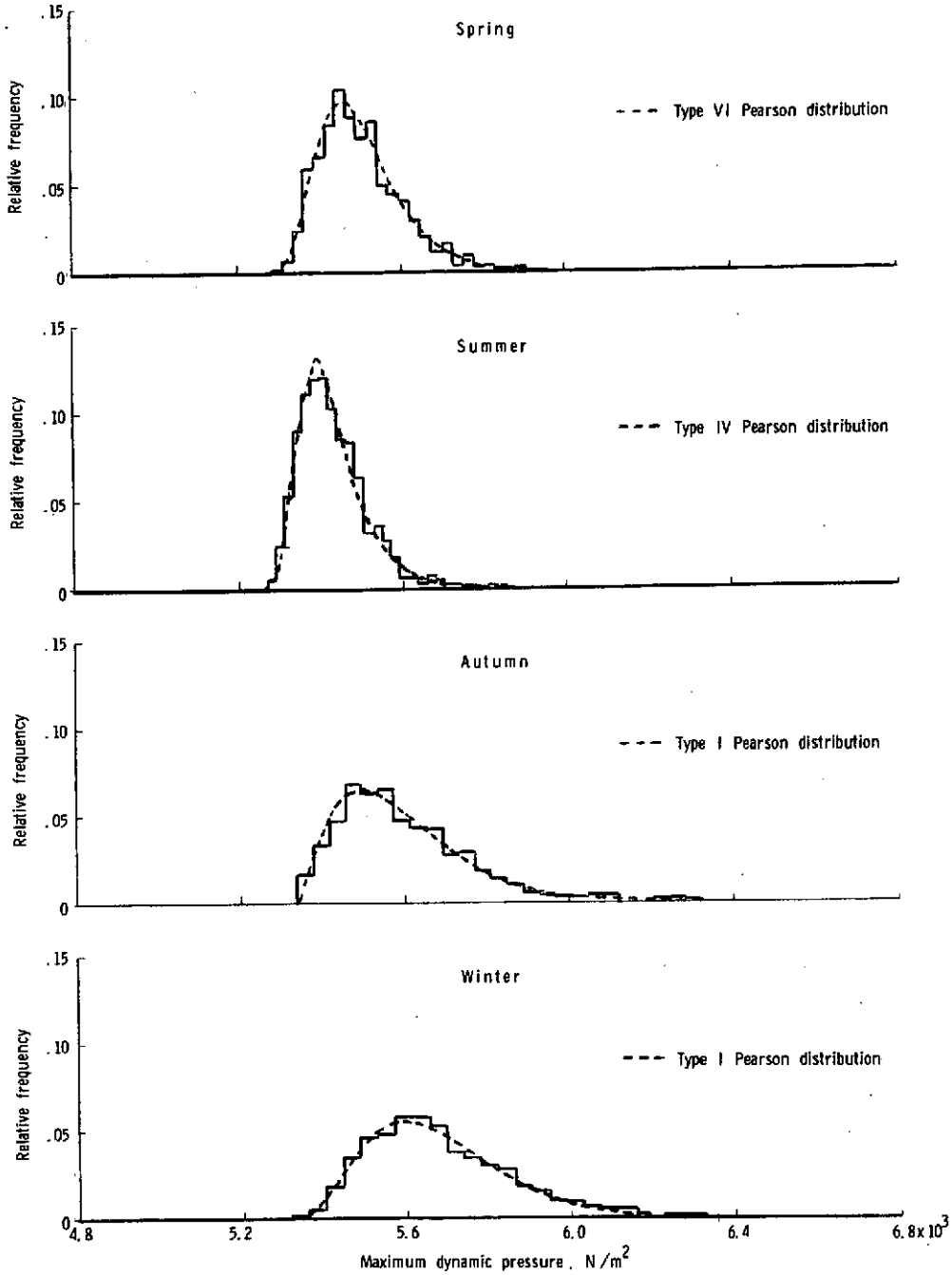

Figure 6.2 - Seasonal distributions of maximum dynamic pressure based on samples of 1000 pseudo-random Shuttle entries.

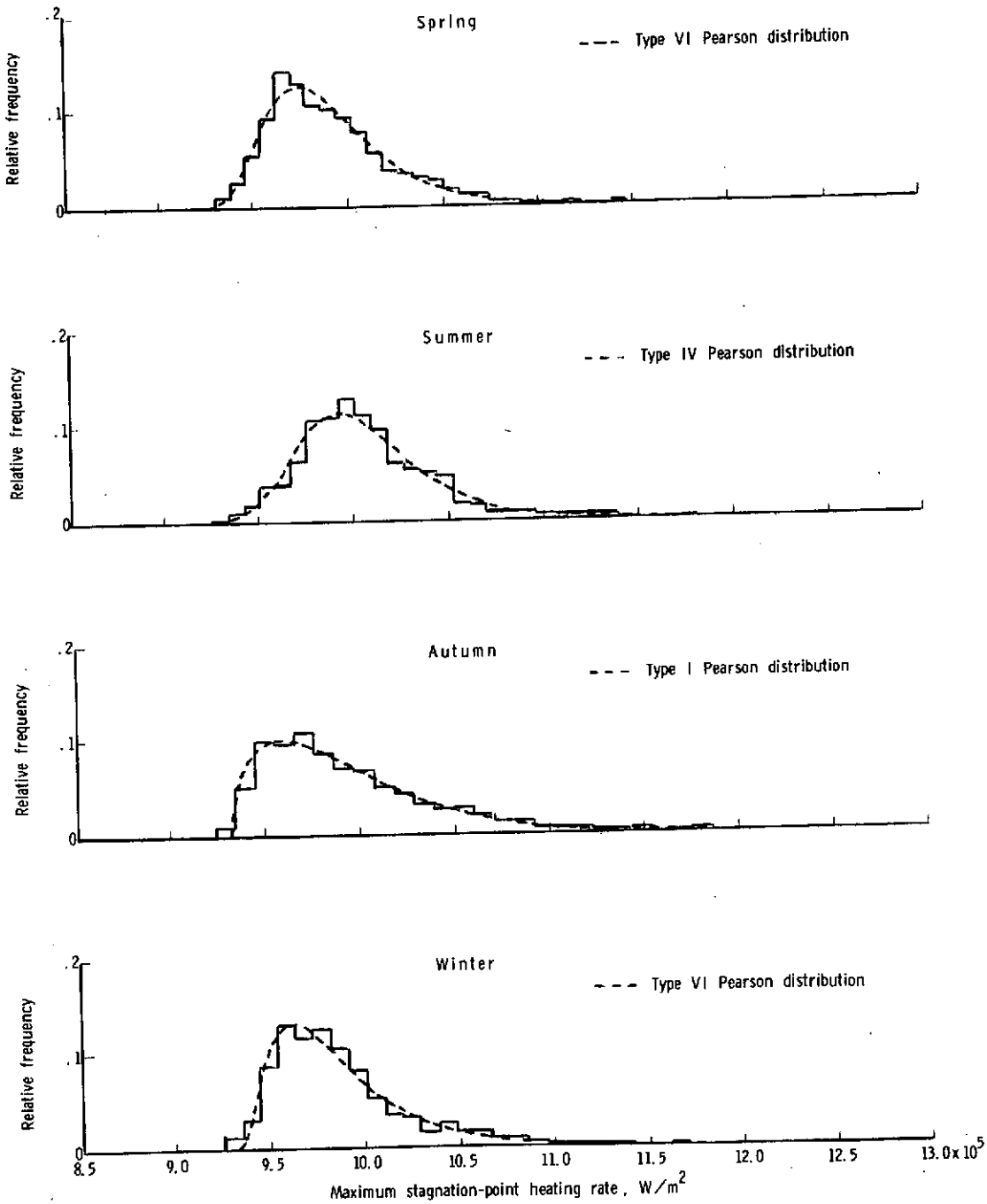

Figure 6.3 - Seasonal distributions of maximum stagnation-point heating rate based on samples of 1000 pseudo-random Shuttle entries.

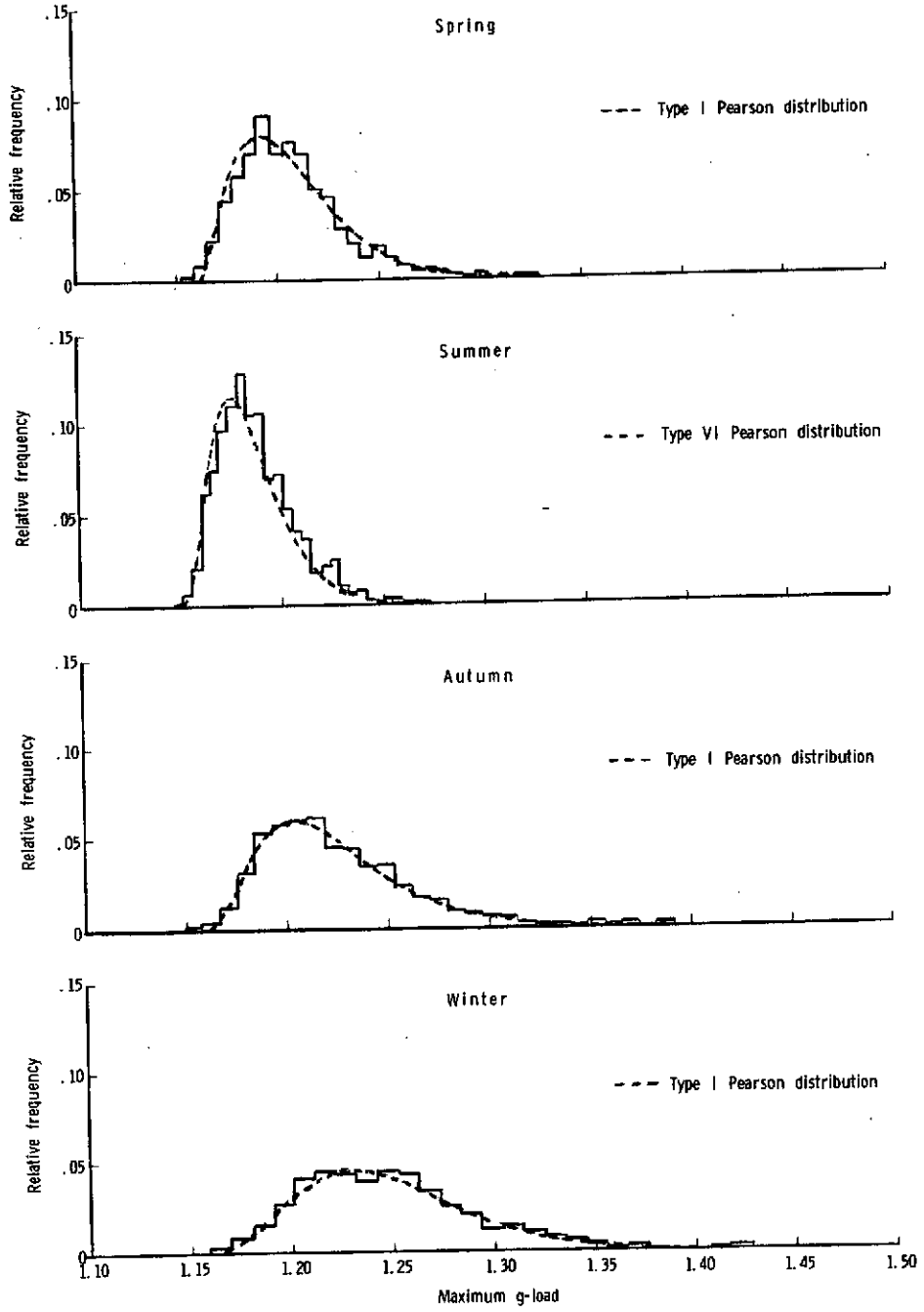

Figure 6.4 - Seasonal distributions of maximum g-load based on samples of 1000 pseudo-random Shuttle entries.

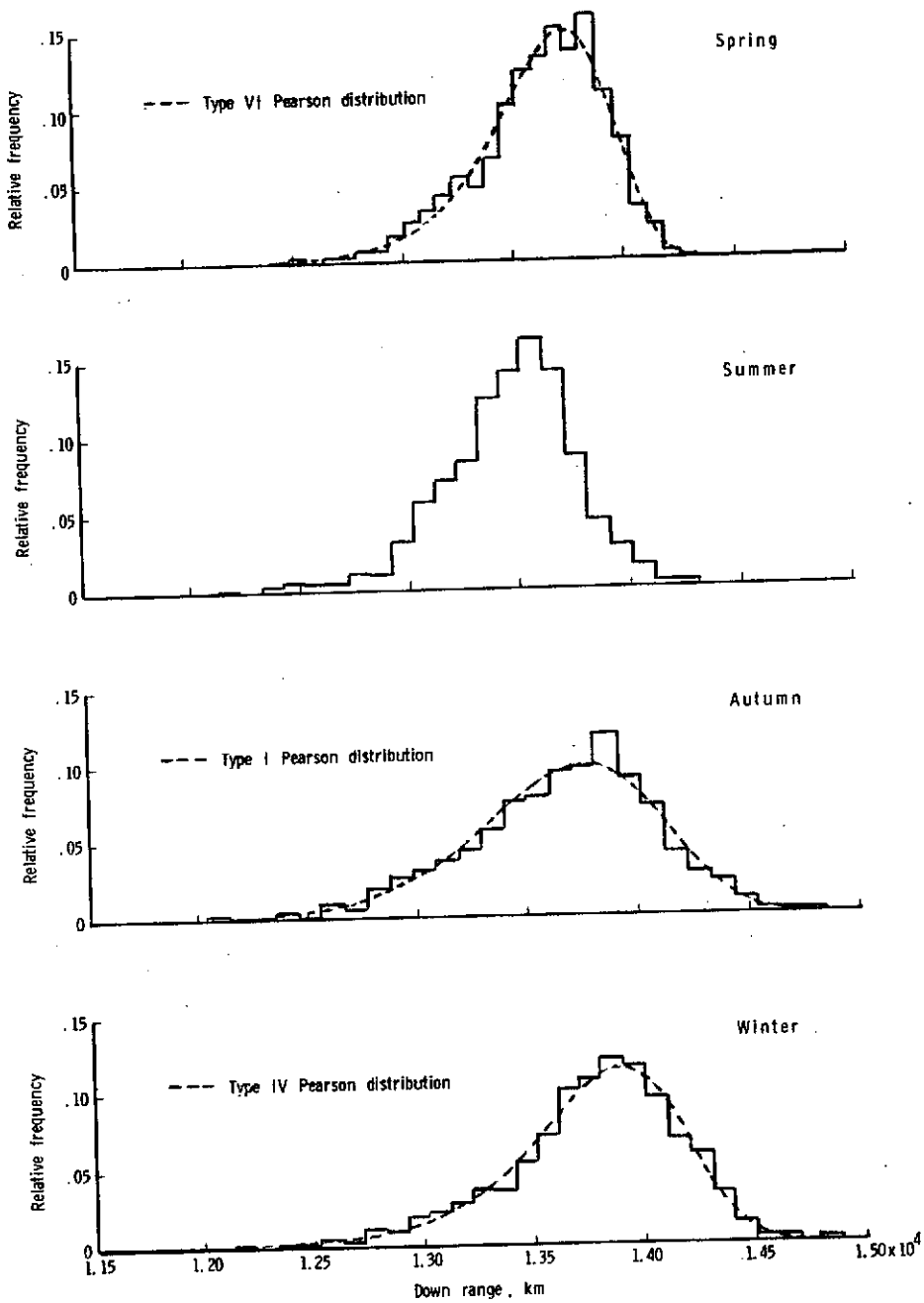

Figure 6.5 - Seasonal distributions of final down-range distance based on samples of 1000 pseudo-random Shuttle entries.

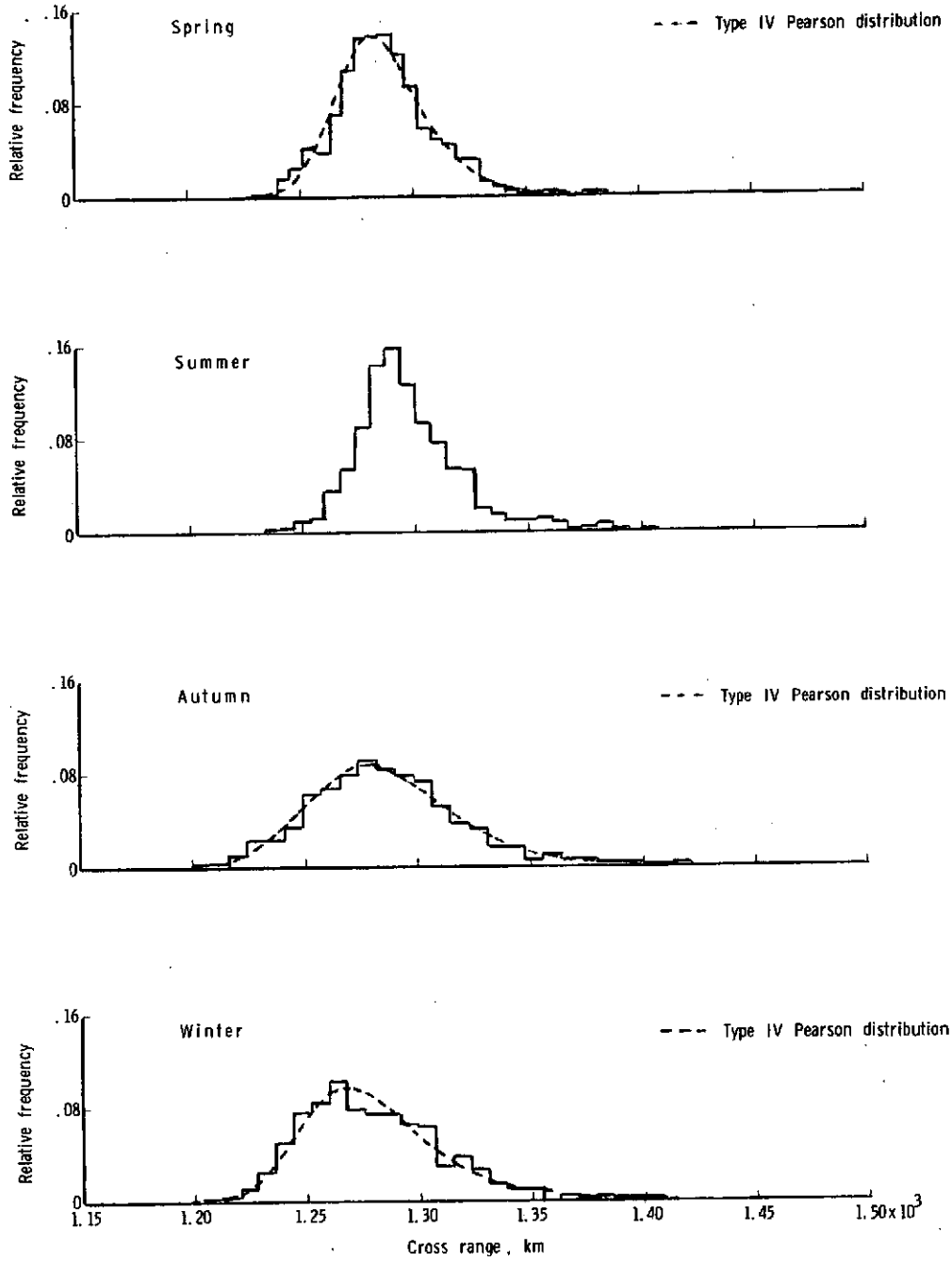

Figure 6.6 - Seasonal distributions of final cross-range distance based on samples of 1000 pseudo-random Shuttle entries.

Table 6.4 - Parameter Design Values

Parameter	A $\bar{X}\pm3s$	B Probability Paper	C Sample Extreme	D Pearson Distribution
(a) Maximum dynamic pressure, N/m^2				
Spring	5817	5903	6192	5997
Summer	5690	5772	6131	5913
Autumn	6067	6201	6298	6310
Winter	6180	6305	6421	6345
(b) Maximum stagnation-point heating rate, $\times 10^{-6}$, W/m^2				
Spring	1.096	1.126	1.226	1.161
Summer	1.119	1.150	1.192	1.174
Autumn	1.130	1.169	1.204	1.192
Winter	1.111	1.150	1.317	1.225
(c) Maximum g-load				
Spring	1.281	1.302	1.325	1.312
Summer	1.239	1.254	1.273	1.265
Autumn	1.327	1.355	1.390	1.377
Winter	1.371	1.401	1.421	1.409
(d) Maximum down range, km				
Spring	14510	14680	14310	14260
Summer	14650	14830	21830	*
Autumn	14900	15090	14780	14610
Winter	14940	15230	14800	14690
(e) Minimum down range, km				
Spring	12750	12550	11900	12420
Summer	12280	12200	12140	*
Autumn	12410	12200	12060	12130
Winter	12580	12330	11450	12100
(f) Maximum cross range, km				
Spring	1355	1374	1431	1393
Summer	1377	1398	1407	*
Autumn	1385	1407	1416	1415
Winter	1374	1400	1482	1428
(g) Minimum cross range, km				
Spring	1221	1223	1233	1230
Summer	1217	1224	905	*
Autumn	1187	1191	1203	1205
Winter	1184	1191	1206	1208

in the direction of skewness (i.e., in the long tail), then the traditional use of $\bar{X} \pm 3s$ as a design value will, in general, lead to an exceedance probability (risk) higher than the intended .0013 . Because of the positive skewness in the maximum dynamic pressure, maximum stagnation-point heating rate, and maximum g-load distributions, it is not surprising, therefore, that the (A) design values ($\bar{X} \pm 3s$) are less conservative (more "risky") than the (B), (C), or (D) design values which are based on sample cumulative frequencies. In other words, the latter three methods estimate the true cumulative distribution function $F(x)$ and select a design value x satisfying $F(x) = .9987$, whereas the (A) design value, x_A , generally has a cumulative frequency $F(x_A)$ less than .9987. Taking the autumn maximum stagnation-point heating rate distribution as an example, and assuming the Pearson distribution shown in Figure 6.3 is the true distribution, the probability of exceeding the (A) design value (11.301), is .0119 instead of .0013 as desired. The chance of exceeding this design value at least once in 100 missions (the anticipated Shuttle lifetime) is 70 percent, whereas the chance of exceeding the (D) design value (11.919) at least once is only 13 percent.

In the cases of the minimum cross-range and the maximum down-range design values, the traditional Method (A) is actually more conservative than the (D) method. This is because these design values lie in the short tails of their respective skewed distributions. Nevertheless, over-conservatism is still not a desirable trait since it adds to the cost of the design.

If it is decided that the optimum exceedance probability for a design value should be .0013, and both greater and smaller exceedance probabilities are to be avoided, then the use of a Pearson fit is recommended whenever possible. Accordingly, the (D) design values listed in Table 6.3 are preferred to those given by the other methods.

A pilot study similar to the present study was made by the author, [43], to determine if random fluctuations in atmospheric density, on the order of those observed, could have an appreciable effect on Shuttle entry parameters. (The same five parameters were studied). In that study a fairly crude stochastic atmosphere model was used. However, in spite of its deficiencies, the pilot study did produce some useful information. It showed, for example, that the shape of a parameter's distribution persisted over a wide range in entry angles of attack, and the coefficient of variation for a particular parameter remained quite constant even though the magnitude of its mean varied considerably for different angles of attack.

There is every reason to believe that these same consistencies would apply in the present study. Therefore, even though angles of attack or other trajectory characteristics may change, thus changing magnitudes of the entry parameters, the shape of a parameter's distribution and its percentage variation due to atmospheric effects should not be seriously affected. For this reason, design values expressed as "design factors" to be multiplied by the parameter's mean are perhaps more valuable than strict design values. Table 6.5 lists these factors based on the (D) design values in Table 6.4. The latter

Table 6.5 - Parameter Design Factors Based on Pearson Distributions

Parameter	Factor
(a) Maximum dynamic pressure	
Spring	1.09
Summer	1.09
Autumn	1.13
Winter	1.12
(b) Maximum stagnation-point heating rate	
Spring	1.17
Summer	1.17
Autumn	1.20
Winter	1.24
(c) Maximum g-load	
Spring	1.09
Summer	1.07
Autumn	1.13
Winter	1.13
(d) Maximum down range	
Spring	1.05
Summer	-
Autumn	1.09
Winter	1.06
(e) Minimum down range	
Spring	0.91
Summer	-
Autumn	0.89
Winter	0.88
(f) Maximum cross range	
Spring	1.08
Summer	-
Autumn	1.10
Winter	1.12
(g) Minimum cross range	
Spring	0.95
Summer	-
Autumn	0.94
Winter	0.94

are obtained by multiplying the design factors in Table 6.5 by the parameter's mean given in Table 6.3.

Conclusions

This study has shown that significant variations can occur in entry parameters as a result of day-to-day atmospheric variability. Parameter distributions showed seasonal trends in both their means and their variances. Largest and smallest means occurred in the summer and winter distributions and intermediate means in the spring and fall. Autumn and winter variances were larger than spring and summer variances in all parameter distributions because the autumn and winter atmosphere models were more variable than the spring and summer models.

Using the design factors in Table 6.5, general conclusions can be drawn about the relative amount of variation one might expect to result from atmospheric variability. Design values for maximum dynamic pressure and maximum g-load range from 7 to 13 percent higher than nominal (mean) values; design values for maximum stagnation-point heating rate range between 17 and 24 percent higher than their nominal values; down-range design values are between +9 and -12 percent, and cross-range design values are between +12 and -6 percent of their nominal.

Interpretation of the design values for maximum dynamic pressure and maximum g-load is straight-forward. The significance of maximum stagnation-point heating rate, however, is its impact on the total integrated heat load and its impact on the maximum stagnation-point surface temperature, T_{max}. The total heat load was not recorded

during the simulations, and hence, its variation is not known. A surface temperature at any point on the vehicle is proportional to the fourth root of the heating rate at that point. Therefore, T_{max} is proportional to the fourth root of the maximum stagnation-point heating rate. This means that a design value for the latter which is 24 percent higher than its nominal is equivalent to a design maximum temperature approximately 6 percent higher than its nominal (i.e., $1.24^{\frac{1}{4}} = 1.06$).

Departures from the nominal down-range and cross-range distances are not to be interpreted as miss distances since on-board guidance systems will allow the Shuttle orbiter to correct for flight path errors. The down-range and cross-range design values obtained here imply that these guidance systems must be capable of correcting for errors of as much as 12 percent caused by natural variations in atmospheric density.

The present study has shown that atmospheric variability is an important source of error to consider in Shuttle entry design studies. It is not the only error source, on the other hand, since uncertainties in the vehicle's weight, aerodynamic coefficients and initial orbital elements will all cause errors in the entry trajectory. Past error analyses have often either ignored atmospheric variability or else used "extreme" atmospheres as described in Chapter I. It is recommended that future error analyses include atmospheric variations and that a statistical approach such as the present one be used.

VII. SUMMARY AND CONCLUSIONS

Summary

A stochastic model of the atmosphere between 30 and 90 km was developed for use in Monte Carlo Shuttle entry studies. The model is actually a family of models, one for each latitude-season category as defined in the 1966 U. S. Standard Atmosphere Supplements, [2].

Each latitude-season model generates a pseudo-random temperature profile whose mean is the appropriate temperature profile from the 1966 Standard Atmosphere Supplements. The standard deviation of temperature for a given latitude-season model is assumed to be the same at all altitudes and is estimated from sounding-rocket data. Departures from the mean temperature at each altitude are produced by assuming a linear regression of temperature $T(z)$ on $\dot{T}_s(z)$, the solar heating rate of ozone. First, a profile of random ozone concentrations is generated using an auxiliary stochastic ozone model, which was also developed as a part of this study. The solar heating rate $\dot{T}_s$ is random since it is a function of the random ozone concentrations. The steps taken in generating a random temperature profile are illustrated schematically in Figure 7.1.

Pressure and density profiles are calculated from each temperature profile by solving simultaneously the hydrostatic equation and the equation of state. Thus, each pseudo-random atmosphere consists of a consistent set of temperature, pressure and density profiles. Isopynic layers, regions where atmospheric density is almost constant, are created

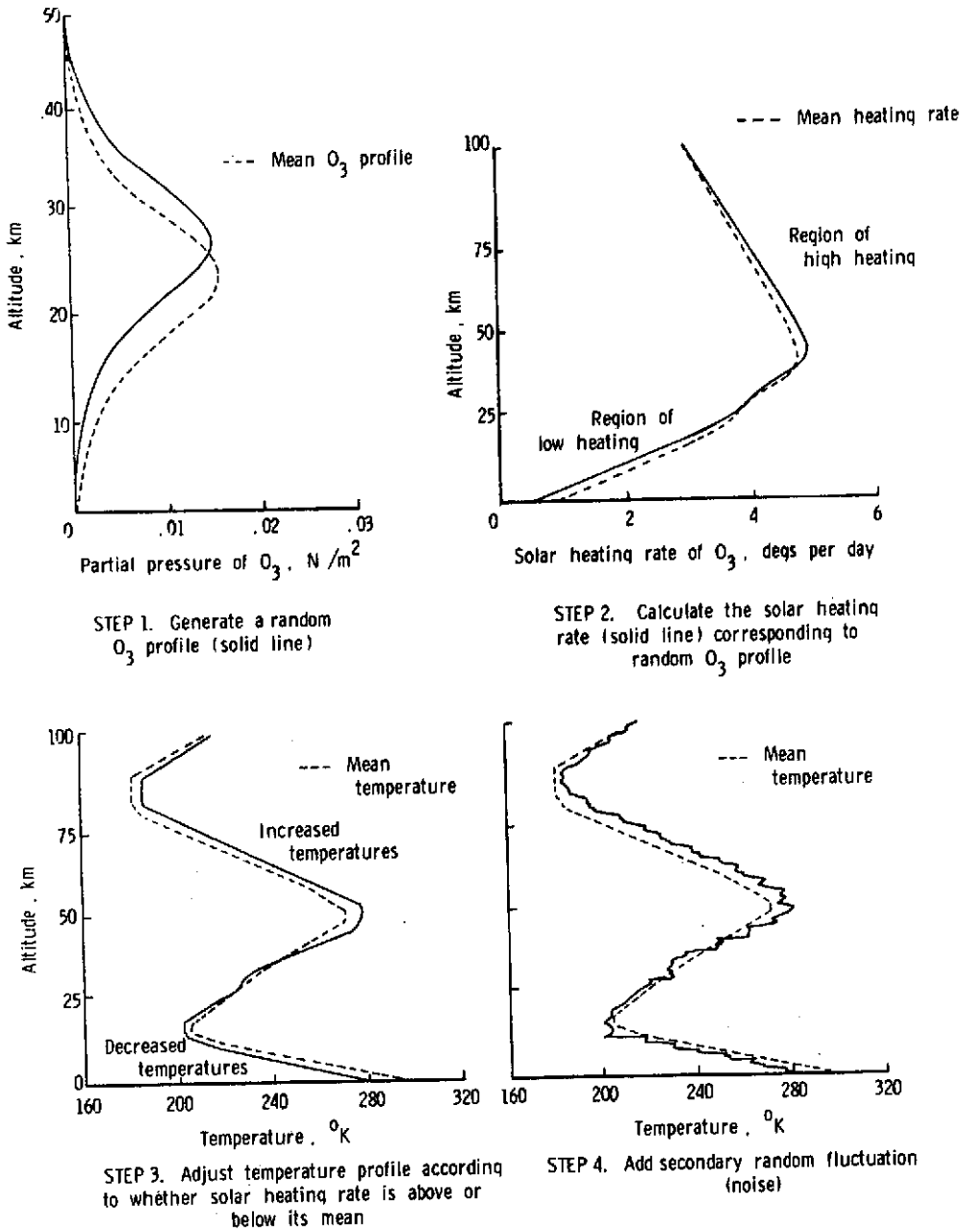

Figure 7.1 - Steps taken in generating one pseudo-random temperature profile.

at 24 and 90 km altitudes by using these two altitudes as boundary points in integrating the hydrostatic equation.

A computer data tape of 442 sounding-rocket measurements of the atmosphere above 35 km was obtained to use in estimating parameters of the temperature distribution. These data were also used for comparing their statistical characteristics with those of the model. After the data were sorted according to latitude-season categories and adjustments were made to assure independence of profiles, the sizes of resultant samples were quite small. For example, in the 30° latitude band, sample sizes ranged from 5 in the summer sample to 20 in the winter sample. Because of such small samples, confidence intervals associated with the sample statistics (e.g., means, standard deviations, and correlations) were so wide that comparison of these statistics with model statistics were inconclusive.

The four 30° latitude models were used in Monte Carlo simulations of Shuttle entries to study the effect of atmospheric variability on five Shuttle entry parameters. The simulations were of point-mass trajectories, and the five parameters studied were maximum dynamic pressure, maximum stagnation-point heating rate, maximum g-load, final down-range distance and final cross-range distance. A sample of 1000 entries was generated for each of the four seasons, and the resultant parameter distributions were analyzed to determine design values. Pearson distributions were fitted to the empirical distributions, and design values obtained from these distributions were compared to the traditional "three-sigma" design values which are based on assumptions that parameter

distributions are normal. Pearson design values were defined as those parameter values with exceedance probabilities equal to .0013 based on the fitted Pearson distribution. (The value .0013 is the exceedance probability associated with a normal random variable located a distance of three standard deviations from its mean.)

In general, the design values based on fitted Pearson distributions were more conservative (farther from the mean) than those obtained with the assumption of normality. This is because all of the empirical distributions were skewed, and most design values lay in the direction of skewness (long tail). Pearson design values ranged from being 24 percent greater than the mean, in the case of winter maximum stagnation-point heating rates, to being within 5 percent of the mean, in the case of spring minimum cross-range distances.

Autumn and winter parameter distributions showed more dispersion than spring and summer distributions, because the autumn and winter atmosphere models were more variable than the spring and summer models. It is apparent from this fact that parameter design values are quite sensitive to the estimates of variances used in the atmosphere models. In particular, two factors contribute to the observed dispersion differences between summer and winter histograms. One is the difference between σ_T(summer) = 6.82° K and σ_T(winter) = 10.89° K, and the other is the difference between summer and winter design density gradients (Table 6.1). Because of this sensitivity, Shuttle parameter design values are only as reliable as these estimates. This further underscores the need to increase the data base used in estimates of atmosphere model

parameters.

Concluding observations

There are two basic philosophies one can use in developing a stochastic model of some random phenomenon. By far the most common approach is to observe the available data relating to that phenomenon and then model that data empirically without any regard to cause-and-effect relationships. By using the data to estimate means, variances, correlations, and higher moments, one can generate artificial data samples with all the statistical characteristics of the original sample.

A second alternate approach is to attempt to identify and model the fundamental random processes which bring about the observed randomness in the phenomenon being modeled. For example, in the case of atmospheric temperature, one would look for underlying random processes which cause temperature to vary.

Believing that a good theoretical model is preferable to a good empirical model, if both were attainable, the author chose the theoretical approach in setting out to model atmospheric variations. Although the development of a workable theoretical model is a much greater challenge, such a model would provide physical insight into the nature of atmospheric variations. A purely empirical model, on the other hand, is strictly limited to describing a particular set of data, and its user must be cautious when projecting the model beyond the range of the original data. Furthermore, empirical models generally are time consuming and require the storage of large correlation matrices.

The fact that the microscopic nature of any gas is basically random was further encouragement for taking a theoretical approach to modeling the atmosphere. For example, the temperature of a gas is actually a direct measure of the variance of molecular velocities in that gas. That is, the velocity of a molecule of gas in any one direction is a normal random variable with mean 0 and variance equal to KT/M, where K is the universal gas constant, M is the molecule's weight, and T is the gas temperature, [44].

In accordance with the "theoretical" philosophy, one fundamental random process, the creation and destruction of atmospheric ozone, was identified as the major cause of temperature variation in the 30-90 km region. An attempt to model it on a microscopic level, using collision rates, etc., lead to the immediate realization that variations in a macroscopic gas property could not be accounted for by modeling random events occurring on a microscopic scale. The law of large numbers steps into play so that, if N is the number of molecules in the gas volume, the collective effect of N random events is virtually non-random at altitudes below 90 km where N is greater than 10^{20} molecules per cubic meter.

Thus, the initial effort to model the causes of temperature variation using purely theoretical considerations failed. It led, instead, to an empirical model of atmospheric ozone based on experimental measurements of ozone concentrations, [37]. Pseudo-random ozone profiles were used to calculate the solar heating rate of ozone at each altitude, and these in turn were linked to temperatures via a linear regression model.

A reasonable question at this point might be, "Why avoid the use of an empirical temperature model and at the same time resort to the use of an empirical ozone model?" Admittedly, this is a compromise, and a theoretical model for ozone variation would be preferable. However, even though the present model contains no insight into the nature of ozone variations, it still uses these to explain, at least partially, the variations in temperature, and particularly the correlations between temperatures at different altitudes. The particular ozone model used here determines the shape of the temperature distribution at each altitude. However, any ozone model showing the same uniform increase and decrease in ozone above 30 km, as exhibited by the data, will give the same interlayer correlation structure for temperatures; it is this feature - the correlation structure - which largely governs the pressure and density distributions. Thus, the pressure and density distributions and the interlayer temperature correlations are somewhat robust to the choice of ozone models.

A number of improvements can and should be made in order to obtain better agreement between the temperature model and data. A better, more quantitative, means of estimating λ should be devised; other sources of variation should be included (e.g., winds, water vapor absorption, etc.), and a more acceptable means of estimating boundary conditions in the hydrostatic equation should be sought. A prerequisite to any improvement attempt, however, is the enlargement of the data base. As it stands now, the model represents an encouraging "first cut" at a workable theoretical model.

REFERENCES

1. COESA, U. S. Standard Atmosphere, 1962, United States Government Printing Office, Washington, D.C., 1962.

2. COESA, U. S. Standard Atmosphere Supplements, 1966, United States Government Printing Office, Washington, D.C., 1966.

3. Cole, Allen E., "Extreme Temperature, Pressure, and Density between 30 and 80 km", AFCRL-70-0462, Environmental Research Paper no. 330, Air Force Cambridge Research Laboratories, Bedford, Mass., 1970.

4. Pitts, David E., "Extreme-Density Profiles for Skylab Command Module Considerations", NASA TM X-58060, NASA Manned Spacecraft Center, Houston, Texas, May 1971.

5. Smith, O. E., J. R. Redus, J.A. Forney, and M. J. Dash, "Effects of Atmospheric Models on Space Shuttle Trajectories and Aerodynamic Heating", preprints of International Conference on Aerospace and Aeronautical Meteorology", Washington, D.C., May 1972, pp. 65-72.

6. Glover, L. S., "Approximate Equations for Evaluating the Impact Dispersion Resulting from Reentry Winds and Deviations in Density", Technical Memorandum TG 1132, Johns Hopkins University Applied Physics Laboratory, September 1970.

7. Smith, O. E., and Don K. Weidner, "A Reference Atmosphere for Patrick AFB, Florida, Annual (1963 Revision)", NASA TM X-53139, Marshall Space Flight Center, Huntsville, Ala., September 1964.

8. Carter, E. A., and S. C. Brown, "A Reference Atmosphere for Vandenburg AFB, Calif., Annual (1971 Revision)", NASA TM X-64590, NASA Marshall Space Flight Center, Huntsville, Ala., May 1971.

9. IRIG Document No. 104-63, Range Reference Atmosphere Documents, Secretariat, Range Commander's Council, White Sands Missile Range, New Mexico, 1963-1970.

10. Theon, J. S., W. S. Smith, and J. F. Casey, "Statistical Models of the Density and Wind Profiles in the Mesosphere Based on 208 Soundings", preprints of 4th National Conference on Aerospace Meteorology, Las Vegas, Nev., May 1970, pp. 306-311.

11. World Data Center A, "Data Report, Meteorological Rocket Network Firings, January 1968", Vol. V, No. 1, U. S. Department of Commerce, Environmental Science Service Administration, National Weather Record Center, Asheville, N.C., January 1968.

12. Weidner, Don K., John L. Chambers, and George Y. Lou, "A Global Model of Atmospheric Temperature, Chemical Composition, and Density (25 to 1000 km altitude)", preprints of 14th COSPAR Plenary Meeting, Seattle, Washington, June-July 1971.

13. Spiegler, D. B., and M. G. Fowler, "Development of Four-Dimensional Atmospheric Models and Application Techniques for Space Mission Simulation", preprints of International Conference on Aerospace and Aeronautical Meteorology, Washington, D.C., May 1972, pp. 18-24.

14. Bowman, W. Allen, "Atmospheric Density Models for Re-entry Heating and Trajectory Applications", preprints of 4th National Conference on Aerospace Meteorology, Las Vegas, Nev., May 1970, pp. 280-286.

15. Goody, R. M., Atmospheric Radiation I: Theoretical Basis, Oxford University Press, London, 1964.

16. Harris, L., and W. Priester, "The Upper Atmosphere", CIRA, 1965, North Holland, Amsterdam.

17. Kuhn, William R., "Infrared Radiative Transfer in the Upper Stratosphere and Mesosphere", PhD Thesis , Department of Astro-Geophysics, Univ. of Colorado, Boulder, Colo., 1966.

18. Manabe, S., and F. Möller, "On the Radiative Equilibrium and Heat Balance of the Atmosphere", Monthly Weather Review, Vol. 89, 1961, pp. 503-532.

19. Manabe, S. and R. F. Strickler, "Thermal Equilibrium of the Atmosphere with a Convective Adjustment", J. of Atmospheric Sciences, Vol. 24, 1964, pp. 361-385.

20. Murgatroyd, R. J., and R. M. Goody, "Sources and Sinks of Radiative Energy from 30 to 90 km", Quarterly J. of the Royal Meteorological Society, 84, 1958, 224-234.

21. Dines, W. H., "The Characteristics of the Free Atmosphere", Geophys. Mem., No. 13, 1919, pp. 46-74.

22. Buell, C. E., "Some Relations Among Atmospheric Statistics", J. of Meteorology, Vol. 11, June, 1954, pp. 238-244.

23. Smith, O. E., S. Clark Brown, Glenn E. Daniels, and Dale L. Johnson, "Inflight Thermodynamic Properties", in Terrestrial Environment (Climatic) Criteria Guidelines for Use in Space Vehicle Development 1971 Revision. NASA TM X-64589, Marshall Space Flight Center, May 1971, pp. 14.1-14.54.

24. Essenwanger, O. M., "Characteristics of Global Atmospheric Conditions by Parameterized Daily Profiles", preprints of International Conference on Aerospace and Aeronautical Meteorological, Washington, D.C., May 1972, pp. 25-31.

25. Engler, Nicholas A. and Mark A. Goldschmidt, "Interrelated Structure of High Altitude Atmospheric Profiles", NASA Contractor Report no. NASA CR-61398, September 1972.

26. Justus, C. G., and Arthur Woodrum, "Atmospheric Pressure, Density, Temperature, and Wind Variations between 50 and 200 km: Interim Report", Contract No. NAS8-26658, January 1972.

27. Morgenstern, Paul, and R. G. Orner, "Multivariate Regression Analysis of Atmospheric Density in the Region 30 to 110 km", report prepared under NASA contract no. NAS12-2125, October 1970.

28. Jacchia, L. G., "The Atmospheric Models Above 120 km: Derivation, Systematic Variations, Sources, Errors, Limitations", Smithsonian Astrophysical Observatory, Cambridge, Mass., 1966.

29. Alexander, Margaret B., S. Clark Brown, Dennis W. Camp, Glenn E. Daniels, George H. Fichtl, Kelly Hill, John Kaufman, O. E. Smith, and William W. Vaughan, "Wind" in Terrestrial Environment (Climatic) Guidelines for Use in Space Vehicle Development, 1971 Revision, NASA TM X-64589, Marshall Space Flight Center, Huntsville, Ala., May 1971, pp. 5.1-5.152.

30. Geissler, E. D., editor, Wind Effects on Launch Vehicles, Circa Publications, Inc., New York, 1970.

31. Fichtl, George H. and G. E. McVehil, "Longitudinal and Lateral Spectra of Turbulence in the Atmospheric Boundary Layer", NASA TN D-5584, Marshall Space Flight Center, Huntsville, Ala., 1969.

32. Henry, Robert M., "A Statistical Model for Synthetic Wind Profiles for Aerospace Vehicle Design and Launching Criteria", NASA TN D-1813, Langley Research Center, 1963.

33. Elsasser, W., "Heat Transfer by Infrared Radiation in the Atmosphere", Harvard Meteorological Studies No. 6, 1942.

34. Plass, G. N., "Models for Spectral Band Absorption", J. Op. Soc. of America, 48, 690, 1958.

35. Goody, R. M., "A Statistical Model for Water-Vapour Absorption", Quart. J. R. Meteor. Soc., 78, 165, 1952.

36. Su, F. Y., "The Radiative Budget for Polluted Layers in the Stratosphere", presented at the American Meteorological Society Conference on Atmospheric Radiation, Fort Collins, Colo., August 1972.

37. Hering, W. S., "Ozonesonde Observations over North America", Vols. I - IV, AFCRL-64-30 (I) - (IV), 1964-1968.

38. Russell, James M., III, "The Measurement of Atmospheric Ozone Using Satellite Infrared Observation in the 9.6 μm Band", PhD Thesis, Department of Meteorology and Oceanography, Univ. of Michigan, 1970.

39. Green, A. E. S., "Attenuation by Ozone and the Earth's Albedo in the Middle Ultraviolet", J. Applied Optics, 3, No. 2, 1964, pp. 203-208.

40. Smith, J. W., "Density Variations and Isopynic Layers", J. of Applied Meteorology, Vol. 3, no. 3, June 1964, pp. 290-298.

41. Proposal for Space Shuttle Program, Vol. III, North American Rockwell Corporation, Downey, California, May 1972.

42. Kendall, M. G., and Allen Stuart, The Advanced Theory of Statistics, Vol. I: Distribution Theory, Hafner Publishing Co., New York, 1963, pp. 148-154.

43. Campbell, Janet W., "The Effects of Random Fluctuations in Atmospheric Density on Significant Space Shuttle Re-entry Parameters", Proceedings of the International Conference on Aerospace and Aeronautical Meteorology, Washington, D.C., May 1972, pp. 65-69.

44. Vincenti, Walter G., and Charles H. Kruger, Jr., Introduction to Physical Gas Dynamics, John Wiley and Sons, Inc., New York, 1965, pp. 27-58.

45. Inn, E. C. Y., and Y. Tanaka, "Absorption Coefficients of Ozone in the Ultraviolet and Visible Regions", J. of the American Optical Society, Vol. 43, 1953, pp. 870-873.

46. Falls, Lee W., "A Computer Program for Standard Statistical Distributions", NASA TM X-64588, Marshall Space Flight Center, Huntsville, Ala., April, 1971.

47. Pearson, E. S., and H. O. Hartley, editors, Biometrika Tables for Statisticians, Vol, I, Cambridge University Press, London, 1958.

APPENDIX A. EQUATIONS FOR CALCULATING ATMOSPHERIC PROPERTIES

List of Symbols

Symbol	Definition	Units/Constants
g	acceleration due to gravity	m/sec^2
g_o	acceleration due to gravity at sea level	m/sec^2
K	universal gas constant	8.314×10^3 $J/^oK$
M	molecular weight of air	28.964 kg
P	atmospheric pressure	N/m^2
P_o	atmospheric pressure at sea level	N/m^2
R_o	radius of earth	m
T	atmospheric temperature	^oK
U	$\log(P/P_o)$	
z	geometric altitude	m
ρ	atmospheric density	kg/m^3
ϕ	earth latitude	degrees

Governing equations

Atmospheric temperature, density and pressure are related by the equation of state

$$\rho = \frac{MP}{KT} \tag{A.1}$$

and the hydrostatic equation

$$dP = -g\rho\, dz \tag{A.2}$$

The molecular weight of air M can be considered constant, for the

present purposes, at altitudes below 90 km.

The acceleration due to gravity g, a function of altitude z, is given by

$$g = g_o \frac{R_o^2}{(R_o + z)^2} \tag{A.3}$$

where g_o, the value of g at sea level, is

$$g_o = 9.780356 \left[1 + .0052885 \sin^2 \phi - .0000059 \sin^2 (2\phi)\right] \tag{A.4}$$

and R_o, the earth's radius, is

$$R_o = 6356798 \, (.9933070 + .0066930 \sin \phi)^{-\frac{1}{2}} \tag{A.5}$$

Equations (A.3) - (A.5) are actually approximations, but they give sufficient accuracy for the model calculations in this study. Equations (A.3) and (A.4) are those used for the calculations in the 1966 Standard Atmosphere Supplements, [2]. The earth's radius $R_o(\phi)$ at latitude ϕ, (A.5), is based on the assumption that the earth is an ellipsoid with an equatorial radius $R_o(0) = 6378178$ m, and a polar radius $R_o(90) = 6356798$ m.

Solving for P and ρ given a temperature-altitude profile

Let the given temperature-altitude profile be of the form

$$\left\{(T_i, z_i): \; z_i = 0, 1, \ldots, 90 \text{ km}\right\} \tag{A.6}$$

and assume that for z between z_i and z_{i+1}, $T(z)$ is found by

linear interpolation. That is,

$$T(z) = T_i + (z - z_i)\, \Delta T_i/\Delta z \qquad (A.7)$$

where $\Delta T_i = T_{i+1} - T_i$ and $\Delta z = z_{i+1} - z_i$. (Δz does not have a subscript since $\Delta z = 1$ km for all i , $i = 0, \ldots, 90$). Assume further that between z_i and z_{i+1} g is constant and is given by (A.3) with $z = z_i$.

In order to solve (A.1) and (A.2) for pressures $\{P_i\}$ and densities $\{\rho_i\}$ it is necessary to have a value of pressure P_b or density ρ_b at some boundary point z_b . Assume that $z_b = z_i$ for some i between 0 and 90 , and that P_b is known at that altitude.

Substituting for ρ from (A.1), equation (A.2) becomes

$$\frac{dP}{P} = - \frac{gM}{KT}\, dz \qquad (A.8)$$

If P_i is known at z_i then, integrating from z_i to z_{i+1} , one gets

$$P_{i+1} = P_i \exp\left[- \frac{g(z_i)M}{K} \int_{z_i}^{z_{i+1}} \frac{dz}{T(z)} \right] \qquad (A.9)$$

Using $T(z)$ from (A.7), the integral in equation (A.9) can be integrated to give

$$P_{i+1} = P_i \left[\frac{T_i}{T_{i+1}} \right]^{\frac{g(z_i)M\Delta z}{K\Delta T_i}} \qquad (A.10)$$

if $\Delta T_i \neq 0$, or

$$P_{i+1} = P_i \exp\left[-\frac{g(z_i)\, M\Delta z}{KT_i}\right] \tag{A.11}$$

if $\Delta T_i = 0$.

Once the pressures $\{P_i\}$ are obtained, the equation of state is used to get densities.

$$\rho_i = \frac{MP_i}{KT_i} \tag{A.12}$$

Solving for z and ρ given a temperature-pressure profile

Let the temperature-pressure profile be of the form

$$\left\{ (T_j, U_j):\ j = 0, 1, \ldots, 90 \right\} \tag{A.13}$$

where $U_j = \log(P_j/P_o)$ and P_o is sea-level pressure. P_o can actually be the pressure at any boundary point z_b , not necessarily $z_b = 0$. Values of U_j ranging from $U_o = 0$ to $U_{90} = -6.4$ cover the atmosphere up to approximately 90 km.

It is assumed that for any U between U_j and U_{j+1} , T(U) can be obtained by linear interpolation. That is,

$$T(U) = T_j + (U - U_j)\, \Delta T_j/\Delta U_j \tag{A.14}$$

where $\Delta T_j = T_{j+1} - T_j$ and $\Delta U_j = U_{j+1} - U_j$.

Equation (A.8) can now be written

$$\frac{K}{M} T\, du = -\frac{g_o R_o^2}{(R_o + z)^2}\, dz \tag{A.15}$$

Integrating from $U_o = 0$ to U_j, ($z_b = 0$ to z_j), one gets

$$\frac{K}{M} \int_{U_o}^{U_j} T(u)\, du = - \frac{g_o R_o z_j}{(R_o + z_j)} \tag{A.16}$$

and solving for z_j yields

$$z_j = \frac{\frac{K}{g_o M} \int_{u_j}^{0} T(u)\, du}{1 - \frac{K}{g_o M R_o} \int_{u_j}^{0} T(u)\, du} \tag{A.17}$$

where the integral is approximated by

$$\int_{u_j}^{0} T(u)\, du = \sum_{i=0}^{j-1} |\Delta u_i| \frac{(T_{i+1} + T_i)}{2} \tag{A.18}$$

The density ρ_j at z_j is again found by using the equation of state.

APPENDIX B. EQUATIONS FOR CALCULATING SOLAR HEATING RATES

List of Symbols

Symbol	Definition	Units/Constants
A	shaping parameter in O_3 model	
a	surface albedo = reflected radiation/ incident radiation	
B	parameter in O_3 model	
c_P	specific heat at constant pressure	1004.7 J/kg/^oK
g	acceleration due to gravity	m/sec^2
g_o	acceleration due to gravity at sea level	m/sec^2
K	universal gas constant	8.3143×10^3 J/^oK
k_i	linear absorption coefficient for step i	m^{-1}
M	molecular weight of air	28.964 kg
MO_3	molecular weight of ozone	47.9982 kg
P	atmospheric pressure	N/m^2
P_o	atmospheric pressure at sea level	N/m^2
PO_3	partial pressure of ozone	N/m^2
PO_3^*	maximum PO_3 (model parameter)	N/m^2
R_o	earth's radius	m
S	flux of solar energy	W/m^2
S_i	flux of solar energy in step i	W/m^2
$S_{\infty,i}$	portion of solar constant in step i	W/m^2
s_R	contribution of Rayleigh scattering to planetary albedo	

Symbol	Definition	Units/Constants
T	atmospheric temperature	^oK
$\dot{T}_s$	solar heating rate of ozone	$^oK/sec$
U	height parameter = $\log(P/P_o)$	
U^*	value of U where $PO_3 = PO_3^*$ (model parameter)	
z	altitude	m
θ	cosine of the sun's zenith angle	
κ	mass absorption coefficient for step i	m^2/kg
λ	wavelength	micron $\mu = 10^{-6}$ m
ρ	atmospheric density	kg/m^3
ρ_3	ozone density	kg/m^3

Ozone absorption coefficients

There are three spectral bands in which ozone absorbs solar radiation. These are the Hartley band with $.2 \leq \lambda \leq .3\ \mu$, the Huggins band with $.3 \leq \lambda \leq .37\ \mu$, and the Chapius band with $.4 \leq \lambda \leq .7\ \mu$.

The present study uses an absorption coefficient model, [36], in which these spectral bands are divided into three "steps" each having a constant mass absorption coefficinet κ_i, $i = 1, 2, 3$. The three steps and their respective mass absorption coefficients are listed in Table B.1. The κ_i's given here are based on ratios of step heights $\kappa_1 : \kappa_2 : \kappa_3 = 1 : .02 : .0005$ calculated from data in Inn and Tanaka, [45]. The value of κ_1 was selected to give a linear absorption coefficient $k_i(z)$, defined by

Table B.1

THREE STEPS IN OZONE ABSORPTION MODEL

Step	Wavelengths, μ	Mass Absorption, Coefficient, m^2/kg	Fraction of Solar Constant*
1	.200 - .300	1292.0	.01203
2	.300 - .335	25.84	.02113
3	.335 - .370; .400 - .700	0.6460	.40982

*Solar Constant = flux of solar energy incident on the "top" of the atmosphere = 1353 W/m^2

$$k_i(z) = \kappa_i \rho_3 (z) \tag{B.1}$$

equal to .0005 m^{-1} at the altitude where ozone density is maximum. This value was chosen by Su, [36], to yield local heating rates in good agreement with those of an earlier model by Manabe and Strickler, [19]. The value of maximum ozone density used for calculating κ_1 was 3.87×10^{-7} kg/m^3 as given by the Mid-Latitude Ozone Model in reference [2].

Solar heating rates

The solar heating rate of ozone at altitude z is

$$\dot{T}_s(z) = - \frac{1}{\rho c_p} \frac{dS}{dz} \tag{B.2}$$

where the solar energy flux $S(z)$ is the sum of three components $S_i(z)$ corresponding to the three steps in the model. These components are

$$S_i(z) = -S_{\infty,i}(1 - s_R)\theta \left\{ \exp\left[- \frac{1}{\theta} \int_z^\infty k_i(x)dx \right] - a \exp\left[- \frac{1}{\theta} \int_0^\infty k_i(x)\, dx \right] \exp\left[- \sqrt{3} \int_0^z k_i(x)\, dx \right] \right\}$$

where the values of $S_{\infty,i}$ are based on Table B.1; s_R and a are respectively, 0.07 and 0.10, as used by Su, [36], and $\theta = .5$ is the cosine of the effective mean zenith angle.

Taking the derivative of (B.3) with respect to z, one gets

$$\frac{dS_i}{dz} = - S_{\infty,i}(1 - s_R)\, k_i(z) \left\{ \exp\left[- \frac{1}{\theta} \int_z^{\infty} k_i(x)\, dx \right] + a\theta \sqrt{3}\ \exp\left[- \frac{1}{\theta} \int_0^{\infty} k_i(x)\, dx \right] \exp\left[- \sqrt{3} \int_0^{z} k_i(x)\, dx \right] \right\} \quad (B.4)$$

Letting $k_i(z) = \kappa_i \rho_3(z)$ and summing (B.4) over all values of i, one gets

$$\dot{T}_s(z) = \frac{(1 - s_R)\, \rho_3(z)}{c_p\, \rho(z)} \sum_{i=1}^{3} S_{\infty,i}\, \kappa_i \left\{ \exp\left[- \frac{\kappa_i}{\theta} \int_z^{\infty} \rho_3(x)\, dx \right] + a\theta \sqrt{3}\ \exp\left[- \frac{\kappa_i}{\theta} \int_0^{\infty} \rho_3(x)\, dx \right] \exp\left[- \kappa_i \sqrt{3} \int_0^{z} \rho_3(x)\, dx \right] \right\} \quad (B.5)$$

The present model uses $U = \log(P/P_o)$ as its independent variable, and, therefore, (B.5) must be expressed as a function of U. The equation of state for a constituent density is

$$\rho_3 = \frac{MO_3\, PO_3}{KT} \quad (B.6)$$

and, therefore, the mixing ratio of O_3 is

$$\frac{\rho_3}{\rho} = \frac{MO_3\, PO_3}{MP} \quad (B.7)$$

Then, utilizing (B.7) and the hydrostatic equation, one can write

$$\int_{z_1}^{z_2} \rho_3(x)\, dx = - \frac{MO_3}{\bar{g}M} \int_{U_1}^{U_2} PO_3(u)\, du \quad (B.8)$$

The acceleration due to gravity g, which actually varies slightly with altitude (i.e., by about 3 percent between sea level and 90 km), is replaced by a constant

$$\bar{g} = g_o \frac{R_o}{(R_o + 90)} \tag{B.9}$$

which represents its effective mean between sea level and 90 km.

Using (B.7), (B.8), and (B.9), the heating rate can now be written as a function of U. That is,

$$\dot{T}_s(U) = \frac{(1 - s_R)\, MO_3\, PO_3(U)}{c_p\, M\, P_o \exp(U)} \sum_{i=1}^{3} S_{\infty,i}\, \kappa_i \left\{ \exp\left[-\frac{Q_i}{\theta} \int_{-\infty}^{U} PO_3(u)\, du \right] + a\theta \sqrt{3} \exp\left[-\frac{Q_i}{\theta} \int_{-\infty}^{0} PO_3(u)\, du \right] \exp\left[-Q_i \sqrt{3} \int_{U}^{0} PO_3(u)\, du \right] \right\} \tag{B.10}$$

where

$$Q_i = \frac{\kappa_i\, MO_3}{\bar{g} M} \tag{B.11}$$

The use of a constant $g = \bar{g}$, and a constant sea-level pressure P_o in (B.10) introduces a small error in the $\dot{T}_s(U)$ profile. However, in the temperature model, $\dot{T}_s(U)$ is standardized so as to become a random variable with mean equal to zero and standard deviation equal to one. Thus, any error which affects the mean and/or standard deviation of $\dot{T}_s(U)$ does not affect the temperature model.

Calculating optical thicknesses

The quantity

$$\frac{1}{\theta}\int_{z_1}^{z_2} k_i(x)\,dx = -\frac{Q_i}{\theta}\int_{U_1}^{U_2} PO_3(u)\,du \qquad (B.12)$$

is called the optical thickness or opacity of the ozone between z_1 and z_2.

The following calculations are based on the ozone model explained in Chapter IV. A value of U located at approximately 50 km altitude, denoted U_{50}, is used as the dividing point for the two different PO_3 formulas. For $U < U_{50}$ (i.e., at altitudes above the dividing point), PO_3 is given by

$$PO_3(U) = \exp(AU - AU^* + B) \qquad (B.13)$$

where for a particular profile A, B, and U^* are constants. Thus, when $U < U_{50}$, the optical thickness above $z(U)$ is

$$\frac{1}{\theta}\int_{z(U)}^{\infty} k_i(x)\,dx = \frac{Q_i}{A\theta}\,PO_3(U) \qquad (B.14)$$

If $U > U_{50}$, Green's formula (Chapter IV) gives

$$PO_3(U) = 4PO_3^* \frac{e^{L(U)}}{(1 + e^{L(U)})^2} \qquad (B.15)$$

where

$$L(U) = A\,(U - U^*) \qquad (B.16)$$

Thus, for $U > U_{50}$,

$$\frac{1}{\theta}\int_{z(U)}^{\infty} k_i(x)\,dx = \frac{Q_i}{A\theta}\exp\left[L(U_{50}) + B\right]$$

$$+ \frac{4PO_3^{*}\,Q_i}{A\theta}\left[\frac{1}{1+e^{L(U_{50})}} - \frac{1}{1+e^{L(U)}}\right] \qquad \text{(B.17)}$$

APPENDIX C. ESTIMATING THE PARAMETERS IN GREEN'S FORMULA USING OZONAGRAMS

List of Symbols

Symbol	Definition	Units/Constants
A	shaping parameter in Green's formula	
dq/du_2	slope of the ozonagram at a point above U* where $PO_3 = q_2$	
M	molecular weight of air	28.964 kg
MO_3	molecular weight of ozone	47.9982 kg
P	atmospheric pressure	N/m^2
P_o	atmospheric pressure at sea level	N/m^2
P*	atmospheric pressure where $PO_3 = PO_3^*$	N/m^2
PO_3	partial pressure of ozone	N/m^2
PO_3^*	maximum partial pressure of ozone	N/m^2
q_1	ozonagram value of PO_3 at height u_1	N/m^2
q_2	arbitrarily selected value of PO_3 where slope dq/du_2 is estimated	N/m^2
TO_3	total ozone	atm-cm
U	height parameter = $\log(P/P_o)$	
u_1	arbitrarily selected value of U above U* where $PO_3 = q_1$ is measured	
U*	value of U where P = P*	
ρ_3	ozone density	kg/m^3

Criteria for a good fit

In fitting Green's formula,

$$PO_3 = 4PO_3^* \frac{e^x}{(1 + e^x)^2} \qquad (C.1)$$

where $x = A \log(P/P^*)$, to an ozonagram, ideally one could read the coordinates (PO_3^*, P^*) off the curve at the location where PO_3 is maximum. Unfortunately, however, the data usually have an appreciable amount of scatter at that point, and, consequently, it is sometimes difficult to determine values of PO_3^* and P^* which produce a good fit.

In the present study, a "good" fit of Green's formula is one which (1) fits the smooth segment of the PO_3 profile above its maximum and (2) has the correct total ozone TO_3 as reported on each ozonagram.

Calculating the shaping parameter A

If PO_3^* is known, the shaping parameter A can be selected to satisfy this latter criterion regarding total ozone. Total ozone, in atmosphere-centimeters, is given by

$$TO_3 = \frac{2240}{MO_3} \int_0^\infty \rho_3(x)\, dx \qquad (C.2)$$

The ozone density ρ_3 can be expressed in terms of PO_3 to give

$$TO_3 = \frac{2240}{\bar{g}M} \int_{-\infty}^0 PO_3(u)\, du \qquad (C.3)$$

where $U = \log(P/P_o)$. (See equations (B.6) - (B.9) in Appendix B).

Using Green's formula for PO_3 , one gets

$$TO_3 = \frac{8960\ PO_3^*}{\bar{g}MA}\ [1 - (1 + e^{-AU^*})^{-1}] \qquad (C.4)$$

and since $P_o >> P^*$ (i.e., U^* is a large negative number), then

$$TO_3 \approx \frac{8960\ PO_3^*}{\bar{g}MA} \qquad (C.5)$$

This approximate expression is used to calculate A for any PO_3^* and TO_3 . That is,

$$A = \frac{8960\ PO_3^*}{\bar{g}M\ TO_3} \qquad (C.6)$$

(The A_o mentioned in Chapter IV is $8960/\bar{g}M$).

Calculating PO_3^* and P^*

Since the portion of the measured PO_3 curve above the maximum is generally smooth, points on this portion can be read with little difficulty. The following information, read from each ozonagram, is used to calculate PO_3^* and P^*:

(a) a point (q_1,u_1) on the curve above (PO_3^*,P^*) , where $PO_3 = q_1$ and $\log(P/P_o) = u_1$, and

(b) the slope $dq/du_2 = \Delta PO_3/\Delta U$ at a second point $PO_3 = q_2$ above (PO_3^*,P^*) .

From this information, i.e., (q_1,u_1) and $(q_2,dq/du_2)$, values of PO_3^* and P^* are calculated such that the fitted curve passes

through (q_1, u_1) and has a slope equal to dq/du_2 at the point above the maximum where $PO_3 = q_2$.

The derivative of Green's formula with respect to U is

$$\frac{dPO_3}{du} = \frac{A\ PO_3^2\ (1 - e^{2x})}{4PO_3^*\ e^x} \tag{C.7}$$

Substituting for A from equation (C.6) and letting $dPO_3/dU = dq/du_2$ and $PO_3 = q_2$, (C.7) becomes

$$\frac{dq}{du_2} = \frac{2240\ q_2^2\ (1 - e^{2x_2})}{\bar{g}M\ TO_3\ e^{x_2}} \tag{C.8}$$

Solving for e^{x_2} one gets

$$e^{x_2} = -y + \sqrt{y^2 + 1} \tag{C.9}$$

where

$$y = \frac{\bar{g}M\ TO_3\ dq/du_2}{4480\ q_2^2} \tag{C.10}$$

Thus, the value of e^x at $PO_3 = q_2$, e^{x_2}, is a function of known quantities and can be calculated. Then, substituting this into Green's formula for q_2, it is possible to solve for

$$PO_3^* = \frac{q_2(1 + e^{x_2})^2}{4\ e^{x_2}} \tag{C.11}$$

where e^{x_2} is given be (C.9).

Now, a value for A can be calculated from (C.6), and $P^* = P_o e^{U^*}$

can be found by solving Green's formula at (q_1, u_1) ,

$$q_1 = 4PO_3^* \frac{e^{x_1}}{(1 + e^{x_1})^2} \tag{C.12}$$

for $U^* = u_1 - x_{1/A}$. Solving (C.12) for e^{x_1} gives

$$e^{x_1} = [\sqrt{r} - \sqrt{r - 1}]^2 \tag{C.13}$$

where $r = PO_3^*/q_1$. Thus,

$$P^* = P_o e^{u_1} (\sqrt{r} - \sqrt{r - 1})^{-2/A} \tag{C.14}$$

APPENDIX D. EQUATIONS FOR FITTING PEARSON DISTRIBUTIONS TO DATA

Let X be a continuous random variable and let $f(x)$ be its probability density function. Karl Pearson, [42], claimed that the probability density functions of most statistical distributions arising in practice belong to the family of density functions satisfying the differential equation

$$\frac{df}{dx} = \frac{(x - a)\, f}{b_0 + b_1 x + b_2 x^2} \qquad (D.1)$$

where a, b_o, b_1, and b_2 are population parameters (constants).

Pearson identified thirteen distribution types which satisfy (D.1). These consist of the normal distribution plus twelve types which are designated Type I - Type XII. Of these, the normal distribution, and the Type I, Type III, Type IV, and Type VI distributions are considered the major Pearson distributions, whereas the other eight are called transitional distributions, [46], and can usually be treated as special degenerate cases of the five major Pearson distributions. Methods are presented here for fitting the five major distributions to empirical distributions (data). In instances where a transitional distribution is identified, it is assigned to one of the five major distribution types.

Any probability density function of the Pearson family can be completely determined by its four moments μ_i, $i = 1, \ldots, 4$, defined by

$$\mu_i = \int_{-\infty}^{\infty} x^i f(x)\, dx \qquad (D.2)$$

Assume that a random sample of size n is drawn from the X population, and let the population moments μ_i be estimated by the sample moments M_i as defined by

$$M_i = \frac{1}{n} \sum_{j=1}^{n} X_j^i \qquad (D.3)$$

Let M_i' denote the i^{th} central moment in the sample as defined by

$$M_i' = \frac{1}{n} \sum_{j=1}^{n} (X_j - \bar{X})^i \qquad (D.4)$$

where $\bar{X} = M_1$ is the sample mean. Then $M_1' = 0$, and $M_2' = s^2$ is the sample variance.

The major Pearson distributions are characterized by three parameters β_1, β_2, and κ which are defined as follows:

$$\beta_1 = \frac{(M_3')^2}{(M_2')^3} \qquad (D.5)$$

$$\beta_2 = \frac{M_4'}{(M_2')^2} \qquad (D.6)$$

and

$$\kappa = \frac{\beta_1 (\beta_2 + 3)^2}{4(4\beta_2 - 3\beta_1)(2\beta_2 - 3\beta_1 - 6)} \qquad (D.7)$$

If the sample variance $s^2 \neq 0$, then, $\beta_1 \geq 0$, $\beta_2 \geq 0$, and

$\kappa = 0$ if and only if $\beta_1 = 0$.

In most cases, the values of β_1 , β_2 , and κ determine the Pearson distribution to which the sample belongs. A fourth parameter is sometimes required to distinguish the transitional distributions. Figure D.1 illustrates the various regions in the $\beta_1 - \beta_2$ plane which are associated with the first seven Pearson distributions. The normal distribution corresponds to the point labeled "N" where $\beta_1 = 0$ and $\beta_2 = 3$. These first seven Pearson distributions plus the normal distribution are listed below with the criteria for their selection and equations for estimating their parameters.

There are two circumstances in which β_1 and β_2 are inadmissible and cannot be used to estimate Pearson distributions. The first is the violation of a constraint on all frequency functions which requires that

$$\beta_2 - \beta_1 > 0 \qquad \text{(D.8)}$$

The second circumstance is the violation of a constraint necessary in order for β_1 and β_2 to lead to a Pearson distribution. This constraint requires that

$$15\,\beta_1 - 8\,\beta_2 + 36 > 0 \qquad \text{(D.9)}$$

Three instances arose in the Monte Carlo Shuttle entry study in which constraint (D.9) was violated. In these cases an attempt was made to find the "closest" Pearson distribution fitting the data. To accomplish this, a line L was drawn through the inadmissible point

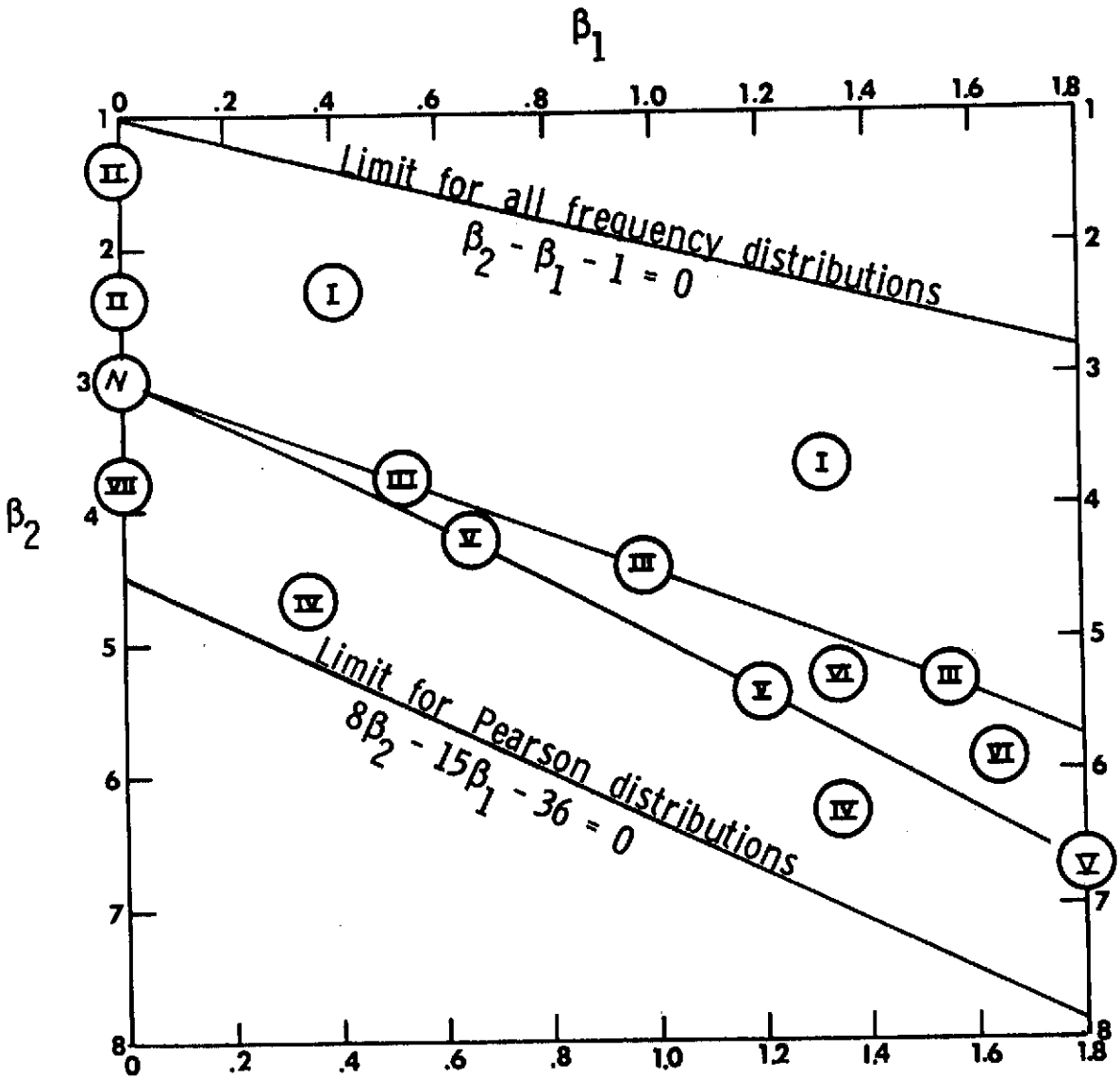

Figure D.1 - Regions of the $\beta_1 - \beta_2$ plane associated with the various Pearson distributions.

(β_1 , β_2) perpendicular to the line $15\beta_1 - 8\beta_2 + 36 = 0$. (See Figure D.1). A point on the line L just inside the admissible region was then selected, and its coordinates (β_1^* , β_2^*) were used as new adjusted values for β_1 and β_2. The third and fourth central moments, M_3' and M_4', were then adjusted to be consistent with the definitions of β_1 and β_2 in equations (D.5) and (D.6), respectively.

In the case of one parameter (i.e., maximum dynamic pressure during the summer entries) this method succeeded in producing a reasonable Pearson fit for the empirical distribution. In the two other cases of inadmissible β_i's, (i.e., summer down range and cross range), this adjustment produced J-shaped Type VI distributions with poor resemblances to the parameter histograms.

The following summaries explain the criteria used for selecting each Pearson distribution and the methods used in estimating their parameters. No effort is made to show derivations of the formulas. If the reader is interested, a good explanation can be found in Kendall and Stuart, Vol. 1, [42].

The Pearson Type I Distribution

(A) Criterion for selection: $\kappa < 0$

(B) Probability density function:

$$f(x) = \begin{cases} y_o\left(1 + \frac{x}{a_1}\right)^{m_1}\left(1 - \frac{x}{a_2}\right)^{m_2} & \frac{x}{a_1} > -1;\ \frac{x}{a_2} < 1 \\ 0 & \text{elsewhere} \end{cases} \qquad (D.10)$$

where $x = X - \mu_1$.

(C) Equations for estimating parameters:

Let

$$R = 6(\beta_2 - \beta_1 - 1)/(6 + 3\beta_1 - 2\beta_2) \tag{D.11}$$

$$S = [\beta_1(R + 2)^2 + 16(R + 1)]^{1/2} \tag{D.12}$$

and

$$T = R(R + 2)\ \beta_1^{1/2}\ /S \tag{D.13}$$

The estimates of m_1 , m_2 , a_1 , a_2 , and Y_o are, respectively,

$$\hat{m}_1 = \begin{cases} (R - 2 + T)/2 & \text{if } M_3' < 0 \\ (R - 2 - T)/2 & \text{if } M_3' \geq 0 \end{cases} \tag{D.14}$$

$$\hat{m}_2 = R - 2 - \hat{m}_1 \tag{D.15}$$

$$\hat{a}_1 = .5\ s\ S(\hat{m}_1 + 1)/(\hat{m}_1 + \hat{m}_2 + 2) \tag{D.16}$$

$$\hat{a}_2 = .5\ s\ S(\hat{m}_2 + 1)/(\hat{m}_1 + \hat{m}_2 + 2) \tag{D.17}$$

and

$$\hat{Y}_o = \frac{\Gamma(\hat{m}_1 + \hat{m}_2 + 2)}{\Gamma(\hat{m}_1 + 1)\Gamma(\hat{m}_2 + 1)}\ \left(\frac{sS}{2}\right)^{-(\hat{m}_1+\hat{m}_2+1)} |\hat{a}_1|^{\hat{m}_1}\ |\hat{a}_2|^{\hat{m}_2} \tag{D.18}$$

The Pearson Type II Distribution

(A) Criterion for selection: $\kappa = 0$, $\beta_2 < 3$

This is one of the transitional distributions, and is treated as a subclass of the Type I distribution.

The Pearson Type III Distribution

(A) Criterion for selection: $\kappa = \pm\infty$

(B) Probability density function:

$$f(x) = \begin{cases} Y_o \left(1 + \frac{x}{a}\right)^{\alpha-1} \exp(-bx) & \frac{x}{a} > -1 \\ 0 & \text{elsewhere} \end{cases} \tag{D.19}$$

(C) Equations for estimating parameters:

The equations for estimating α , b , a , and Y_o are, respectively,

$$\hat{\alpha} = 4/\beta_1 \tag{D.20}$$

$$\hat{b} = 2s^2/M_3' \tag{D.21}$$

$$\hat{a} = \hat{\alpha}/\hat{b} \tag{D.22}$$

and

$$\hat{Y}_o = \frac{|\hat{b}|\ \hat{\alpha}^{(\hat{\alpha}-1)} \exp(-\hat{\alpha})}{\Gamma(\hat{\alpha})} \tag{D.23}$$

The Pearson Type IV Distribution

(A) Criterion for selection: $0 < \kappa < 1$

(B) Probability density function:

$$f(x) = Y_o \left[1 + \left(\frac{x}{a} - \frac{v}{r}\right)^2\right]^{-m} \exp\left[-v \tan^{-1}\left(\frac{x}{a} - \frac{v}{r}\right)\right] \tag{D.24}$$

where $x = X - \mu_1$.

(C) Equations for estimating parameters:

Let

$$R = 6(\beta_2 - \beta_1 - 1)/(2\beta_2 - 3\beta_1 - 6) \tag{D.25}$$

$$S = [16(R - 1) - \beta_1(R - 2)^2\ ]^{1/2} \tag{D.26}$$

and

$$T = R(R - 2)\ \beta_1^{1/2}\ /S \tag{D.27}$$

Then the equations for estimating m, a, v, r, and Y_o are, respectively,

$$\hat{m} = (R + 2)/2 \tag{D.28}$$

$$\hat{a} = sS/4 \tag{D.29}$$

$$\hat{v} = \begin{cases} T & \text{if } M_3' < 0 \\ -T & \text{if } M_3' \geq 0 \end{cases} \tag{D.30}$$

$$\hat{r} = R \tag{D.31}$$

and

$$\hat{Y}_o = \frac{0.3989432\ \hat{r}^{1/2}}{\hat{a}(\cos\ \phi)^{\hat{r}+1}} \left\{ \frac{\cos^2 \phi}{3\hat{r}} - \frac{1}{12\hat{r}} - \phi\hat{r} \right\} \tag{D.32}$$

where

$$\phi = \tan^{-1} \left(\frac{\hat{v}}{\hat{r}}\right) \tag{D.33}$$

The Pearson Type V Distribution

(A) Criterion for selection: $\kappa = 1$

This is one of the transitional distributions and is treated as a subclass of the Type VI distribution.

The Pearson Type VI Distribution

(A) Criterion for selection: $\kappa > 1$

(B) Probability density function:

$$f(x) = \begin{cases} Y_o \left(1 + \frac{x}{a_1}\right)^{m_1} \left(1 + \frac{x}{a_2}\right)^{-m_2} & \frac{x}{a_1} > -1 \; ; \; \frac{x}{a_2} > -1 \\ 0 & \text{elsewhere} \end{cases} \tag{D.34}$$

where $x = X - \mu_1$.

(C) Equations for estimating parameters:

Let

$$R = 6(\beta_2 - \beta_1 - 1)/(6 + 3\beta_1 - 2\beta_2) \tag{D.35}$$

$$S = [\beta_1(R + 2)^2 + 16 (R + 1)]^{1/2} \tag{D.36}$$

and

$$T = R(R + 2) \beta_1^{1/2} /S \tag{D.37}$$

Then the equations for estimating m_1 , m_2 , a_1 , a_2 , and Y_o are, respectively:

$$\hat{m}_1 = (T - R + 2)/2 \tag{D.38}$$

$$\hat{m}_2 = (T + R - 2)/2 \tag{D.39}$$

$$\hat{a}_1 = \begin{cases} -.5 \; s \; S(\hat{m}_1 - 1)/(\hat{m}_1 - \hat{m}_2 - 2) & \text{if } M_3' < 0 \\ .5 \; s \; S(\hat{m}_1 - 1)/(\hat{m}_1 - \hat{m}_2 - 2) & \text{if } M_3' \geq 0 \end{cases}$$

$$\hat{a}_2 = \begin{cases} \hat{a}_1 + s \; S/2 & \text{if } M_3' < 0 \\ \hat{a}_1 - s \; S/2 & \text{if } M_3' \geq 0 \end{cases} \tag{D.41}$$

and

$$\hat{Y}_o = \frac{\Gamma(\hat{m}_1)}{\Gamma(\hat{m}_2 + 1)\Gamma(\hat{m}_1 - \hat{m}_2 - 1)} \left(\frac{sS}{2}\right)^{(\hat{m}_1 - \hat{m}_2 - 1)} |\hat{a}_1|^{-\hat{m}_1} |\hat{a}_2|^{\hat{m}_2} \qquad (D.42)$$

The Pearson Type VII Distribution

(A) Criterion for selection: $\kappa = 0$, $\beta_2 > 3$

This is one of the transitional distributions and is treated as a subclass of the Type IV distribution.

The Normal Distribution

(A) Criterion for selection: $\beta_1 = 0$ $\beta_2 = 3$

(B) Probability density function:

$$f(x) = \frac{1}{\sigma\sqrt{2\pi}} \exp\left(-x^2/2\sigma^2\right) \qquad (D.43)$$

where $x = X - \mu_1$.

(C) Equations for estimating parameters .

An estimate of σ is s , the sample standard deviation.

VITA

The author was born in [redacted], on [redacted]. As the daughter of an Air Force officer, she attended schools in different parts of the country and abroad. After graduation from the American High School in San Salvador, El Salvador, she entered Mary Baldwin College in September, 1962, and graduated with High Honors in June, 1966, receiving a Bachelor of Arts degree in mathematics. She attended Vanderbilt University from September, 1966, until June, 1967, on a National Aeronautics and Space Administration graduate fellowship administered by the university, and received a Master of Arts degree in mathematics in January, 1968.

The author has been employed at the Langley Research Center of the National Aeronautics and Space Administration in Hampton, Virginia, since September, 1967. She was granted Graduate Study Leave to attend Virginia Polytechnic Institute and State University in September, 1969, at which time she began the course work leading to the present degree. In the meantime, she was awarded a Master of Sciences degree (without thesis) in statistics in June, 1971. Her husband, James F. Campbell, has recently completed the requirements for a Doctor of Philosophy degree in aerospace engineering from Virginia Polytechnic Institute and State University. He is also employed at the Langley Research Center.